FIRST-PRINCIPLE INVESTIGATIONS OF SOME NANOSTRUCTURED SYSTEMS FOR GAS SENSING APPLICATIONS

BY

MOHAMMED MOHAMMED ESMAIL AL-EZZI

A Thesis Presented to the
DEANSHIP OF GRADUATE STUDIES

KING FAHD UNIVERSITY OF PETROLEUM & MINERALS

DHAHRAN, SAUDI ARABIA

In Partial Fulfillment of the
Requirements for the Degree of

MASTER OF SCIENCE

In

PHYSICS

MAY 2017

KING FAHD UNIVERSITY OF PETROLEUM & MINERALS

DHAHRAN- 31261, SAUDI ARABIA

DEANSHIP OF GRADUATE STUDIES

This thesis, written by **MOHAMMED MOHAMMED ESMAIL ALEZZI** under the direction his thesis advisor and approved by his thesis committee, has been presented and accepted by the Dean of Graduate Studies, in partial fulfillment of the requirements for the degree of **MASTER OF SCIENCE IN PHYSICS.**

Dr. Hocine Bahlouli
(Advisor)

Dr. Abdullah Al-Sunaidi
Department Chairman

Dr. Nacir Tit
(Member)

Dr. Salam A. Zummo
Dean of Graduate Studies

Dr. Saeed Al-Marzoug
(Member)

5/16/17
Date

© Mohammed Mohammed Esmail Alezzi

2017

To my Mother

ACKNOWLEDGMENTS

All my appreciation and thanks to my thesis advisor, Prof. Hocine Bahlouli for his guidance and help all the way till the achievement of this thesis. He taught me physics 101 and motivated me to major in physics. Thanks for his constant motivation and asking about my progress during my undergraduate. Because of him, SCTP paid the master's degree tuitions. Without him, it would have been impossible to finish my master program.

I would like also to thank my thesis committee member, Prof. Nacir Tit and Dr. Saeed Al-Marzoug for their cooperation and constructive comments. I am grateful to Prof. Tit, who introduced me to the field of computational physics and trained me on DFTB+. He is truly humble. He is more than a professor to me; he is a big brother. A very special gratitude goes out to Dr. Berdiyorov, who hosted me in Doha for one week, trained my on ATK and tremendously worked with me on the second problem of this thesis.

I would like to thank the Saudi Center for Theoretical Physics (SCTP) for their financial support. I would like to thank Dr. Al Jalal. He motivated me and hugely supported my application to study physics as a double major during my undergraduate. He also supported me financially during my master. My deepest appreciation, thanks and acknowledgment to King Fahd University of Petroleum and Minerals (KFUPM) for their full support during my undergraduate study and their partial support during my graduate program.

With a special mention to Mohammed Ameen, Al-Areeq, Qasem, Hassan, Talal, Thamari, Mustafa, Darwbi, Salah, Galal, Zead, Sadam, Anwar, Ali Qadri, Mazen, Qais, Omar, Saleem, Madean, Ismail, Manda, it was fantastic to have the opportunity to live in such a supportive and encouraging environment.

Last but not least, my ultimate thank and love for my parents and family for their endless support and love.

TABLE OF CONTENTS

ACKNOWLEDGMENTS ..... **v**

TABLE OF CONTENTS ..... **vii**

LIST OF TABLES ..... **ix**

LIST OF FIGURES ..... **x**

LIST OF ABBREVIATIONS ..... **xiv**

ABSTRACT ..... **xv**

ملخص الرسالة ..... **xvii**

CHAPTER 1 INTRODUCTION **1**

1.1 Objectives **6**

1.2 Methodology **7**

CHAPTER 2 DETECTION OF CO_2 USING CNT-BASED SENSORS **10**

2.1 Background **11**

2.2 Computational Details and Model Systems **14**

2.3 Results and Discussion **21**

2.3.1 Atomic Relaxations **21**

2.3.2 Study of Sensitivity **30**

2.3.3 Effect of Energy Gap on Sensitivity **34**

2.3.4 Study of Selectivity **39**

2.4 Conclusion **44**

CHAPTER 3 CO_2 ADSORPTION ON FE-DOPED GRAPHENE NANORIBBONS.. 46

3.1 Introduction..... 47

3.2 Computational Details 48

3.3 Results and Discussion..... 51

3.4 Conclusion..... 65

CHAPTER 4 ADSORPTION OF H2 ON GRAPHITIC ZNO 66

4.1 Introduction..... 67

4.2 Computational Method..... 70

4.3 Results and Discussions 74

4.3.1 Relaxation and Atomic Structures..... 75

4.3.2 Density of States..... 79

4.3.3 Simulation of Gas Sensing..... 82

4.3.4 Defected ZnO 87

4.3.5 Band Structures 89

4.4 Conclusion..... 91

CHAPTER 5 CONCLUSIONS..... 93

APPENDIX METALLIC CONDUCTIVITY AND GAS SENSITIVITY 97

REFERENCES..... 100

VITAE..... 108

LIST OF TABLES

Table 1: Comparison of geometrical parameters of four relaxed structures: (i) ac-CNT with 1 Fe (on-site) and 1 CO_2 molecule; (ii) graphene with 1 Fe (on-site) and 1 CO_2 molecule; (iii) ac-CNT with 1 Fe (on hollow site) and 1 CO_2 molecule; and (iv) graphene with 1 Fe (on hollow site) and 1 CO_2 molecule. Note that in the pictures: C, Fe and O atoms are shown in yellow, red and green colors, respectively. 21

Table 2: Results of relaxations of 1 Fe atom on either on-site or on hollow-site as well as of1 CO2 molecule on top of Fe ad-atom for: (A) Graphene and (B) ac-CNT 22

Table 3: Results of relaxation of 1 Fe atom on hollow sites of both zz-CNT and ac-CNT (for sake of comparison), followed by the relaxation of 1 CO_2 on the Fe ad-atom..... 39

Table 4: Results of selectivity analysis of CO_2, O_2, N_2, H_2, H_2O and CO gases are shown. The results include: the Fe-molecule distance, angular distortion of molecule, binding energy of molecule and type of adsorption. 43

Table 5 : Summary of energetics and geometry results of relaxations of H_2 molecule on: (i) Zn-site; (ii) O-site; (iii) Bridge-site; and (iv) Hollow-site. Both EF and Ebind are in eV-units; whereas the Zn-H and O-H distances are in Å-units. 77

Table 6: Density of states at Fermi level (NF) and the response-function (i.e., gas sensitivity) are shown versus gas dose (i.e., N = 1-4 molecules). 84

LIST OF FIGURES

Figure 1: (a) Pristine graphene sheet of size 6x6 primitive cells used in the calculations. The primitive lattice vectors (a1, a2) are shown. (b) Supercell of graphene; (c) Supercell of ac-CNT; and (d) Supercell of zz-CNT. 16

Figure 2: Comparison between relaxed atomic structures of two systems showing the chemisorption of CO_2 on: (a) ac-CNT with 1 Fe ad-atom, and (b) Pristine graphene with 1 Fe ad-atom. Note that in both latter cases Fe ad-atoms are placed on hollow sites. Note that C, Fe and O atoms are shown in yellow, red and green colors, respectively.....27

Figure 3: Relaxed atomic structures of ac-CNT with 5 Fe ad-atoms dispersed on its surface before the arrival of CO_2 gas molecules, (b) After chemisorption of 1 CO_2 molecule, and (c) After chemisorption of 5 CO_2 molecules. 29

Figure 4: (a) TDOS and PDOS of a relaxed system of ac-CNT with 5 Fe ad-atoms and 1 CO_2 molecule on its surface are shown. (b) TDOS of 6 systems: each consisting of ac-CNT and 5 Fe ad-atoms on its surface as well as CO_2 molecules, the number of which is varied between 0 and 5. Fermi level is taken as an energy reference in both panels.....31

Figure 5: (a) DOS at Fermi level, (b) Sensitivity, and (c) Average charge of O atom versus the number of CO_2 molecules chemisorbed on a surface of the ac-CNT with 5 Fe ad-atoms.....33

Figure 6: Charge density plots presenting the magnitudes of the HOMO and LUMO states in Graphene-Fe-CO_2 systems. Colors used for: C (grey), Fe (red), and O (green); while the eigen-states are in blue color. 35

Figure 7: Comparison of band structures and DOS of ac-CNT (containing 144 carbon atoms) and zz-CNT (containing 160 carbon atoms). The numbers associated to letters stand for: (1) pure CNT, (2) CNT with 1 Fe ad-atom, and (3) CNT-Fe compound after chemisorption of 1 CO_2 molecule. In the bands, vacuum level is taken as an energy reference. Whereas, for DOS, either Fermi

level (EF) or valence-band edge (EV) is taken as an energy reference. TDOS is normalized to 8 electrons per hexagon in case of pure CNT. 37

Figure 8: Bar chart of the binding energy in green color (a) of a single gas molecule and the gas sensitivity in red color (b) versus different gases is shown. The adsorbent is ac-CNT with 1 Fe ad-atom. 40

Figure 9: Device geometries: hydrogen passivated graphene nanoribbons with a single CO_2 molecule adsorbed directly (a) or through Fe atoms (b, c). The transmission is calculated along the z-direction and a vacuum space of 20 ˚A is left along the x-direction..... 50

Figure 10: (a) Zero bias transmission spectra (T(E)) of pristine graphene without (solid-black curve) and with a single CO_2 molecule adsorbed (dashed-red curve) as a function of electron energy. Insets show the enlargement of the transmission spectra. (b) Device density of states projected onC atom (solid black curve) and O atoms (dashed-red curve) of the molecule as a function of energy. Energy origin coincides with the Fermi energy. 52

Figure 11: (a) Zero bias transmission spectra of aFe-graphene without (solid-black curve) an with a single CO_2 molecule adsorbed (dashed-red curve) as a function of electron energy. (b) device density of states (DDOS) of aFe-graphene projected on Fe atom. (c) DDOS of aFe-graphene+CO_2 system projected on the Fe atom (solid-black curve), C atom of the molecule (dashed-red curve) and the O atoms of the molecule (dotted-blue curve)..... 54

Figure 12: Isosurface plots of the projected self consistent Hamiltonian eigenstates for the aFe-graphene (a) and aFe-graphene+CO_2 (b) systems. The isovalues are 0.005 ˚A−3/2 (a) in both cases. The energies for the corresponding isoplots are given in each panel..... 55

Figure 13: The same as in Fig. 11, but for sFe-graphene system. 58

Figure 14: Isosurface plots of the projected self-consistent Hamiltonian eigenstates for the sFe-graphene (a) and sFe-graphene+CO_2 (b) systems. The isovalues are 0.01 ˚A−3/2. The energies of the corresponding isoplots are given in each panel. 60

Figure 15: Electrostatic difference potential along the transport direction for zero bias across the samples. The results are shown for pristine graphene (a), aFe-graphene (b) and sFe-graphene (c) without (solid-black curves) and with CO_2 molecule (dashed-red curves)..... 61

Figure 16: Transmission spectra of graphene (a), aFe-graphene (b) and sFe-graphene (c) without (solid-black curve) and with a single CO_2 molecule adsorbed (dashed-red curve) for the voltage biasing V= 0.5 V. 64

Figure 17: Both top-view and side-view of relaxed atomic structures of H_2 molecule on ZnO-2d starting from putting the H_2 molecule on: (a) Zn-site; (b) O-site; (c) Bridge-site; and (iv) Hollow-site. Only case (b) is found to yield chemisorption. 76

Figure 18: Density of electronic states of relaxed: (a) pristine ZnO containing 6x6 primitive cells (72 atoms); (b) isolated H_2 molecule; and (c) H_2 molecule chemisorbed on ZnO associated with its dissociation and the formation of Zn-H and O-H single bonds. These latter two bonds form acceptor and donor states, respectively. Fermi level is taken as an energy reference. 81

Figure 19: Relaxed structures of H_2 molecule(s) on ZnO, starting from on O-sites and leading to chemisorption versus gas dose (i.e., versus N = 1-4 molecules). 83

Figure 20: (a-d) DOS of relaxed structures of Figure 19. Fermi level is taken as an energy reference. (e) The DOS at Fermi level and sensitivity are shown versus number of H_2 molecules (i.e., versus gas dose). 86

Figure 21: Relaxed atomic structures of ZnO with VO (a) and with H_2 molecule (b). The corresponding DOSs to (a-b) are shown in (c), with Fermi level as an energy reference. 88

Figure 22: Band structures are shown for: (a) Pristine ZnO-2d; (2) Relaxed H_2 on ZnO in case of chemisorption (i.e., stating from on O-site); (c) Reconstructed oxygen vacancy; (d) relaxed H_2 on reconstructed VO, which yields physisorption. 90

LIST OF ABBREVIATIONS

DFT	:	Density functional theory
DFTB	:	Density functional tight binding theory
SCC-DFTB	:	self-consistent-charge density functional tight-binding method.
CNT	:	Carbon nano tubes
ac-CNT	:	armchairs carbon nanotube
ac-CNT-Fe	:	armchairs carbon nanotube + Fe atom
GNR	:	Graphene nano ribbons
aFe-graphene:		Fe add atom on graphene
sFe-graphene	:	Substitutional Fe atom on graphene
VO	:	oxygen vacancy
ZnO-2d	:	2 dimensional sheets of ZnO

ABSTRACT

Full Name : [Mohammed Mohammed Esmail Al-Ezzi]

Thesis Title : [First-Principle Investigations of Some Nanostructured Systems for Gas Sensing Applications]

Major Field : [Physics]

Date of Degree : [May 2017]

Using computational methods to design novel solid state gas sensor is crucial to further improve technological applications based on nanostructured materials. In this thesis, we used quantum computational method to study three novel nanostructured systems and investigated the feasibility to employ them in the detection of different gases of interest. The first problem involves the adsorption of CO_2 on surfaces of graphene and carbon nanotubes (CNTs), decorated with Fe atoms, using the self-consistent-charge density-functional tight-binding (SCC-DFTB) method. Comparative study of sensitivity of ac-CNT-Fe composite towards various gases (e.g., O_2, N_2, H_2, H_2O, CO and CO_2) has shown high sensitivity and selectivity towards CO, CO_2 and H_2O gases. In the second problem, we studied graphene nanoribbons (GNR) to detect CO_2. We used density functional theory in combination with the nonequilibrium Green's function formalism to study the conductance response of Fe-doped graphene nanoribbons to CO_2 gas adsorption. A single Fe atom is either adsorbed on graphene's surface (aFe-graphene) or it substitutes the carbon atom (sFe-graphene). Metal atom doping reduces the electronic transmission of pristine graphene due to the localization of electronic states near the impurities. The reduction in the transmission is more pronounced in the case of aFe-graphene. In addition, the aFe-graphene is found to be less sensitive to the CO_2 molecule attachment as compared to the

sFe-graphene system. Pristine graphene is also found to be less sensitive to the molecular adsorption. We think our findings will be useful in developing graphene-based solid-state gas sensor. Finally, the adsorption of H_2 molecules on graphitic ZnO-2d is investigated using (SCC-DFTB) method. We inspected the chemical activity of (a) Zn site, (b) O site, (iii) bridge site, (iv) hollow site, and (v) oxygen-vacancy "VO" site. The results show that the chemisorption can occur only if H_2 molecule lands on the oxygen site. In that case, the H_2 molecules gets dissociated into two separate hydrogen atoms. Moreover, oxygen vacancies do intentionally exist in real samples as native defects. Our simulations show that the relaxed oxygen vacancy in ZnO-2d would introduce a triplet of donor states and a singlet of acceptor state as well as to shift Fermi level upper than the donor states (i.e., $E_F \geq E_D$). Furthermore, the chemisorption of H_2 on oxygen site yields to formation of one shallow donor state (attributed to O-H bond) and one deep acceptor state (attributed to Zn-H bond). These two scenarios would simultaneously enhance the majority charge carrier density and yield a degenerate n-type ZnO. Because of these reasons, our results show an enhanced conductance and sensitivity versus gas dose, and clearly display the suitability of ZnO for H_2 gas sensing.

ملخص الرسالة

الاسم الكامل: محمد محمد إسماعيل العزي

عنوان الرسالة: دراسات حسابية لبعض المركبات النانومترية لاستخدامها في تطبيقات استشعار الغازات

التخصص: فيزياء

تاريخ الدرجة العلمية: مايو 2017

في هذه الرسالة العلمية تم توظيف طرق حسابية فيزيائية في ثلاث دراسات مختلفة لغرض تصميم مركبات نانومترية جديدة كي تستخدم في صناعة أجهزة استشعار بعض الغازات ذات الأهمية البيئية والاقتصادية. كل الطرق الحسابية المستخدمة هي طرق تابعة لميكانيكا الكم. تم استخدام الطرق الحسابية لدراسة ثلاث مركبات نانومترية جديدة من أجل فحص إمكانية استخدمها في أجهزة استشعار الغازات. الدراسة الأولى تتضمن بحث عمليات التصاق جزيئات ثاني أكسيد الكربون على سطح الجرافين والكربون نانو تيوب, مع وبدون إضافة ذرات الحديد باستخدام نظرية ال self-consistent-charge density-functional tight-binding والتي يرمز لها بالاختصار (SCC-DFTB). وقد أظهرت الدراسة المقارنة حساسية الكربون نانوتيوب ac-CNT-Fe المطعم بذرات الحديد تجاه عدة غازات وهي الأكسجين و النيتروجين والهيدروجين وبخار الماء و أول أكسيد الكربون بالإضافة لثاني أكسيد الكربون أن المادة النانومترية المركبة الجديدة حساسة وانتقائية فقط تجاه أول وثاني أكسيد الكربون بالإضافة لبخار الماء. أما الدراسة الثانية فقد تضمنت بحث قدرة أشرطة الجرافين graphene nanoribbons (GNR) على استشعار غاز ثاني أكسيد الكربون. في هذه الدراسة استخدمنا density functional theory بالإضافة ل nonequilibrium Green's function formalism لبحث تغير خصائص أشرطة الجرافين المطعمة بالحديد بعد تعرضها لالتصاق غاز ثاني أكسيد الكربون على سطحها. تم إضافة ذرة الحديد لشريط الجرافين بطريقتين: إما على السطح بالاتصاق (aFe-graphene) أو بطريقة تعويضية بعد إزالة ذرة كربون وإبدالها بذرة الحديد (sFe-graphene) . وقد وجدنا - كما هو معلوم - أن التطعيم بذرات المعادن يعمل على إضعاف التوصيل الإلكتروني للجرافين نتيجة تمركز الإلكترونات بالقرب من الشوائب المضافة للجرافين. وجدنا أيضا أن إضافة

الحديد على سطح أشرطة الجرافين يضعف التوصيل الإلكتروني أكثر مما يحدث في حالة إضافة الحديد بالإبدال. على العكس من ذلك , فإن غاز ثاني أكسيد الكربون له القدرة على تغيير خصائص أشرطة الجرافين المدعمة بالحديد بطريقة الإبدال بمقدار كبير في حالة المقارنة مع ال (aFe-graphene) . و يجدر الإشارة بإن الجرافين بدون إضافات لا يستطيع استشعار غاز ثاني أكسيد الكربون. ونريد التنويه بإن نتائج دراستنا الثانية من الممكن توظيفها في تطوير أجهزة استشعار قائمة على مادة الجرافين. أما دراستنا الثالثة فقد هدفت لبحث التصاق غاز الهيدروجين على مادة الزنك أكسيد النانومترية ذات الدرجة الثانية ZnO-2d باستخدام نظرية ال (SCC-DFTB) . في هذه الدراسة بحثنا النشاط الكيميائي لخمسة مواقع التصاق على سطح ال ZnO-2d وهي (أ) فوق ذرة الزنك (ب) فوق ذرة الأكسجين (ج) فوق الرابطة (د) في المواقع الجوفاء بالإضافة ل (هـ) مواقع ذرات الأكسجين الشاغرة. أظهرت نتائجنا أن الالتصاق الكيميائي يحصل فقط في حالة وضع جزيئات الهيدروجين فوق ذرات الأكسجين. في هذه الحالة فإن جزيئات الهيدروجين تتحلل إلى ذرتين منفصلتين. أما الدور الذي تعلبها مواقع الأكسجين الشاغرة فهو إضافة electronic states جديدة تعمل على زيادة كثافة الناقلات السالبة مما يؤدي تشكيل degenerate n-type ZnO . بما أن دراستنا الثالثة أظهرت تحسن في التوصيل الكهربي وزيادة في قدرته على التفريق بين عدد جزئيات الهيدروجين الملتصق على السطح فإن نستطيع القول بإن ZnO-2d مادة مناسبة للاستخدام في أجهزة استشعار الهيدروجين.

CHAPTER 1

INTRODUCTION

Challenges resulting from global warming are forcing mankind to seek alternatives to traditional energy resources, such as the renewable energy resources, as well as seek solutions to currently existing environmental problems [1]. Amongst plausible solutions is to search for suitable materials (of high efficiency and low cost) capable of capturing CO_2 gas molecule, which is one of the most important green-house gases, and to incorporate these materials into fabrication of devices such as sensors and filters for aim of environmental-safety and health-security applications. Generally, there are several basic criteria for good and efficient gas sensing systems: (i) high selectivity and sensitivity; (ii) fast response and recovery time; (iii) minimal analyst intervention; (iv) operating under low temperature, preferably at ambient temperatures; (v) stability in performance; and (vi) portability, whenever possible. In the last decade, research has focused on materials that control CO_2 emissions by capture and separation technologies, such as absorption, adsorption, separation membranes, and so forth [2]. These include adsorption technologies that use semiconducting metal oxides [3], zeolites[4] , metal-organic frameworks (MOFs)[5] , activated carbons [6], and other porous structured materials such as porous silicon [7]. In recent years, several novel adsorbers of various atmospheric gases (including

CO_2), like carbon nanotubes (CNTs), graphene and their nano-ribbons (GNRs), have been experimentally and theoretically investigated as candidates for adsorption beds[8-13] .

Carbon nanotubes attracted enormous number of researchers since their discovery by Iijima in 1991 [14], for their unique morphology, geometry and other properties [15]. Furthermore, it is because of its unique surface morphology, remarkably large surface-to-volume ratio, huge conductivity and little thermal noise, graphene is also considered as a promising material for gas sensing applications [16-18]. Graphene based sensors have advantages over the other solid-state gas sensors in terms of sensitivity, response and recovery time, low power consumption and low cost[19-22] . Moreover, they run at room temperature and under ambient conditions. In addition, gas sensing and catalytic properties of graphene can be further enhanced by decorating it with metal and metaloxide nanoparticles [8, 23-25].

Because of their suitability for adsorption carbon nanomaterials were proposed and actually investigated like graphene [26, 27] nanotubes [28], and activated carbons [29-31]. Gas sensing is dependent on two events: (i) Occurrence of chemisorption and (ii) if this latter affects the conductivity. Both are related to surface phenomena. For this reason, systems with high surface-to-volume ration and porosity would be efficient for gas sensing. Because of these trends, I decided to work on novel one and two dimensional materials, namely are: (1) Honeycomb Graphene “G”; (2) Carbon Nanotubes “CNT” (3) Graphene Nanoribbons “GNR”; (4) Graphetic ZnO-2d; and probably (5) ZnO Nanotubes “ZnO-NT”. The aim is to search for efficient gas sensor with low cost in fabrication to detect two gases of interest (CO_2 and/or H_2). CO_2 is one of the most active green-house gases which is the

main cause of climate change and global warming and should be of great interest for environmental and health applications. H_2 is a gas needed to produce energy.

Graphene, graphene nanoribbons, CNTs and zinc-oxide nanostructures are categorized as materials possessing multi-functional characters altering diversity of applications in various fields such as: (1) nano-electronics (e.g., synthesis of smallest transistors CNTFET)[32, 33] ; (2) photonics (e.g., utilization of CNTs in fabrications of LED[34] and dye-sensitized solar cells[35]); (3) biomedical field (e.g., CNTs in coatings [36]); (4) spintronics (e.g., the curvature can enhance spin-orbit coupling to yield spintronics) [37]; and (5) gas sensing (e.g., gas-sensors able to work at low temperatures) [38, 39]. Graphene and CNTs are considered potential materials for gas sensing that may even exceed the semiconducting metal oxides in sensitivity and selectivity towards certain gases and, thus, may gain a leading position in the field of gas-sensing [13, 20, 40-44].

To be specific, these nano materials possess tremendously high surface-to-volume ratio with high porosity (hollow structure), which are ideal for gas molecule adsorption and storage. In addition, the curvature of CNTs and zinc-oxide nanotubes (ZNTs) permits relatively stronger binding with other ad-atoms or gas molecules.

Keeping in mind that gas sensing principles relate to the adsorption and desorption of

gas molecules on the surface of the sensing materials, the sensitivity can be significantly enhanced by increasing the contact interfaces between the catalyst and the sensing materials. This has been demonstrated in the experimental work of Mishra and

Ramaprabhu[45], who proved that chemisorption of CO_2 molecules on CNTs takes place only if the CNTs have been decorated with magnetite (Fe_3O_4) nanoparticles. These latter

authors reported that such nanocomposites have the ability to be CO_2 absorbent with very high uptake capacity, much larger than that of activated carbon and zeolites, working in temperatures up to about 100 ^{0}C.

There is experimental evidence that metal nanoparticle decoration would further enhance both sensitivity and selectivity of graphene based sensors for the detection of toxic gases [46]. Among the other transition metals [47-49], Fe atoms are also considered to be effective dopants to improve the catalytic and gas sensing properties of graphene [50]. Although, the choice of this non-noble metal as a dopant is mainly motivated by its low cost, Fe atoms can perform as good as noble metal atoms (such as Pt-atoms) in terms of improving the sensitivity of graphene, as was revealed in recent first principles calculations [50].

Further to this, a recent theoretical modelling used ab-initio calculations to study the absorption of H_2S on a ZnO 2D-honeycomb sheets doped with iron atoms has showed the roles of metal catalysts in enhancing the chemisorption [50]. These authors

compared four metal catalysts (Fe, Ti , Pt) deposited on a graphitic sheet of ZnO and found that iron yields the highest sensitivity and selectivity amongst the other metals because it has the least electro-negativity (i.e., the highest electro-positivity).

Since the changes in the resistivity after the gas molecule absorption is the main output of solid-state sensors, a fundamental understanding of the electronic transport properties of graphene, carbon nanotubes, and graphene nanoribbons under these conditions enables the utilization of the full potential for their practical applications.

Based on this, I have decided to divide my thesis into three main problems. (1) The first one is the utilization of iron (Fe) as a catalyst deposited on CNT, and to assess the adsorption properties of CO_2 on the CNT-Fe composites. (2) The second one is the utilization of (Fe) as a catalyst deposited on graphene nanoribbons and to assess the adsorption properties of CO_2 on the GNR-Fe composites. (3) Finally, Zinc oxide in 2D-honeycomb sheet will be utilized to detect CO_2 and/or H_2 based on their adsorption of the nanostructure.

It is worth mentioning that recent experimental investigations [51, 52] have shown that C-doped ZnO nanorods have been experimentally shown to be high-active photo-catalyst for water splitting and hydrogen production. Throughout our investigation, we want to understand the reasons behind such behaviors. Hence ZnO presenting its multi-functionality becomes clear and rather obvious.

1.1 OBJECTIVES

(a) Investigate the adsorption of CO_2 on surfaces of carbon nanotubes (CNTs) and graphene sheet both decorated with Fe atoms and the feasibility of using these two materials as a gas sensor for CO_2 after we check the selectivity towards gases including CO_2, O_2, H_2, N_2, H_2O, and CO.

(b) Study the conductance response of Fe-doped graphene nanoribbons to CO_2 gas adsorption where a single Fe atom is either adsorbed on graphene's surface (aFe-graphene) or it substitutes the carbon atom (sFe-graphene). Then I investigate the feasibility of Fe-doped graphene nanoribbon as a CO_2 gas sensor by studying its adsorption properties.

(c) Study the absorption of H_2 on a ZnO nanostructure and investigate the role of intrinsic defects (like oxygen vacancy "VO on the gas sensitivity and to investigate the feasibility of using ZnO 2D-honeycomb sheet as a gas sensor for H_2.

(d) Investigate the possible physical mechanisms involved in detecting these gases and attempt to employ some theoretical models to explain the physical and chemical phenomena behind the sensing effect.

1.2 METHODOLOGY

(I) As a computational method, in the first problem we employ the self-consistent-charge density-functional tight-binding (SCC-DFTB) technique, which uses DFT and has the ability to deal with large systems containing thousands of atoms, and perform accurate

(II) atomic relaxation in an efficient way [53, 54]. The aim is also to relax Fe atom(s) on either graphene or armchair CNTs, then to relax CO_2 molecules on Fe ad-atoms. As output, we calculate the global minimum total energy and obtain the fully relaxed structures as well as their corresponding band structures and density of states (DOS). From total energy calculations, one can estimate the binding energy of both Fe ad-atoms and CO_2 molecules. On the other hand, from DOS calculations, one can estimate the DOS at Fermi level from which conductance and gas detection sensitivity are evaluated. The selectivity is inspected by studying the sensitivity of acCNT-Fe composite to various gases (most of them are components of air, such as: N_2, O_2, H_2, H_2O, CO, and CO_2). A comparative study of selectivity includes a comparison with zigzag CNTs (i.e., zz-CNT-Fe compound) and graphene.

(III) In the second problem, we use density functional theory (DFT) in combination with the nonequilibrium Green's function formalism to study the electronic transport response of zigzag graphene nanoribbons doped with Fe atom and its effect on adsorption of CO_2 molecule. This is using ATK-code (Atomistic ToolKit). Capturing, storing and converting CO_2 has become a major problem due to present climate changes [55-59]. We consider two different cases, either the Fe atom substitutes the carbon atom of graphene (sFe-graphene) or it is adsorbed on graphene's surface (aFe-graphene). As a

reference, we also study the electronic transport properties of pristine graphene without and with a single adsorbed CO_2 molecule. The main purpose of this study is to fully explore the effect of the CO_2 molecule adsorption on the electronic transport properties of pristine and functionalized graphene. The obtained results are explained in terms of electron localization in the system. The variation of the electrostatic potential is also studied in all cases which is one of the important factors affecting the transport properties of the system. Our findings will be useful to design more sensitive graphene based gas sensors.

(IV) In the third problem, I will again employ the self-consistent-charge density-functional tight-binding (SCC-DFTB) technique, which uses DFT and has the ability to deal with large systems containing thousands of atoms, and perform accurate atomic relaxation in an efficient way [53, 54]. The aim is also to relax defects like oxygen vacancies and substitutional dopants like C, Si (C_{Zn}, C_O, Si_{Zn}, Si_O) and metals like K and Mg. As said before, the aim is to understand the selectivity and sensitivity of ZnO nano-system towards detection of CO_2 and/or H_2.

Concerning part III, the first thing to do in computation is usually to check the "bond-length". I will do this for both 2D-graphetic sheet of ZnO (containing 6x6 primitive cells of 72 atoms). Because we need to find the lattice constant or bond-length, only for these bulk structure the atomic relaxations should include "Relaxation of Supercell Lattice Vectors". After we relax our structure we need then to find the total energy and binding energy for five different configurations corresponding to the following molecule positions: (i) on-site, (ii) on-bridge site, (iii) on hollow site, (iv) C substituting Zn-atom

(CZn) and C substituting O-atom (CO) (FeO). Finally based on the binding energies one can study the adsorption of CO_2 and/or H_2 and other molecules on ZnO nano-systems.

CHAPTER 2

DETECTION OF CO_2 USING CNT-BASED SENSORS

The adsorption of CO_2 on surfaces of graphene and carbon nanotubes (CNTs), decorated with Fe atoms, are investigated using the self-consistent-charge density-functional tight-binding (SCC-DFTB) method, neglecting the heat effects. Fe ad-atoms are more stable when they are dispersed on hollow sites. They introduce a large density of states at the Fermi level (NF); where keeping such density low would help in gas sensing. Furthermore, the Fe ad-atom can weaken the C=O double bonds of the chemisorbed CO_2 molecule, paving the way for oxygen atoms to drain more charges from Fe. Consequently, chemisorption of CO_2 molecules reduces both NF and the conductance while it enhances the sensitivity with the increasing gas dose. Conducting armchair CNTs (ac-CNTs) have higher sensitivity than graphene and semiconducting zigzag CNTs (zz-CNTs). Comparative study of sensitivity of ac-CNT-Fe composite towards various gases (e.g., O_2, N_2, H_2, H_2O, CO and CO_2) has shown high sensitivity and selectivity towards CO, CO_2 and H_2O gases.

2.1 Background

Challenges resulting from global warming are forcing mankind to seek alternatives to traditional energy resources, such as the renewable energy resources, as well as seek solutions to currently existing environmental problems [1]. Amongst plausible solutions is to search for suitable materials (of high efficiency and low cost) capable of capturing CO_2 gas molecule, which is one of the most important green-house gases, and to incorporate these materials into fabrication of devices such as sensors and filters for aim of environmental-safety and health-security applications. Generally, there are several basic criteria for good and efficient gas sensing systems: (i) high sensitivity and selectivity; (ii) fast response time and recovery time; (iii) minimal analyst intervention; (iv) low operating temperature, preferably at ambient temperatures; (v) stability in performance; and (vi) portability, as possible. In the last decade, research has focused on materials that control CO_2 emissions by capture and separation technologies, such as absorption, adsorption, membranes, and so forth [2] . These include adsorption technologies that use semiconducting metal oxides [3], zeolites [4], metal-organic frameworks (MOFs) [5], activated carbons [6], and other porous structured materials such as porous silicon [7]. In the recent years, several novel adsorbers of various atmospheric gases (including CO_2), such as carbon nanotubes (CNTs), graphene and graphene nano-ribbons (GNRs), have been experimentally and theoretically investigated as candidates for adsorption beds [8-13, 60, 61].

Carbon nanotubes have attracted enormous research interest since their discovery by Iijima in 1991 [14], due to their unique geometry, morphology, and other properties [15].

Their distinction from graphene, by virtue of their curvature properties, presents additional characteristics that are advantageous in the development of next generation high-speed electronic devices with properties exceeding those of silicon and conventional semiconductors. CNTs are categorized as materials possessing multi-functional characters with diversity of applications in various fields such as: (1) nano-electronics (e.g., synthesis of smallest transistors CNTFET) [32, 62]; (2) photonics (e.g., utilization of CNTs in fabrications of LED [34] and dye-sensitized solar cells [35]); (3) biomedical field (e.g., CNTs in coatings [36]); (4) spintronics (e.g., the curvature can enhance spin-orbit coupling to yield spintronics) [37]; and (5) gas sensing (e.g., gas-sensors able to work at low temperatures)[38, 39]. Graphene and CNTs are considered potential materials for gas-sensing that may even exceed the semiconducting metal oxides in sensitivity and selectivity towards certain gases and, thus, may gain a leading position in the field of gas-sensing [13, 20, 40-44] .

To be specific, CNTs possess extremely high surface-to-volume ratio with high porosity (hollow structure), which are ideal for gas molecule adsorption and storage. In addition, the curvature permits relatively stronger binding with other ad-atoms or gas molecules. Keeping in mind that gas sensing principles relate to the adsorption and desorption of gas molecules on the sensing materials, it is quite understandable that by increasing the contact interfaces between the catalyst and the sensing materials, the sensitivity can be significantly enhanced. This has been demonstrated in the experimental work of Mishra and Ramaprabhu[63], who proved that chemisorption of CO_2 molecules on CNTs takes place only if the CNTs have been decorated with magnetite (Fe_3O_4) nanoparticles. These

latter authors reported that such nano-composites have the ability to be CO_2 absorbent

with very high uptake capacity, much larger than that of activated carbon and much larger than zeolites, up to a temperature of about 100 ^oC. Further to this, a recent theoretical modelling used ab-initio calculations to study the absorption of H_2S on a ZnO 2D-honey$_{co}$mb sheets and has noted the roles of metal catalysts in enhancing the chemisorption [50]. These authors compared four metal catalysts (Fe, Co, Pd and Au) deposited on a graphitic sheet of ZnO and found that iron yields the highest sensitivity and selectivity amongst the other metals because it has the least electro-negativity (i.e., the highest electro-positivity). Based on this, we have decided to use iron (Fe) as a catalyst deposited on CNT, and to assess the adsorption properties of CO_2 on the CNT-Fe composites.

The present work aims to study the adsorption properties of CO_2 molecules on both graphene and CNTs, in the presence of metal Fe catalysts. As a computational method, we employ the self-consistent-charge density-functional tight-binding (SCC-DFTB) technique, which uses DFT and has the ability to deal with large systems containing thousands of atoms, and perform accurate atomic relaxation in an efficient way [53, 54]. The aim is also to relax Fe atom(s) on either graphene or armchair CNTs, then to relax CO_2 molecules on Fe ad-atoms. As output, we calculate the global-minimum total energy and obtain the fully relaxed structures as well as their corresponding band structures and density of states (DOS). From total energy calculations, one can estimate the binding energy of both Fe ad-atoms and CO_2 molecules. On the other hand, from DOS calculations, one can estimate the DOS at Fermi level from which conductance and gas detection sensitivity are evaluated. The selectivity is inspected by studying the sensitivity of ac-CNT-Fe composite

to various gases (most of them are components of air, such as: N_2, O_2, H_2, H_2O, CO, and CO_2). A comparative study of selectivity includes a comparison with zigzag CNTs (i.e., zz-CNT-Fe compound) and graphene. This chapter is organized as follows: Section 2 describes both the method and the models to be used in the computation. Section 3 gives a detailed discussion of the results. The last section summarizes our main findings.

2.2 Computational Details and Model Systems

In the present work, three different systems have been modeled: (i) Graphene being modeled by a hexagonal supercell shown in Figure 1b; the basis of which is a triangular lattice shown in Figure 1a. In Figure 1a, the vectors $\overrightarrow{a_1} = \frac{3}{2}\, a\hat{\imath} + \frac{\sqrt{3}}{2}\, a\hat{\jmath}$ and $\overrightarrow{a_2} = \frac{3}{2}\, a\hat{\imath} - \frac{\sqrt{3}}{2}\, a\hat{\jmath}$ are the lattice primitive vectors of pristine graphene structure, with a being the bond length a=1.42 Å (i.e., note that the primitive cell contains 2 basis atoms of coordinates $\overrightarrow{r_1} = a\hat{\imath}$ and $\overrightarrow{r_2} = 2a\hat{\imath}$, respectively; and any other Bravais lattice site can be referred to by a vector $\vec{r} = n_1\, \overrightarrow{a_1} + n_2\, \overrightarrow{a_2}$, where n_1 and n_2 are integers). We use a supercell composed of 6x6 primitive cells, containing 72 carbon atoms (i.e., A= B= $6a\sqrt{3}$ =14.76 Å, whereas the supercell c-axis is kept of size C=20 Å, with a vacuum large enough to ensure the separation of adjacent periodic images of the sheet). In case of graphene, the Brillouin zone (BZ) was sampled using the Monkhorst-Pack (MP) technique [64], with a mesh of 26x26x1 (i.e., 340 k-vectors were selected from within the

irreducible wedge of the BZ and such number of k-vectors is tested to be sufficient to achieve the full convergences of both charge density and density of states "DOS"). (ii) Single-walled armchair CNT (ac-CNT) can be obtained by rolling the graphene sheet along

the x-axis direction (i.e., along$\vec{r} = \overrightarrow{a_1} + \overrightarrow{a_2}$). In our present case, we have rolled the sheet along the vector $\vec{r} = 6\,\overrightarrow{a_1} + 6\,\overrightarrow{a_2}$ then repeated the ring structure for 6 periods along the tube axis (i.e., making an ac-CNT of radius R = 4.07 Å and length L = 14.76 Å; and the ac-CNT contains 144 carbon atoms). The length of the ac-CNT must be the size of the tetragonal supercell, used for computation, to ensure the validity of periodic boundary conditions along the tube. So, we use the tetragonal supercell, shown in Figure 1c, of dimensionalities: A=14.76 Å and B = C= 20 Å; this latter size is much larger than the radius of ac-CNT to ensure the complete isolation from adjacent periodic images of the tube. The sampling of the one-dimensional BZ is performed using MP technique with a mesh of 50x1x1 (i.e., 26 k-vectors were selected from within the irreducible wedge to warrant full convergences of both charge density and DOS). (iii) Single-walled zigzag CNT (zz-CNT) can be obtained by rolling the graphene sheet along either $\overrightarrow{a_1}$ or $\overrightarrow{a_2}$ primitive graphene-lattice vectors. In our present case, we have rolled the graphene sheet along $\vec{r} = 10\,\overrightarrow{a_1}$ then repeated the ring structure for 4 periods along the tube axis (i.e., making zz-CNT of radius R = 3.92 Å and length L = 17.05 Å; containing 160 carbon atoms). Same procedures are taken regarding the supercell size and the BZ sampling as in the case of ac-CNT. The supercell of zz-CNT, which is used in one of our realizations in the present investigation, is shown in Figure 1d.

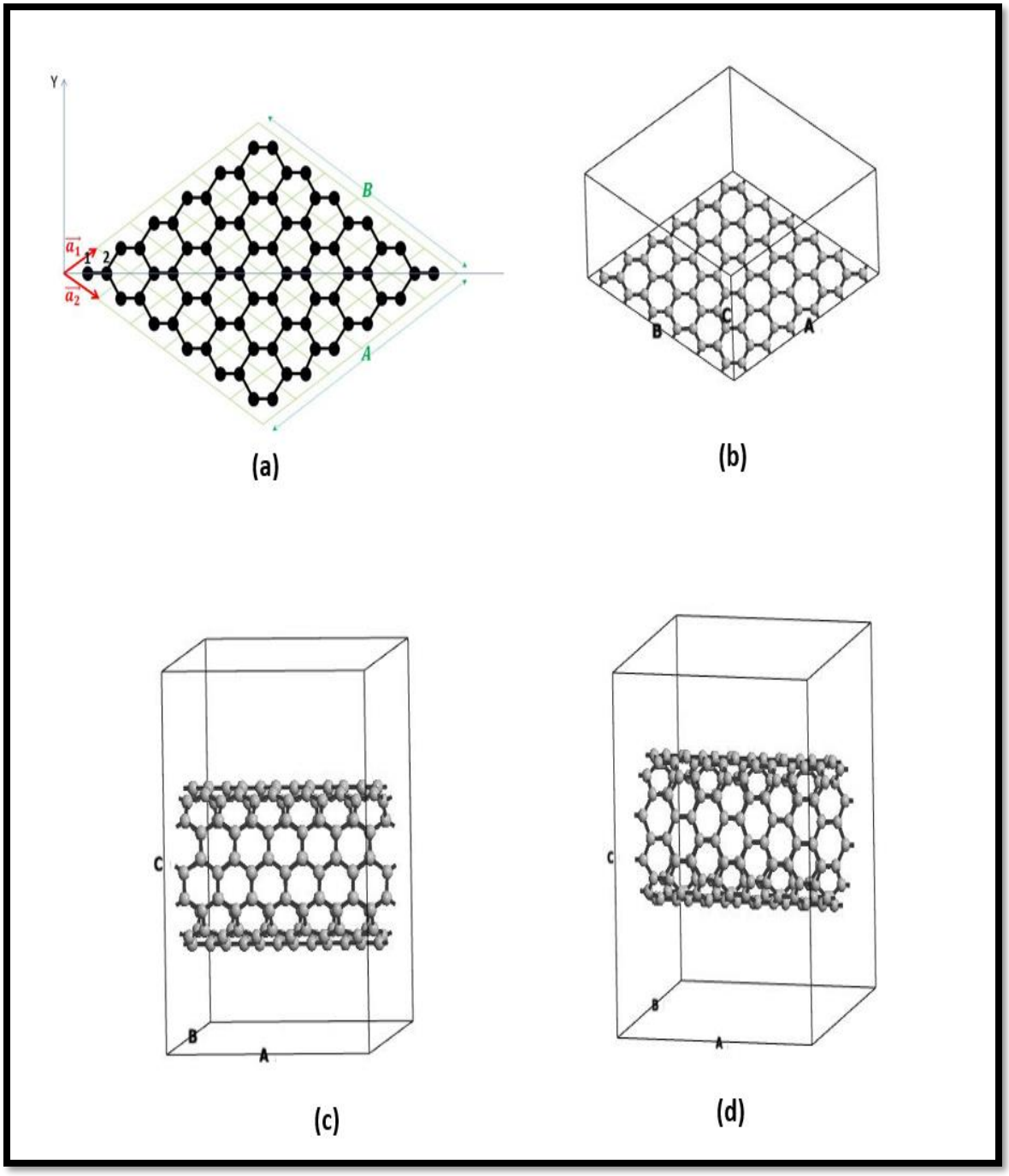

Figure 1: (a) Pristine graphene sheet of size 6x6 primitive cells used in the calculations. The primitive lattice vectors ($\overrightarrow{a_1}$, $\overrightarrow{a_2}$) are shown. (b) Supercell of graphene; (c) Supercell of ac-CNT; and (d) Supercell of zz-CNT.

In our computation, we investigate the adsorption properties of CO_2 molecule (and other molecules are studied for the aim of inspecting the selectivity) on the surfaces of the previously mentioned three systems in presence of Fe catalyst atom(s) in configuration of ad-atom(s). The relaxation processes are carried out mainly using the SCC-DFTB method [34,35], which is implemented in the DFTB+ package. We use Slater-Koster (SK) parameter files [65] from the 'mio-0-1' [66, 67] set to parameterize the inter-atomic interactions of carbon with other organic elements; whereas parameters of Fe's interactions with other elements are taken from the 'trans3d' [68]. van der Waals (vdW) interaction is accounted for by using the Lenard-Jones dispersion model used in DFTB+, with parameters taken from the universal force field (UFF). It is worth to emphasize that DFTB can deal with large systems containing hundreds to few thousands of atoms and efficiently carry out atomic relaxations. On one hand, approximating and parameterizing Fock-Matrix elements, an effective one-electron Kohn-Sham (KS) Hamiltonian is derived from density functional theory (DFT) calculations. On the other hand, DFTB is in close connection to tight-binding method. So, it can be seen as tight-binding method, parameterized from DFT, and this overcomes the problem of parameters' transferability and makes the method more accurate. So, its basis set does not rely on plane-waves or Gaussian functions, but rather is a minimal basis set based on pseudo-atomic orbitals (Slater orbitals and spherical harmonics). Based on this basis set, DFTB gains its speed and ability to deal with large systems. So, in contrast to "full" DFT methods such as quantum Espresso, DFTB can easily handle calculations of large systems with reasonably large MP grid and perform atomic relaxations. Furthermore, DFTB was augmented by a

self-consistency treatment based on atomic charges in the so-called self-consistent charge density-functional tight-binding (SCC-DFTB) method; charge density is expressed in terms of Milliken charges [69]. Because the wave functions in DFTB are well defined as KS-like orbitals, one can easily derive expressions for any property in the same way as within a "full" DFT scheme. This has indeed paved the way for DFTB to extend its domain applications to even comprise biological systems [70]. Its strength stems from the transparent derivation, the inclusion of electron correlation on the DFT-GGA level and the updating parameterization process. This led to a robust method that predicts molecular geometries quite reliably. Among the limitations in DFTB is the availability of Slater-Koster files for all elements in the periodic table and this remains among the main challenges in the next years.

For the purpose of benchmarking the binding energy results, we explore another ab-initio code, which is quantum espresso (QE) package [71]. QE is based on DFT, plane-wave basis sets and pseudopotentials (both norm-conserving and ultra-soft). In our particular study of adsorption of molecules on surfaces, as the charge density is expected to vary rapidly in space, we use a generalized gradient approximation (GGA) of Perdew Burke-Ernzerhof (PBE) parameterized form [72] and the interaction between ionic core and valence electrons is represented using ultra-soft pseudo-potentials[73]. Furthermore, we use Grimme scheme[74] to capture the long-range interactions namely van der Waals (vdW) like. We use plane-wave-basis set with energy cutoffs of 30 Ry and 180 Ry in representing orbital wave-functions and charge density, respectively. For the Brillouin-zone sampling, for instance in the case of sample of graphene, a uniform mesh of 5x5x1

k-points is used, and the occupation numbers of electronic states is smoothened with a smearing width of order kBT (i.e., about 0.04 eV) using Fermi-Dirac distribution function. Regarding the accuracy of the two methods, we carried out a small test of total energy calculations on a pristine graphene sample of size 5x5 primitive cells (i.e., containing 50 carbon atoms) and both DFTB and QE agree within a discrepancy of 10 meV when a relatively large MP mesh of about 12x12x1 is used in QE code.

The atomic relaxed structures are determined via DFTB through the minimization of the total energy until Hellmann-Feynman force on each atom becomes smaller than 0.03 eV/Å in magnitude [75, 76]. The atomic relaxation further comprises the relaxation of supercell lattice primitive vectors in order to release the stress and further minimizes the total energy. The calculation would, at the end, yield both the total energy and Fermi energy of the most stable geometry as well as its related total and partial densities of states.

The binding energy of the Fe ad-atom on the substrate is calculated using the following convention:

$$E_{bind} = E_{(Fe+substrate)} - E_{(substrate)} - E_{(Fe)} \qquad (2.1)$$

where $E_{(Fe+substrate)}$, $E_{(substrate)}$, and $E_{(Fe)}$stand for the total energies of the relaxed Fe ad-atom on the substrate (here the substrate is either graphene or CNT), isolated substrate, and isolated Fe atom, respectively. We also define the adsorption energy of the CO_2 molecule on the adsorbent as follows:

$$E_{ad} = E_{(CO2+substrate)} - E_{(adsorbent)} - E_{(CO2)} \qquad (2.2)$$

Where $E_{(CO2+substrate)}$, $E_{(adsorbent)}$, and $E_{(CO2)}$ stand for the total energies of system of CO_2 molecule and the adsorbent (the adsorbent can be either graphene-Fe composite or CNT-Fe compound), isolated adsorbent, and isolated CO_2 molecule.

In the case of adsorption of several molecules (for instance "N" molecules of CO_2), the average adsorption energy per molecule would be defined as

$$E_{ad}^{avg} = \frac{E_{(CO2+adsorbent)} - E_{(adsorbent)} - N*E_{(CO2)}}{N} \qquad (2.3)$$

The sensitivity of a gas sensor is studied by looking at the variation of the electrical conductance versus gas dose (i.e., conductance versus number of molecules landed on the adsorbent). Appendix-1 shows the derivation of gas sensitivity and how it is related to density of states at Fermi level within the framework of free-electron gas.

Last but not the least, the selectivity is studied by keeping the gas dose constant but varying the gas type. All sensitivities are compared on a unified scale. In the present work, in case of studying the selectivity, we focus on ac-CNT decorated with just one Fe atom and sensitivity tests are carried out versus different gas molecules (namely, CO_2, CO, O_2, N_2, H_2, and H_2O). The results of structural relaxations, electronic structure calculations, and both sensitivity and selectivity will be discussed in the next section.

2.3 Results and Discussion

2.3.1 Atomic Relaxations

The first assessment is of the stability of the Fe atom on both the pristine graphene and CNTs. As initial states, on graphene, an Fe atom was placed above the surface in three different positions within an expected Fe-C bond length and the system was allowed to relax. These three initial positions correspond to: (i) on-site, (ii) bridge-site and (iii) hollow-site positions. It was found that the hollow site position in both graphene as well as CNTs corresponds to the most stable configuration by having the lowest total energy. Specifically, we noticed that the binding energies corresponding to the mentioned three possible configurations of Fe ad-atom are ordered as follows: $\boldsymbol{E_{bind}^{Fe-Onsite} = -1.279\ eV >}$ $\boldsymbol{E_{bind}^{Fe-Onbridge} = -1.314\ eV >\ E_{bind}^{Fe-Onhollow} = -1.412\ eV}$. The Fe on hollow-site is found to be the most stable configuration. Likely, the coordination of Fe and the number of bonds it makes with carbon atoms do matter in its stability on the graphene substrate. In addition to this, the adsorption energies of CO_2 molecule on Fe are also found to be in the same respective ranking. Hence, the results of just the two extreme cases (on-site and on-hollow-site) are selected and displayed in Tables 1 and 2.

Table 1: Comparison of geometrical parameters of four relaxed structures: (i) ac-CNT with 1 Fe (on-site) and 1 CO_2 molecule; (ii) graphene with 1 Fe (on-site) and 1 CO_2 molecule; (iii) ac-CNT with 1 Fe (on hollow site) and 1 CO_2 molecule; and (iv) graphene

with 1 Fe (on hollow site) and 1 CO_2 molecule. Note that in the pictures: C, Fe and O atoms are shown in yellow, red and green colors, respectively.

System	Fe on-site		Fe on hollow site	
	CNT-Fe-CO_2	**G-Fe-CO_2**	**CNT-Fe-CO_2**	**G-Fe-CO_2**
Relaxed Structure	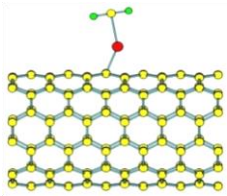		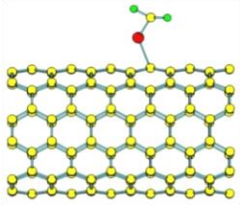	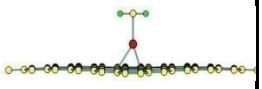
D(Surf-Fe) Å	2.248	2.270	2.240	2.319
D(Fe-CO_2) Å	2.492	2.501	1.857	2.491
D(C=O) Å	1.172	1.172	1.272	1.172
Angle(Surf-Fe-C)	144.8°	178.6°	131.7°	154.5°
Angle(Fe-C-O)	89.2°	88.9°	76.7°& 129.5°	89.3°
Angle(O-C-O)	178.4°	177.7°	153.7°	178.5°

Table 2: Results of relaxations of 1 Fe atom on either on-site or on hollow-site as well as of1 CO_2 molecule on top of Fe ad-atom for: (A) Graphene and (B) ac-CNT

System	On-Site	On hollow site

	G-Fe	G-Fe-CO_2	G-Fe	G-Fe-CO_2
E_{TOT} (eV)	-3413.767	-3644.469	-3413.900	-3644.623
E_F (eV)	-4.254	-4.219	-4.224	-4.195
E_{bind} (eV)	-1.279	-2.075	-1.412	-2.096
N_F (1/eV per Hexagon)	0.4941	0.4738	0.3248	0.2840
Sensitivity (%)	N/A	4.11 %	N/A	12.56 %
Charge of O atom (e units)	N/A	6.328	N/A	6.330

Table 2B

System	On-Site		On hollow site	
	CNT-Fe	CNT-Fe-CO_2	CNT-Fe	CNT-Fe-CO_2
E_{TOT} (eV)	-6777.891	-7008.719	-6778.013	-7009.358
E_F (eV)	-4.367	-4.313	-4.339	-4.503
E_{bind} (eV)	-1.559	-2.200	-1.680	-2.718
N_F (1/eV per Hexagon)	0.2480	0.1764	0.2057	0.1340
Sensitivity (%)	N/A	28.3 %	N/A	34.85 %
Charge of O atom (e units)	N/A	6.3395	N/A	6.3991

In the next step, a CO_2 molecule was placed just nominally above the Fe atom at a distance of about the C-Fe bond length from the Fe atom, after which, a second relaxation process was applied. Tracking the bond lengths and bond angles, the obtained converged configurations for both graphene and CNT clearly show evidence for chemisorption with the geometrical parameters shown in Table-1. The results for Fe positioned on on-site and hollow sites of graphene, as well as ac-CNT, are also shown for comparison. Focusing on the case of hollow sites, it is clear that ac-CNT-Fe compound exhibits stronger chemisorption with the CO_2 molecule than graphene-Fe $_{co}$mposite does. Essentially, the surface-Fe and Fe-CO_2 distances are shorter in the case of CNT-Fe composite than those for graphene-Fe compound. Additionally, in the case of graphene, the CO_2 molecule

possesses C-O bond length 1.17 Å, close to the value for the free molecule; and remains about linear with a bit distorted O-C-O angle of about 179o. On the other hand, the linearity and bond angle are much disturbed in the case of a CO_2 molecule on ac-CNT-Fe, where the C-O bond length (increased to 1.27 Å) became larger than the value for the free molecule; and the bond angle O-C-O decreased to about 154o. Thus, the double bonds O=C and C=O are indeed weakened, as π-bond broke down, paving the way for the molecule to have a stronger coupling/bonding to the Fe ad-atom.

From the point of view of energetics, Tables 2A and 2B correspond to pristine graphene and ac-CNT, respectively. These Tables summarize the results for total energy, Fermi energy, binding energies of Fe on the surface, and CO_2 on Fe, density of states at Fermi level, gas sensing sensitivity, and average electronic charge of oxygen atom. Both Tables 2A and 2B present evidence that Fe on the hollow site is more stable than when it is on-site. Focusing on the hollow site cases, both the binding energy of Fe on the surface and the binding energy of CO_2 on the Fe ad-atom, in the case of ac-CNT, are much stronger than those in the case of graphene; these are consistent with shortening of both surface-Fe and Fe-CO_2 bond lengths, displayed in Table-1. Furthermore, the Fe atom introduces a huge DOS at Fermi level (NF). Still, this NF is more moderate in the case of ac-CNT (i.e., in ac-CNT, the atomic ratio is 1 Fe: 144 C atoms; whereas in graphene the atomic ratio is 1 Fe: 72 C atoms). These characteristics would make NF in the case of ac-CNT to be more sensitive to the landing of CO_2 on Fe than for graphene. In other words, the variation of DOS at Fermi level, before and after the landing of CO_2 on an Fe ad-atom, is considerably larger in the case of ac-CNT than on the case of graphene.

Figure 2 corroborates the observation of DOS at Fermi level. It shows that the shape of the CO_2 molecule deviates from its original linearity when it gets adsorbed on ac-CNT-Fe compound more than when it get adsorbed on graphene-Fe compound. One final remark is that the average charge of the oxygen atom in the case of ac-CNT is also larger than that in the case of graphene, because oxygen is more electronegative than carbon and as the O=C and C=O double bonds weaken (i.e., π-bond breaks down) on ac-CNT, oxygen atoms will get the opportunity to drain more charge and reduce the DOS at Fermi level, consequently causing more surface resistance and higher sensitivity. A rough estimate of sensitivity shows that in ac-CNT-Fe composite, it is about 35 % compared to 12.5 % in case of graphene-Fe compound of similar concentrations. This stimulated us to focus more on CNTs for the remainder of the investigation.

One further use of graphene in this investigation was to assess the effect of metal ad-atom clustering on the sensitivity. To this aim, in our model we have first relaxed the group of 5 Fe atoms on a graphene super-cell of 6x6 primitive cells in three different configurations: (i) linear chain of Fe-atoms; (ii) planar cluster of Fe-atoms and (iii) scattered Fe-atoms. Then, we deposited and relaxed CO_2 molecules on the Fe ad-atoms. We found that the average binding energies, surface-Fe distance, and Fe-CO_2 distance have minimal values in the case of scattered $_{co}$nfiguration of Fe ad-atoms. The sensitivity in the latter configuration is much higher because the Fermi level becomes populated with a lower density of localized states originating from the Fe metal atoms. Based on these findings, we decided to deal with scattered Fe atoms on the CNT surface and study the variation of sensitivity versus gas dose for the ac-CNT-Fe composite.

System	Top view	Side view
(a) CNT-ac + 1 Fe + 1 CO_2		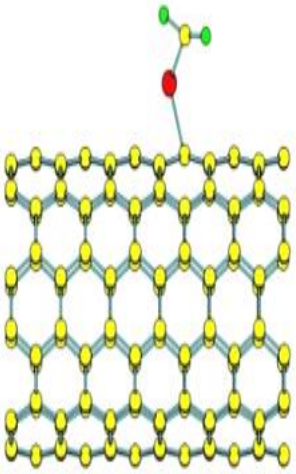
(b) Graphene + 1 Fe + 1 CO_2	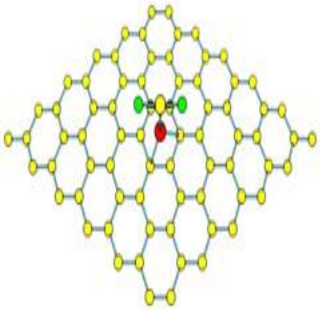	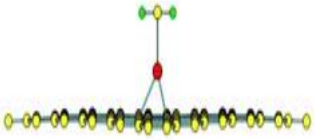

Figure 2: Comparison between relaxed atomic structures of two systems showing the chemisorption of CO_2 on: (a) ac-CNT with 1 Fe ad-atom, and (b) Pristine graphene with 1 Fe ad-atom. Note that in both latter cases Fe ad-atoms are placed on hollow sites. Note that C, Fe and O atoms are shown in yellow, red and green colors, respectively.

To study the sensitivity as a function of CO_2 gas dose, the first step was to relax 5 Fe ad-atoms that were initially scattered on the surface of ac-CNT. Then, we relaxed 5 CO_2 molecules that were originally positioned above the Fe ad-atoms, in a consecutive way, one after the other (making a total of five different samples to be relaxed). Figure 3a shows the relaxed configurations of (ac-CNT + 5 Fe atoms) and Figures 3b and 3c show two among the mentioned 5 samples, which include CO_2 molecules. These latter two samples are: (2b) ac-CNT + 5 Fe + 1 CO_2 and (2c) ac-CNT + 5 Fe + 5 CO_2. Basically, the configuration and geometry of CO_2 are independent of gas dose and remain similar to those in the case of (ac-CNT + 1 Fe + 1 CO_2), shown in Figure 2. However, the increase in the number of CO_2 molecules would allow oxygen to drain more electrons from the Fermi level after the weakening of O=C and C=O bonds (breaking of π-bonds) of the adsorbed CO_2 molecule. The reduction of the DOS at Fermi level with the increasing number of CO_2 molecules would yield more surface resistance and, thus, greater sensitivity due to the enhanced variations in the DOS at Fermi level.

System	Top View	Side View
(a) CNT-ac + 5 Fe	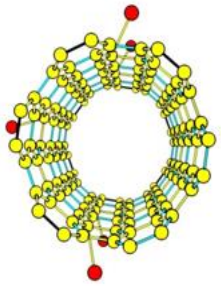	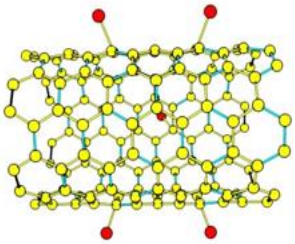
(b) CNT-ac + 5 Fe + 1 CO_2	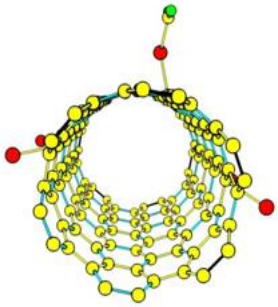	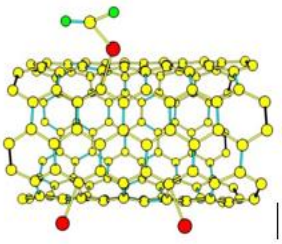
(c) CNT-ac + 5 Fe + 5 CO_2	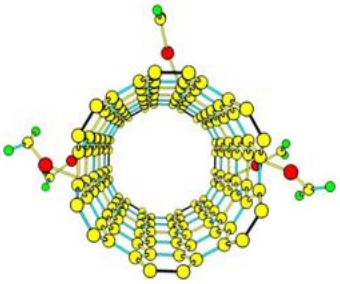	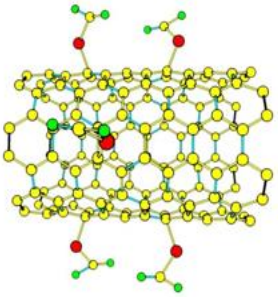

Figure 3: Relaxed atomic structures of ac-CNT with 5 Fe ad-atoms dispersed on its surface before the arrival of CO_2 gas molecules, (b) After chemisorption of 1 CO_2 molecule, and (c) After chemisorption of 5 $CO2$ molecules.

2.3.2 Study of Sensitivity

Figure 4a displays the partial densities of states (PDOS) and the total densities of states (TDOS) of the system composed of ac-CNT (containing 144 carbon atoms), 5 Fe atoms and 1 CO_2 molecule. This latter molecule has been chemisorbed on one of the five iron atoms. PDOS contributions of C, Fe, O atoms are shown in Figure 4a in black, blue, and green curves, respectively. The five metal Fe ad-atoms, in fact, introduce a huge DOS at the Fermi level, as well as spread DOS along the conduction band (i.e., energy range [-1, +8] eV). The DOS of Fe atoms being spread over the conduction band (CB) reveals the formation of bonds with carbon atoms of CNT. Figure 4b shows the TDOS of 6 systems containing zero to five CO_2 molecules, after they have been relaxed on the available five Fe ad-atoms. The energy range [-1.5, 1.5] eV is concentrated around the Fermi level, which is taken to be the common energy reference for all of the 6 composites. Figure 4b shows clearly the decrease of DOS at Fermi level (NF) associated with increasing number of CO_2 molecules getting attached to Fe ad-atoms on the CNT's surface. This reduction of DOS at Fermi level is caused by the effect of chemisorption of CO_2 molecules on Fe atoms, as described in the previous sub-section. The double bonds of O=C and C=O weaken, as π-bonds break down, paving the way to oxygen atoms to drain more charge from the Fe atoms. Furthermore, it was emphasized that the change of DOS at Fermi level due to the landing of CO_2 molecules is also sensitive to the clustering of Fe atoms and their ratio to the total number of carbon atoms in CNT.

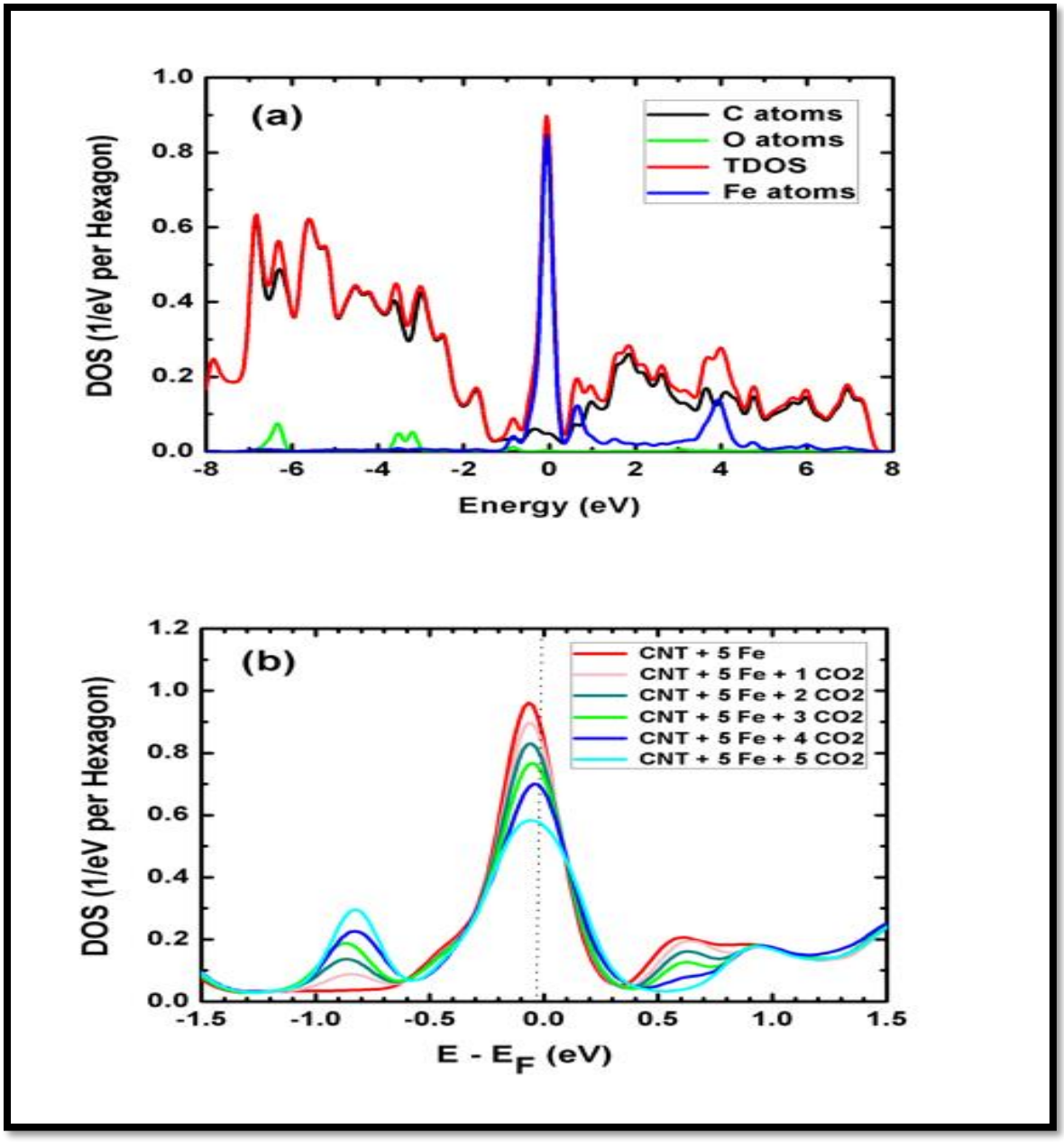

Figure 4: (a) TDOS and PDOS of a relaxed system of ac-CNT with 5 Fe ad-atoms and 1 CO_2 molecule on its surface are shown. (b) TDOS of 6 systems: each consisting of ac-CNT and 5 Fe ad-atoms on its surface as well as CO_2 molecules, the number of which is varied be between 0 and 5. Fermi level is taken as an energy reference in both panels.

Figure 5 summarizes the results of variations of DOS at Fermi level, sensitivity, and average charge of oxygen atom versus the gas dose (with the number of CO_2 molecules varying from 0 to 5). Figure 5a shows a linear decrease of NF against the number of CO_2 molecules. Consequently, the conductance is expected to decrease as the number of CO_2 molecules increases. In addition to this, the sensitivity increases with the increasing CO_2 gas dose, as shown in Figure 5b. Figure 5c corroborates the plot of sensitivity versus gas dose by showing the increase in the average charge of oxygen atoms versus dose. Oxygen atoms are more electronegative than carbon atoms and should drain more charge from the system after the occurrence of chemisorption of various CO_2 molecules on Fe atoms.

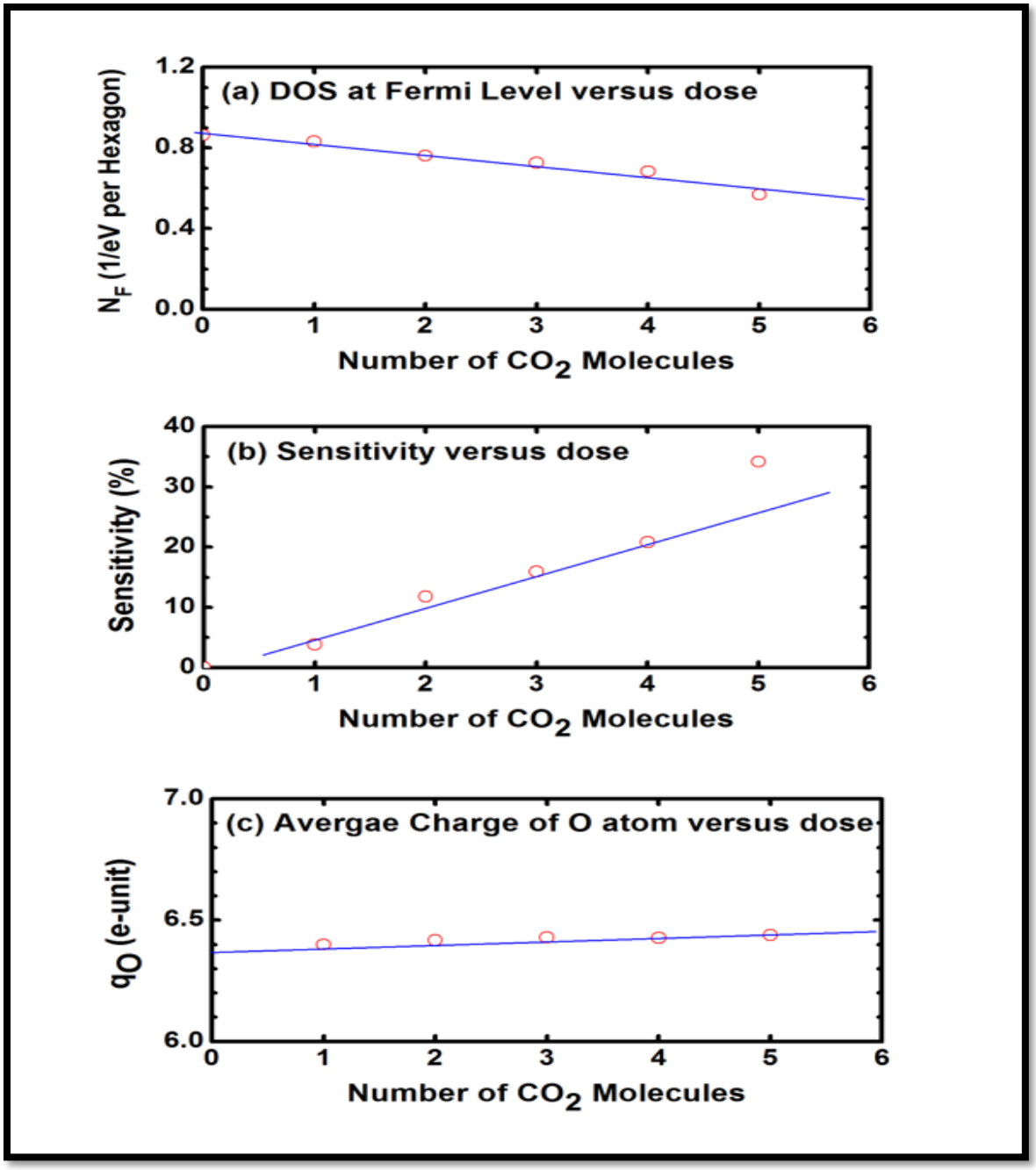

Figure 5: (a) DOS at Fermi level, (b) Sensitivity, and (c) Average charge of O atom versus the number of CO_2 molecules chemisorbed on a surface of the ac-CNT with 5 Fe ad-atoms.

In order to show the evidence of occurrence of both bonding and charge transfer from the adsorbent to the CO_2 molecule. We took the case of graphene-Fe $_{co}$mpound as adsorbent. Figure 6 displays the charge-density plots of the valence-band-edge and conduction-band-edge eigen-states' magnitudes (i.e., so named in chemistry highest-occupied molecular orbital "HOMO" and lowest-occupied molecular orbital "LUMO" states). Both top view and side view are shown. The C, Fe and O atoms are shown in grey, red and green colors, respectively. The HOMO and LUMO eigen-states are shown in blue color. The side view of HOMO state is shown to be delocalized over all sites including all C, Fe and O atoms. This reveals the occurrence of covalent bonding. Whereas, the side view of LUMO state is shown to be distributed over all sites but not the CO_2 molecule. This reveals that the CB-edge has permissible states to accommodate more charge transfers as behaving like the role of a cationic electro-positive element. In brief, the occurrence of bonding of CO_2 molecule with Fe is obviously shown through the HOMO state. Such charge transfer occurring from surface to molecule has also been reported in the Bader analysis reported by Bendavid and Carter [11], where transfer of charge occurs from CuO2 surface to the adsorbed CO_2 molecule, and more efficiently on V_{Cu} site.

2.3.3 Effect of Energy Gap on Sensitivity

We have considered two types of CNTs having two different electrical characteristics; namely: (i) ac-CNT Containing 144 carbon atoms, representing an example of a conducting CNT, and containing a single Fe ad-atom on a hollow site; and (ii) zz-CNT containing 160 carbon atoms of geometry 10x4 avoiding multiples of 3 in circumference, in order to make it a suitable representative of a semiconducting CNT. The calculated

	HOMO state	LUMO state
Top View	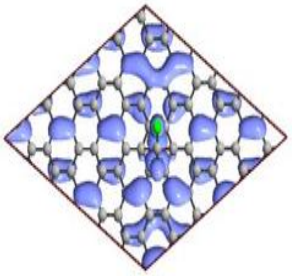	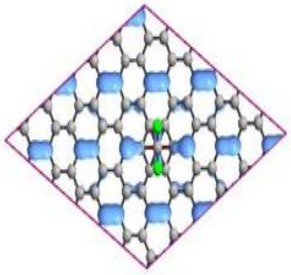
Side View	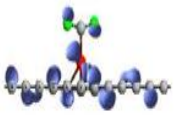	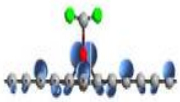

Figure 6: Charge density plots presenting the magnitudes of the HOMO and LUMO states in Graphene-Fe-CO_2 systems. Colors used for: C (grey), Fe (red), and O (green); while the eigen-states are in blue color.

band-gap energy for this latter zz-CNT is found to be 1.143 eV, in the absence of Fe ad-atom. Then, on the top of each Fe ad-atom of CNT, a CO_2 molecule is deposited and relaxed. We quote that in displaying the band structures, the energy reference is taken to be the vacuum level so that one can follow the changes introduced by adding 1 Fe atom on a hollow site of the CNT, and also subsequent changes introduced by adding 1 CO_2 molecule on Fe ad-atom. On the other hand, in DOS plots, the Fermi level is taken as the common energy reference. The order in each panel is performed to correspond to: (1) Pure CNT, (2) CNT with 1 Fe ad-atom after relaxation, and (3) CNT with 1 Fe ad-atom and above it a chemisorbed CO_2 molecule, after relaxation process.

For the ac-CNT, Figure 7a displays the bands along the Γ-X-high symmetry line for three relaxed structures: (a1) pure CNT, (a2) CNT+1Fe, and (a3) CNT+1Fe+1CO_2. Panel (a1) shows two bands crossing at Fermi level to yield a conducting CNT. Panel (a2) shows the shift of Fermi level towards the states introduced by the Fe ad-atom. Many bands above Fermi level originating from the Fe atom apparently lack dispersion (as they correspond to localized states on d orbitals of Fe). Panel (a3) shows the effect of chemisorption of CO_2 on the Fe atom in making some localized d-states coupled to the CO_2 molecule. The corresponding DOS to these three structures is shown in panels b1 to b3, respectively. Panel b1 shows a flat DOS at Fermi level (in the energy range [-1, 1]) revealing the metallic character of this ac-CNT. Panel (b2) shows that the Fe ad-atom introduces a large DOS at Fermi level, of more than 0.20 states/eV per hexagon for each single Fe ad-atom. Panel (b3) shows that the chemisorption of CO_2 molecule reduces the DOS at Fermi level to about 0.13 states/eV per hexagon. Thus, the sensitivity produced is enormous of about 35%.

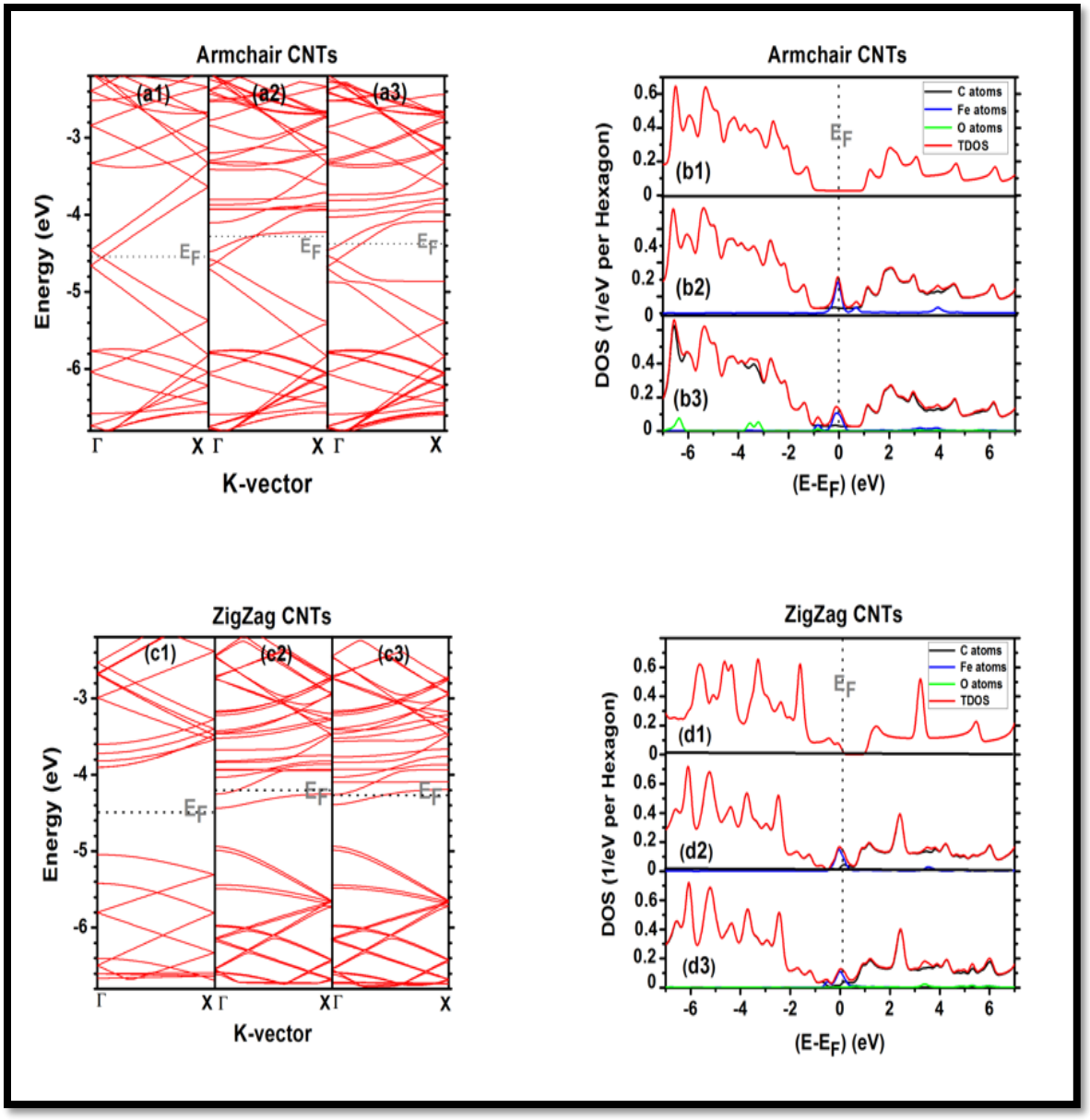

Figure 7: Comparison of band structures and DOS of ac-CNT (containing 144 carbon atoms) and zz-CNT (containing 160 carbon atoms). The numbers associated to letters stand for: (1) pure CNT, (2) CNT with 1 Fe ad-atom, and (3) CNT-Fe compound after chemisorption of 1 CO_2 molecule. In the bands, vacuum level is taken as an energy reference. Whereas, for DOS, either Fermi level (EF) or valence-band edge (EV) is taken as an energy reference. TDOS is normalized to 8 electrons per hexagon in case of pure CNT.

In the case of zz-CNT, Figure 7c displays the bands for three relaxed structures: (c1) pure CNT, (c2) CNT+1Fe, and (c3) CNT+1Fe+1CO_2. Panel (c1) shows an energy bandgap of about 1.143 eV with Fermi level lying in the middle of the gap. Panel (c2) shows that the Fe ad-atom introduces both delocalized states due the bonding with CNT, and localized d-states likely due to dangling bonds. Nevertheless, the Fermi level is shifted to lie on Fe states below the conduction-band edge of zz-CNT. Panel (c3) shows the effect of chemisorption of CO_2 molecule on the Fe ad-atom. The Fermi level continues to lie on Fe states below the conduction-band edge of zz-CNT. Hence, one expects a poor conductivity and consequently less sensitivity. As an overestimation, the sensitivity of zz-CNT would not exceed 22%. As a matter of fact, this latter system does not reach the necessary values of conductivity to validate the Drude formula. Figure 7d shows the DOS corresponding to the three structures of Figure 7c. The Fe ad-atom introduces a large DOS at Fermi level of about 0.16 states/eV per hexagon. The chemisorbed CO_2 molecule on the Fe ad-atom reduces this DOS to become about 0.13 states/eV per hexagon. However, this DOS at Fermi level is due to states, which are still very localized on the Fe atom and should not contribute to conductivity as EF < EC (zz-CNT). This, in turn, will make the sensitivity of zz-CNT much lower than that of ac-CNT. Table 3 summarizes a quantitative comparison of the obtained results between ac-CNT and zz-CNT.

Table 3: Results of relaxation of 1 Fe atom on hollow sites of both zz-CNT and ac-CNT (for sake of comparison), followed by the relaxation of 1 CO_2 on the Fe ad-atom.

System	Zigzag		Armchair	
	CNT-Fe	**CNT-Fe-CO_2**	**CNT-Fe**	**CNT-Fe-CO_2**
E_{TOT} (eV)	-7526.305	-7757.358	-6778.289	-7009.630
E_F (eV)	-4.206	-4.397	-4.344	-4.506
E_{bind} (eV)	-1.511	-2.426	-1.701	-2.714
N_F (1/eV per Hexagon)	0.165	0.130	0.206	0.135
Sensitivity (%)	N/A	22.42 %	N/A	34.64 %
Charge of O atom (e units)	N/A	6.387	N/A	6.399

2.3.4 Study of Selectivity

To study selectivity, we have considered the ac-CNT containing 144 carbon atoms, with one Fe ad-atom relaxed on a hollow site. Following this, we performed relaxations above this Fe ad-atom of various gas molecules (namely: O_2, N_2, H_2, H_2O, CO and CO_2), in addition to the adsorption of CO_2 molecule on graphene-Fe and on zz-CNT-Fe.

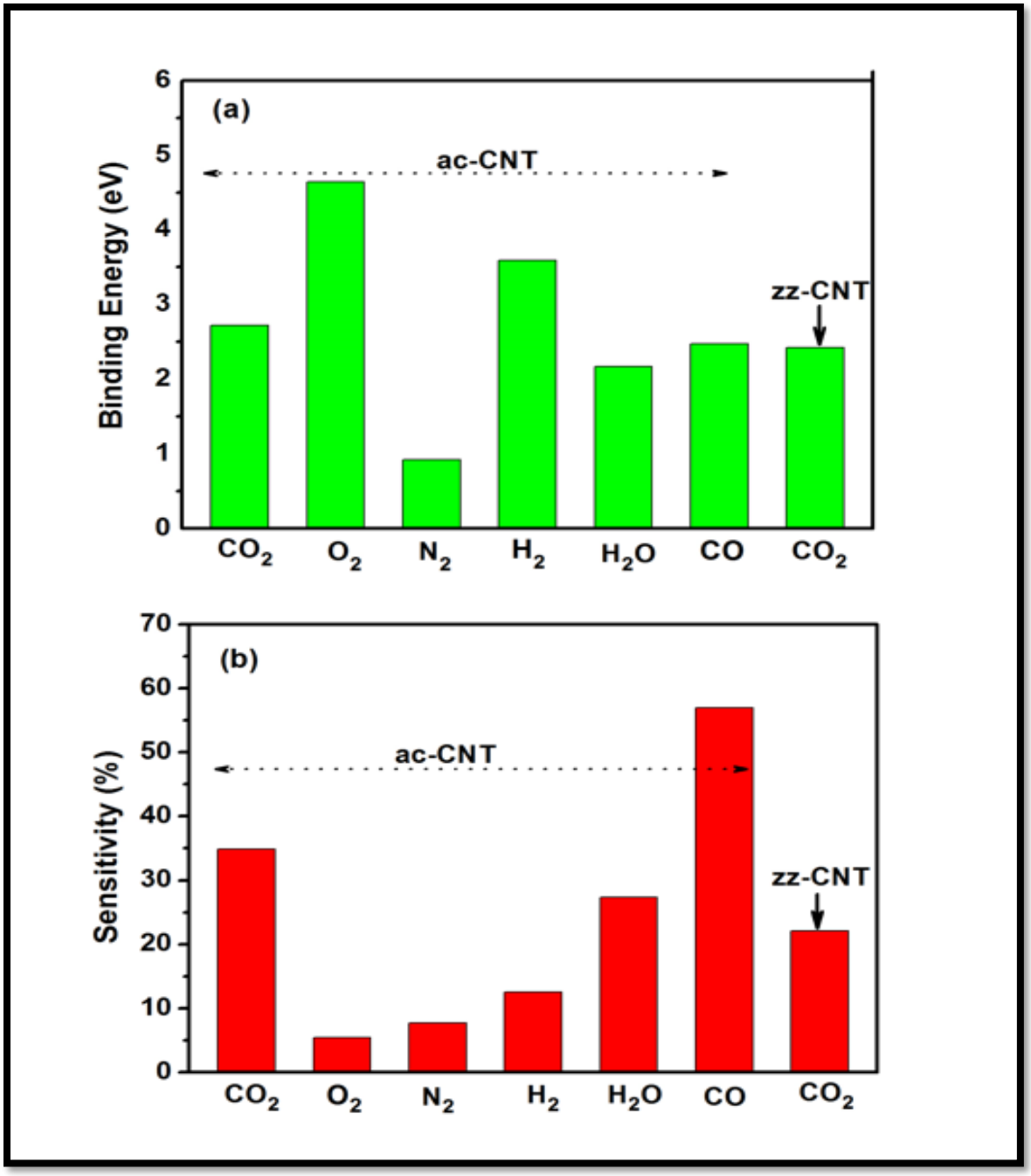

Figure 8: Bar chart of the binding energy in green color (a) of a single gas molecule and the gas sensitivity in red color (b) versus different gases is shown. The adsorbent is ac-CNT with 1 Fe ad-atom.

Figure 8a displays a bar chart of the binding energy of CO_2 and other gases while Figure 8b displays the sensitivity of same gases on CNT-Fe compound. Table 4 summarizes some geometrical parameters of the converged structures. All molecules endure chemisorption processes except N2 which exhibits physisorption. It seems that the triple bond N≡N is so strong and stable that the molecule N_2 does not prefer interacting even with a metal catalyst. At the other extreme, H_2 molecule exhibits chemisorption with dissociation. The Fe atom is able to split H_2 and make two separate Fe-H single bonds. In case of CO chemisorption, the oxygen atom is found to be the one to bond to Fe ad-atom instead of C atom. This is because O atom is more electronegative than C atom. On the other hand, in the chemisorption of CO_2 molecule, this latter breaks its linear shape as C=O bonds get weaker (due break down of π-bonds) in paving the way for the molecule to $_{co}$uple with Fe ad-atom. The fact that this chemisorption occurs without dissociation of molecule would suggest that the recovery process is plausible. Moreover, one should emphasize that the sensitivity in the case of zz-CNT towards detecting CO_2 (values are displayed in Table 4) is overestimated because the studied zz-CNT is a semiconductor and Drude model should not be valid. Yet the sensitivity of zz-CNT remains much lower than the one of ac-CNT. In case of O2 molecule, Fe is able to break one of the O=O double bond (specifically, the π-bond breaks down) and able to make a sigma bond with each of the two oxygen atoms without dissociating the O2 molecule. The last molecule to discuss its chemisorption on ac-CNT is H_2O. The O atom makes a bond with Fe ad-atom while it maintains the other two bonds with its two H atoms. Nonetheless, it seems to have comparable binding energy and sensitivity to those of CO_2. In summary, the ac-CNT decorated with Fe metal catalyst is highly sensitive and selective towards the detection of CO_2, CO and H_2O gases.

Table 4: Results of selectivity analysis of CO_2, O_2, N_2, H_2, H_2O and CO gases are shown. The results include: the Fe-molecule distance, angular distortion of molecule, binding energy of molecule and type of adsorption.

Molecule	D(Fe-Molecule) (Å)	Angle (degrees)	Type of Adsorption	E_{bind} of Molecule (eV)	Comment about Molecule
CO_2	1.857	O-C-O: 153.7°	Chemisorption	-2.718	No split: Fe-C bond is the shortest
O_2	1.938	O-Fe-O: 54.2°	Chemisorption	-4.639	No split: O-Fe-O is isosceles triangle
N_2	2.582	N-Fe-N: 25.2°	Physisorption	-0.923	No Split: both N atoms are equidistant to Fe
H_2	1.531	H-Fe-H: 95.2°	Chemisorption	-3.586	Split
H_2O	1.942	H-O-H: 106.3°	Chemisorption	-2.169	No split: D(Fe-H) = 1.699 Å is the shortest
CO	1.686	O-C-Fe:89.6°	Chemisorption	-2.472	No split: Fe-C bond is the shortest

2.4 Conclusions

The self-consistent-charge density-functional tight-binding (SCC-DFTB) method was employed to study the adsorption properties of CO_2 molecules on both pristine graphene and pure conducting ac-CNT, after being decorated with Fe metal-catalyst atoms. It was found that the catalyst plays a crucial role in inducing and enhancing the interaction to a level of achieving chemisorption state. The results of chemisorption of CO_2 molecule on G-Fe and ac-CNT-Fe compounds can be summarized as follows:

(1) It is recommended to deposit Fe atoms in a scattered manner on the surface of graphene or CNT, since any clustering of Fe atoms yields less binding to the surface and less coupling with CO_2 molecules. Thus, the clustering is found to yield lower sensitivity. The Fe atoms should be scattered and their ratio should be restricted with respect to the total number of existing carbon atoms. The optimum number should not exceed the order of a doping density in semiconductors (i.e., much less than 1% of total number of carbon atoms). Below that limit, Fe will enhance the DOS at Fermi level and lead to considerable reduction of NF by the chemisorption of CO_2 molecules. The reduction of NF will enhance both the surface electrical resistance and sensitivity versus gas dose.

(2) The atomic relaxations demonstrate that the deposition of Fe on hollow site yields the most stable configuration. Additionally, the ac-CNT were found to have sensitivity much higher than those of graphene and zz-CNT. Thus, our study of sensitivity and selectivity was focused only on ac-CNT.

(3) In the study of sensitivity, CO_2 molecules were deposited on ac-CNT-Fe compound one by one (N = 0-5 molecules). NF was found to decrease, resulting in enhancement of resistance and sensitivity. The C=O double bonds were found to partially break down and become weaker and longer than those in free CO_2 molecule. The O-C-O angle was found to decrease to 154o (this angle is likely dependent on curvature). Meanwhile, the average charge of oxygen increases against gas dose, because oxygen has higher electronegativity than carbon and would drain more charge from Fe atom with increasing gas dose.

(4) On the issue of selectivity, ac-CNT-Fe compound was found to be highly sensitive and selective towards three gases (CO, CO_2 and H_2O) to a greater degree than any other gas studied (such as O_2, N_2, H_2). The cost of production of ac-CNT-Fe systems being relatively low, would make them promising candidates for mass production of ac-CNT-Fe based sensors, filters, and storage devices.

CHAPTER 3

CO_2 ADSORPTION ON FE-DOPED GRAPHENE NANORIBBONS

Decoration of graphene with metals and metal-oxides is known to be one of the effective methods to enhance gas sensing and catalytic properties of graphene. We use density functional theory in combination with the nonequilibrium Green's function formalism to study the conductance response of Fe-doped graphene nanoribbons to CO_2 gas adsorption. A single Fe atom is either adsorbed on graphene's surface (aFe-graphene) or it substitutes the carbon atom (sFe-graphene). Metal atom doping reduces the electronic transmission of pristine graphene due to the localization of electronic states near the impurities. The reduction in the transmission is more pronounced in the case of aFegraphene. In addition, the aFe-graphene is found to be less sensitive to the CO_2 molecule attachment as compared to the sFe-graphene system. Pristine graphene is also found to be less sensitive to the molecular adsorption. Since the change in the conductivity is one of the main outputs of sensors, our findings will be useful in developing graphene-based solid-state gas sensors

3.1 Introduction

Due to its unique surface morphology, exceptionally high surface-to-volume ratio, high conductivity and low thermal noise, graphene is known to be a promising material for gas sensing applications [16-18]. Graphene based sensors have advantages over the other solid-state gas sensors in terms of sensitivity, response and recovery time, low power consumption and low cost (see, Refs. [19-22] for reviews). Moreover, they can operate at room temperature and under ambient conditions. In addition, gas sensing and catalytic properties of graphene can be further enhanced by decorating it with metal and metaloxide nanoparticles (see, Ref. [23-25] for review). Metal nanoparticle decoration also increases both sensitivity and selectivity of graphene based sensors for the detection of toxic metal ions [46]. Among the other transition metals [47-49, 77], Fe atoms are also considered to be effective dopants to improve the catalytic and gas sensing properties of graphene [50, 78, 79]. Although, the choice of this non-noble metal as a dopant is mainly motivated by its low cost, Fe atoms can perform as good as noble metal atoms (such as Pt-atoms) in terms of improving the sensitivity of graphene, as was revealed in recent first principles calculations [50, 78]. Since the changes in the resistivity after the gas molecule absorbtion is the main output of solid-state sensors, a fundamental understanding of the electronic transport properties of graphene under these conditions enables the utilization of the full potential of graphene for practical applications.

Here, we use density functional theory (DFT) in combination with the nonequilibrium Green's function formalism to study the electronic transport response of zigzag graphene

nanoribbons [80, 81] doped with Fe atom and its effect on adsorption of a carbon dioxide (CO_2) molecule, which is one of the major greenhouse gases. Capturing, storing and converting CO_2 has become a major problem due to present climate changes[55-59]. We consider two different cases, either the Fe atom substitutes the carbon atom of graphene (sFe-graphene) or it is adsorbed on graphene's surface (aFe-graphene). As a reference, we also study the electronic transport properties of pristine graphene without and with a single adsorbed CO_2 molecule. The main purpose of this study is to fully explore the effect of the CO_2 molecule adsorption on the electronic transport properties of pristine and functionalized graphene. The obtained results are explained in terms of electron localization in the system. The variation of the electrostatic potential is also studied in all cases which is one of the important factors affecting the transport properties of the system. Our findings will be useful to design more sensitive graphene based gas sensors.

3.2 Computational Details

As a typical example, we consider a hydrogen passivated zig-zag graphene nanoribbon of width 11.37 ˚A. A single CO_2 molecule is adsorbed on graphene's surface either directly (Fig. 9(a)) or through Fe atoms (Figs. 9(b, c)). The Fe atom either substitutes one of the carbon atoms (sFe-graphene, Fig. 9(c)) or is adsorbed on the hollow site of graphene (aFe-graphene, Fig. 9(b)). The considered samples are first optimized using DFT within the generalized gradient approximation (GGA) of Perdew-Burke-Ernzerhof (PBE) for the exchange-correlation energy[73]. The Brillouin zone sampling was performed using 1×1×100 Monkhorst k point sampling [64]. The convergence criteria for total energy and

Hellman-Feynman forces were 0.001 eV and 0.01 eV/˚A, respectively. The electrostatic potentials were determined on a real-space grid with a mesh cutoff energy of 148 Ry and double-zeta polarized basis sets of local numerical orbitals were applied to all atoms. Dispersive interactions (i.e. van der Waals interactions) were accounted for by using Grimme's DFT-D2 empirical dispersion correction [74] to the PBE. Optimizations were conducted for the device geometries (see Fig. 9) after the doping. The device structures consist of left and right regions and the central (scattering) region (i.e., a two probe configurations). Both electrodes are modelled as an electron gas with a given chemical potential. The transmission is always along the z-direction. The nonequilibrium Green's function formalism is used to calculate the electronic transport with (1, 1, 100) Brillouin zone sampling. All simulations were obtained using the first-principles computational package Atomistic toolkit[82].

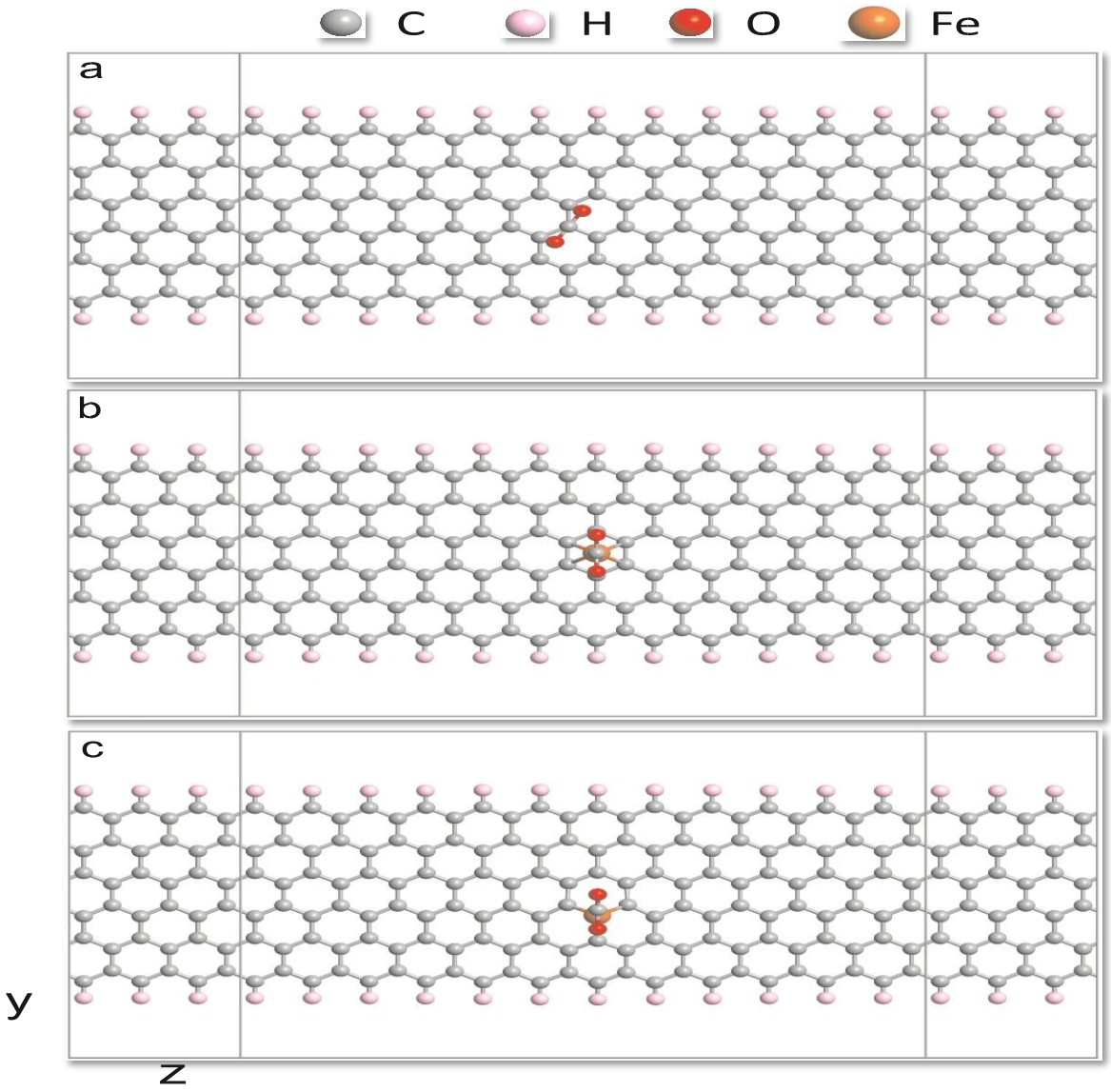

Figure 9: Device geometries: hydrogen passivated graphene nanoribbons with a single CO_2 molecule adsorbed directly (a) or through Fe atoms (b, c). The transmission is calculated along the z-direction and a vacuum space of 20 ˚A is left along the x-direction.

3.3 Results and Discussion

We start by considering the transport response of a pristine graphene nanoribbon to the CO_2 molecule attachment. We terminate the edge carbon atoms by hydrogen atoms to get better structural and electronic stability as compared to bare graphene nanoribbon. In the device geometries (see Fig. 9), the size of the active layer was 29.532 ˚A and the size of the electrodes was 7.383 ˚A. The active region is long enough to study the effect of a single impurity[83, 84]. As a reference, the solid black curve in Fig. 10(a) presents the zero-bias transmission spectrum of pristine graphene nanoribbon without the CO_2 molecule. The transmission curve shows a step-like behavior with an enhanced transmission at the Fermi level, which are typical for graphene nanoribbons. These features originate from the edge-localized electronic states with energies close to the Fermi energy. Interestingly, the CO_2 molecule adsorption has a minor impact on the transmission of the system; it still exhibits a sequence of steps of integer transmission and an enhanced transmission at the Fermi level (dashed red curve in Fig. 10(a)). A small reduction of the electron transmission is obtained only at the Fermi level and at energies -1.5 eV and 1.5 eV, where the T(E) curve exhibits a jump

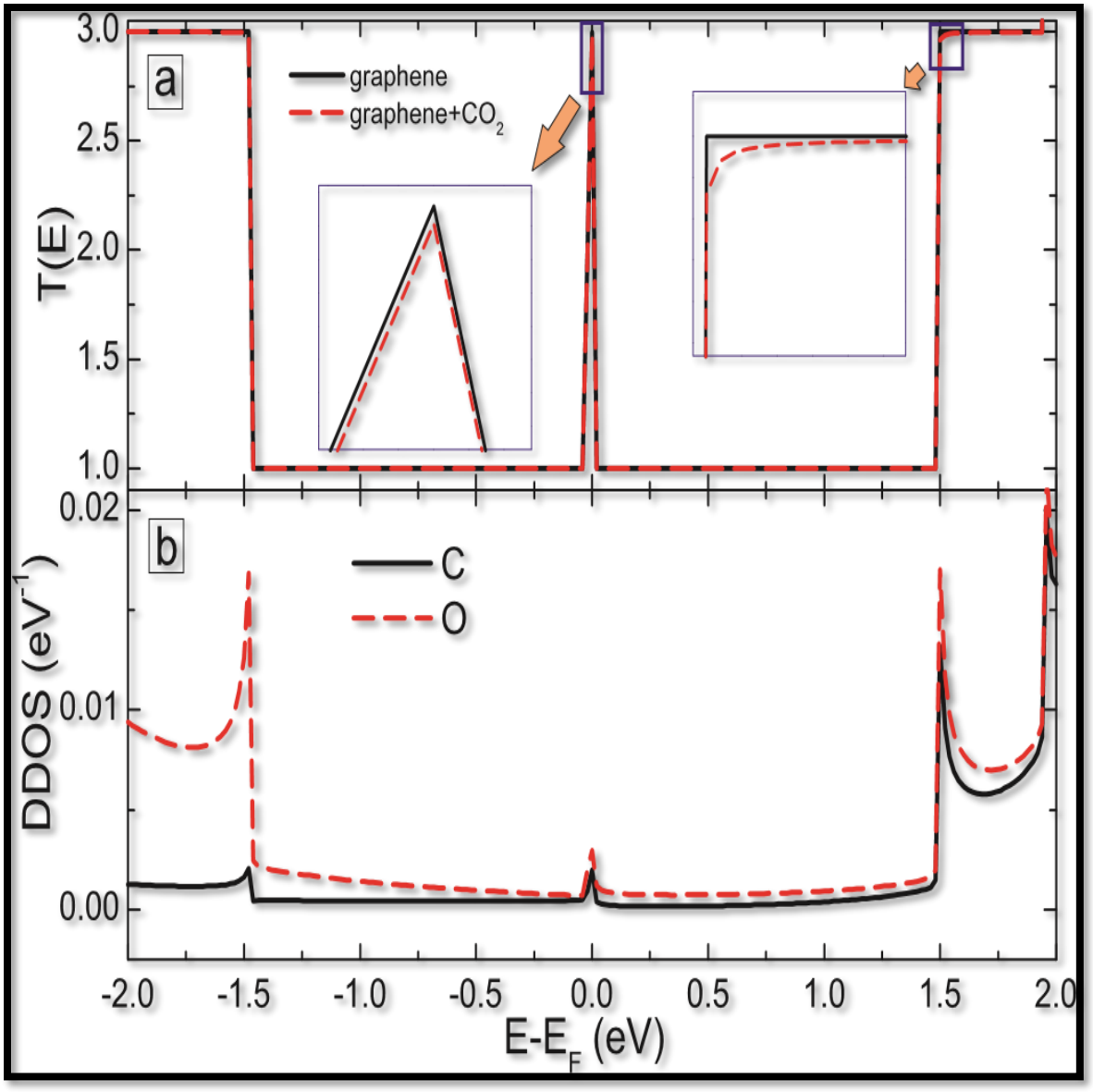

Figure 10: (a) Zero bias transmission spectra (T(E)) of pristine graphene without (solid-black curve) and with a single CO_2 molecule adsorbed (dashed-red curve) as a function of electron energy. Insets show the enlargement of the transmission spectra. (b) Device density of states projected onC atom (solid black curve) and O atoms (dashed-red curve) of the molecule as a function of energy. Energy origin coincides with the Fermi energy.

(see the insets in Fig. 10(a)). Such a negligible transport response of the system to the physical adsorption of the CO_2 molecule can be attributed to the weak interaction between the CO_2 gas molecules and graphene.

Figure 10(b) shows the density of states of the device (DDOS) projected on the C and O atoms of the molecule. It is seen from this figure that despite smaller contribution to the DDOS of the system (in the considered range of the spectrum the maximum DOS is ∼80 eV−1), clear peaks are obtained at the Fermi energy and at the energy values corresponding to the jumps in the transmission. The location of the peaks also corresponds to the reduction in the transmission.

Figure 11(a) shows the zero-bias transmission spectra of aFe-graphene without (solid-black curve) and with the CO_2 molecule attached (dashed-red curve). As in the case of the other transition metals, the Fe-atom is adsorbed on the hollow site of graphene with a Fe-C distance of 2.05 ˚A. The Fe atom locally disturbs the planar lattice structure of graphene. Notice that we have only considered the case when the Fe atom is adsorbed in the middle of the sample. However, the effect of the foreign atom doping on the structural and electronic properties

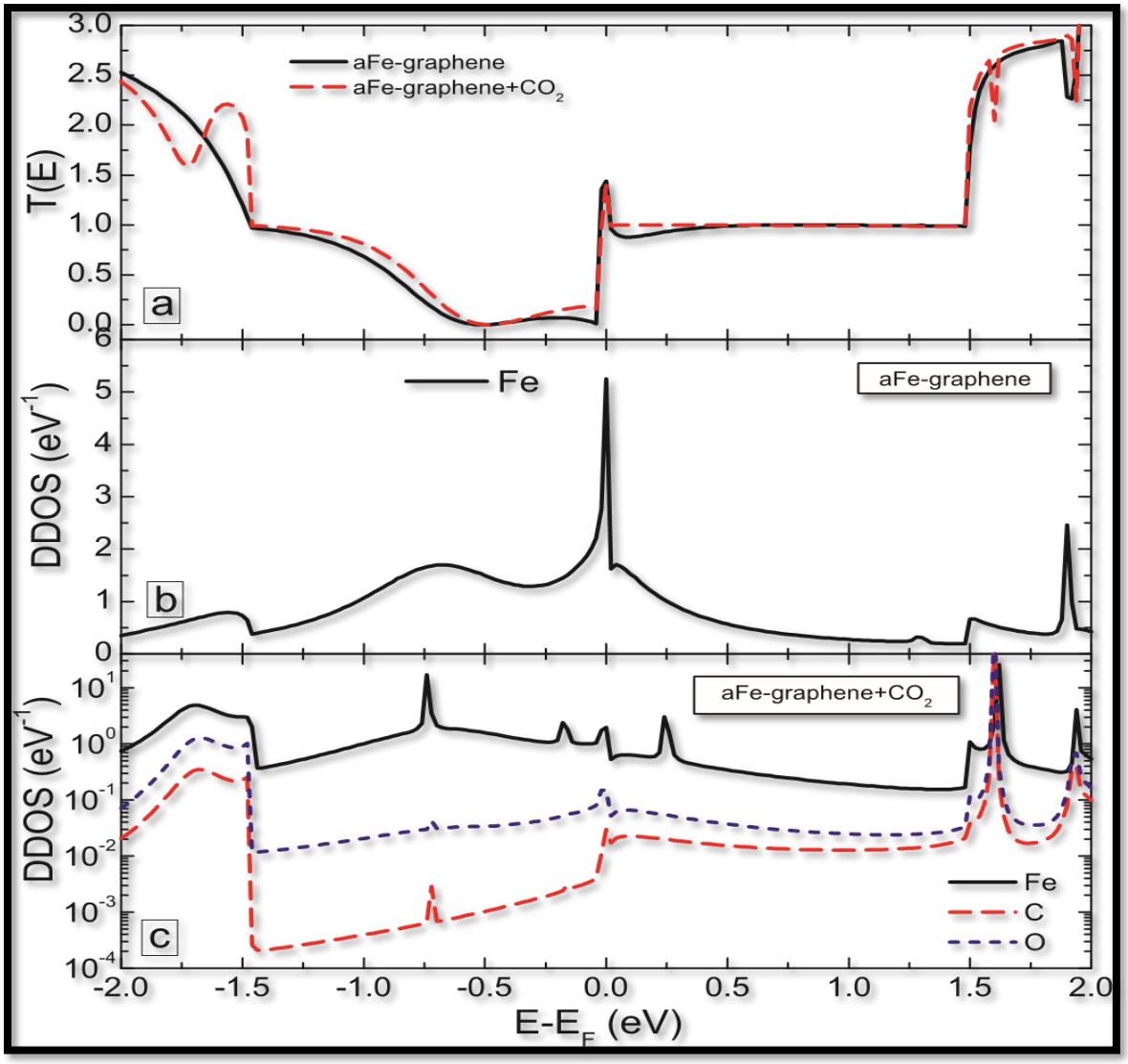

Figure 11: (a) Zero bias transmission spectra of aFe-graphene without (solid-black curve) an with a single CO_2 molecule adsorbed (dashed-red curve) as a function of electron energy. (b) device density of states (DDOS) of aFe-graphene projected on Fe atom. (c) DDOS of aFe-graphene+CO_2 system projected on the Fe atom (solid-black curve), C atom of the molecule (dashed-red curve) and the O atoms of the molecule (dotted-blue curve).

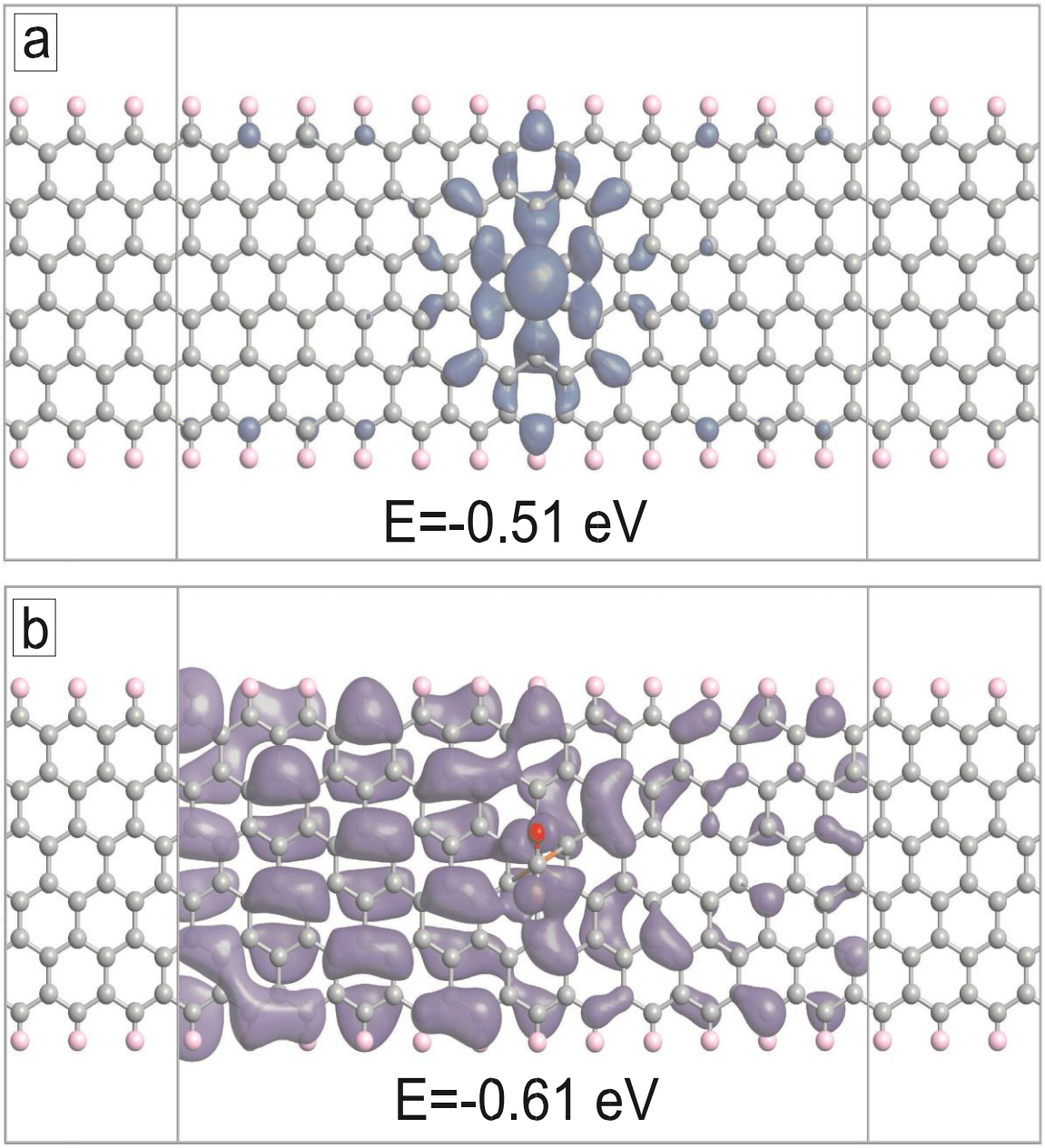

Figure 12: Isosurface plots of the projected self consistent Hamiltonian eigenstates for the aFe-graphene (a) and aFe-graphene+CO_2 (b) systems. The isovalues are 0.005 ˚A−3/2 (a) in both cases. The energies for the corresponding isoplots are given in each panel.

of the graphene strongly depends on the location of the dopants with respect to the edges [84-86]. The transmission spectrum changes drastically when the Fe-atom is present in the

system; the Fe atom adsorption results in considerably reduction of electron transmission as compared to pristine graphene (compare solid black curves in Figs. 10(a) and 3(a)). T(E) becomes smaller at the Fermi level and it drops sharply when decreasing the electron energy below the Fermi energy. In fact, total reflection of the electrons can be obtained at these small energies. As we have discussed above, the minima in the T(E) curves are reflected in the DDOS of the system projected on the Fe atom (see Fig. 11(b)).

In order to get a better insight into the origin of the obtained changes in the transmission spectrum due to the doping, we calculated the projected self-consistent Hamiltonian (PSH) eigenstates. These eigenstates are associated with the poles of the Green's function at the given electron energy. Figure 12(a) shows the PSH eigenstates of the aFe-graphene sample without the CO_2 molecule at the electron energy $E = -0.51$ eV, where we found a profound minima in the transmission spectrum with zero electronic transmission. It is seen from this isosurface plot that the electronic states are localized near the Fe-atom. It is very well known that such nanoscale charge localizations reduce the probability of electrons to transit across the system.

Dashed-red curve in Fig. 11(a) shows the transmission spectrum of aFe-graphene when the CO_2 molecule is attached to the Fe atom (see Fig. 9(b) for the optimized geometry). Interestingly, the gas molecule adsorption slightly increases the transmission spectrum of this hybrid system in the considered range of the spectrum. Extra features (such as local transmission maxima and minima) are also observed in the transmission spectrum due to the contributions of the electronic states of the molecule to the DDOS of the system (dashed-red and dotted-blue curves in Fig. 11(c)). The locations of the maxima of DDOS

of the system projected on the Fe atom also changes due to the gas molecule, indicating the structural changes near the Fe-impurity. The structural analysis show that the Fe-C bond distance now changes between 2.05 ˚A and 2.08 ˚A. However, the system still shows reduced transmission for the electrons as compared to the pristine graphene due to the localization of electronic states (see Fig. 12(b)).

The gas molecule attachment results in the appearance of extra features in the transmission spectrum (see dashed-red curve in Fig. 13(a)). For example, the transmission increases for the electron energies above the Fermi level and it decreases considerably below the Fermi energy. Such a reduction of the electron transmission also originates from the charge localization near the Fe-CO_2 complex. One example of such electron localizations is shown in Fig. 14(b), where we plot the PSH eigenstates of the system at electron energy E = −0.51 eV corresponding to a local minima in the T(E) curve. Note that in this range of the electron energy we obtained extended electronic states for the sFe-graphene without the gas molecule (see Fig. 14(a)), which result in larger transmission. Note also that the contribution of the metal atom orbitals to the DDOS of the system also changes considerably due to the presence of the gas molecule (compare solid-black curves in Figs. 11(b) and 13(b)) due to the local structural changes. Again, all the minima in the T(E) curve are reflected in the projected DDOS as a local maxima.

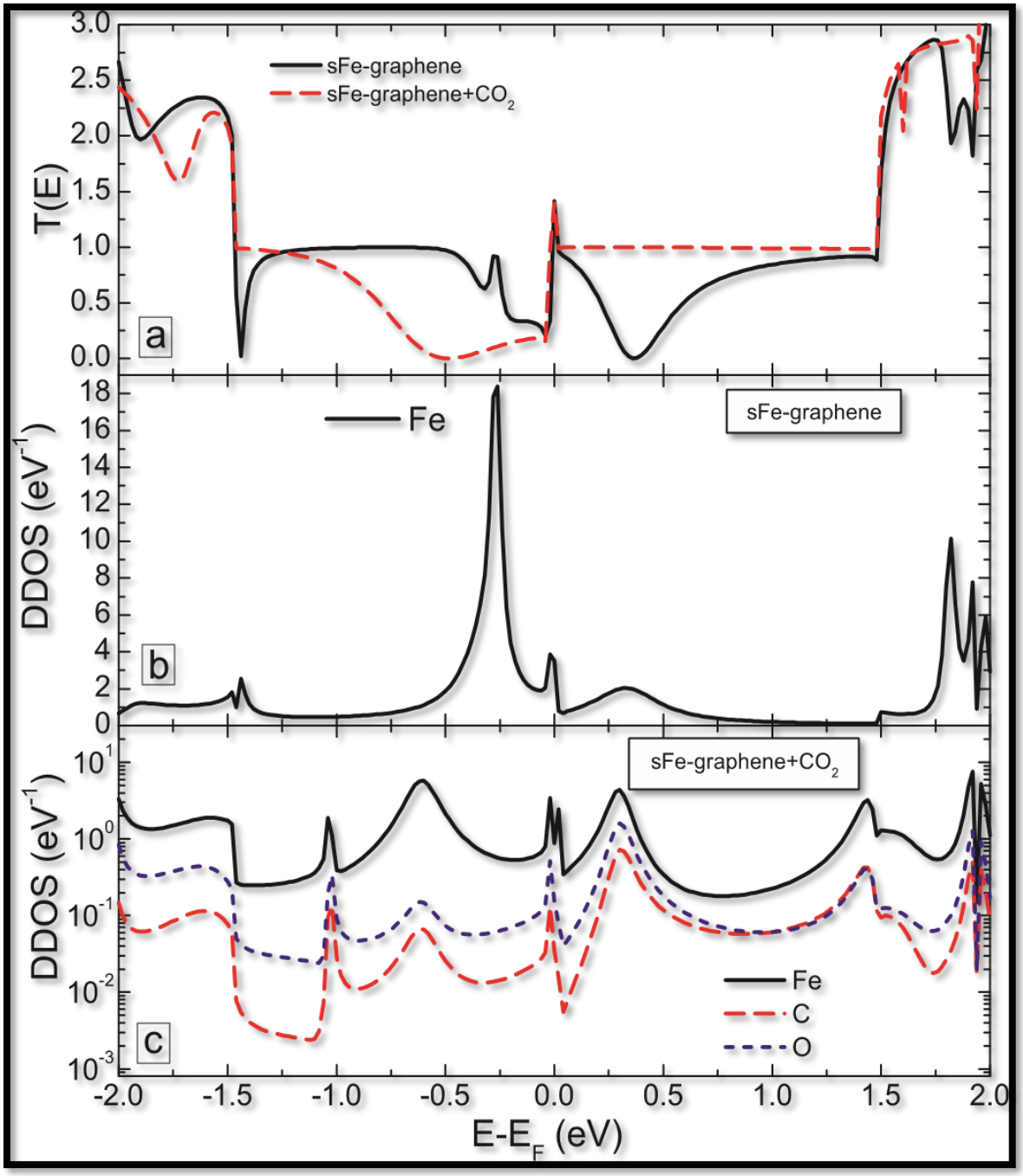

Figure 13: The same as in Fig. 11, but for sFe-graphene system.

Figure 13(a) shows the zero-bias transmission spectra of graphene nanoribbon as a function of electron energy when the Fe atom substitutes a single C atom in the middle of the system

(i.e., the sFe-graphene). The Fe atom is vertically displaced with Fe-C distance of 1.75 ˚A. In the absence of the gas molecule, this sample shows better electronic transport as compared to the aFe-system (compare solid black curves in Figs. 11(a) and 13(a)). We still observe pronounced minima in the transmission spectrum due to the presence of the metal atom. The locations of the transmission minima correspond to the positions of the maxima in the DDOS of the system projected on the Fe-atom (Fig. 13(b)).

Another important factor which influences the charge carrier transport in nanoscale systems is the change in the electrostatic potential profile along the transport direction. In order to see the effect of the metallic dopants and gas molecule adsorption on the electrostatic potential variation, we present in Fig. 15 the averaged electrostatic difference potential along the transport direction.

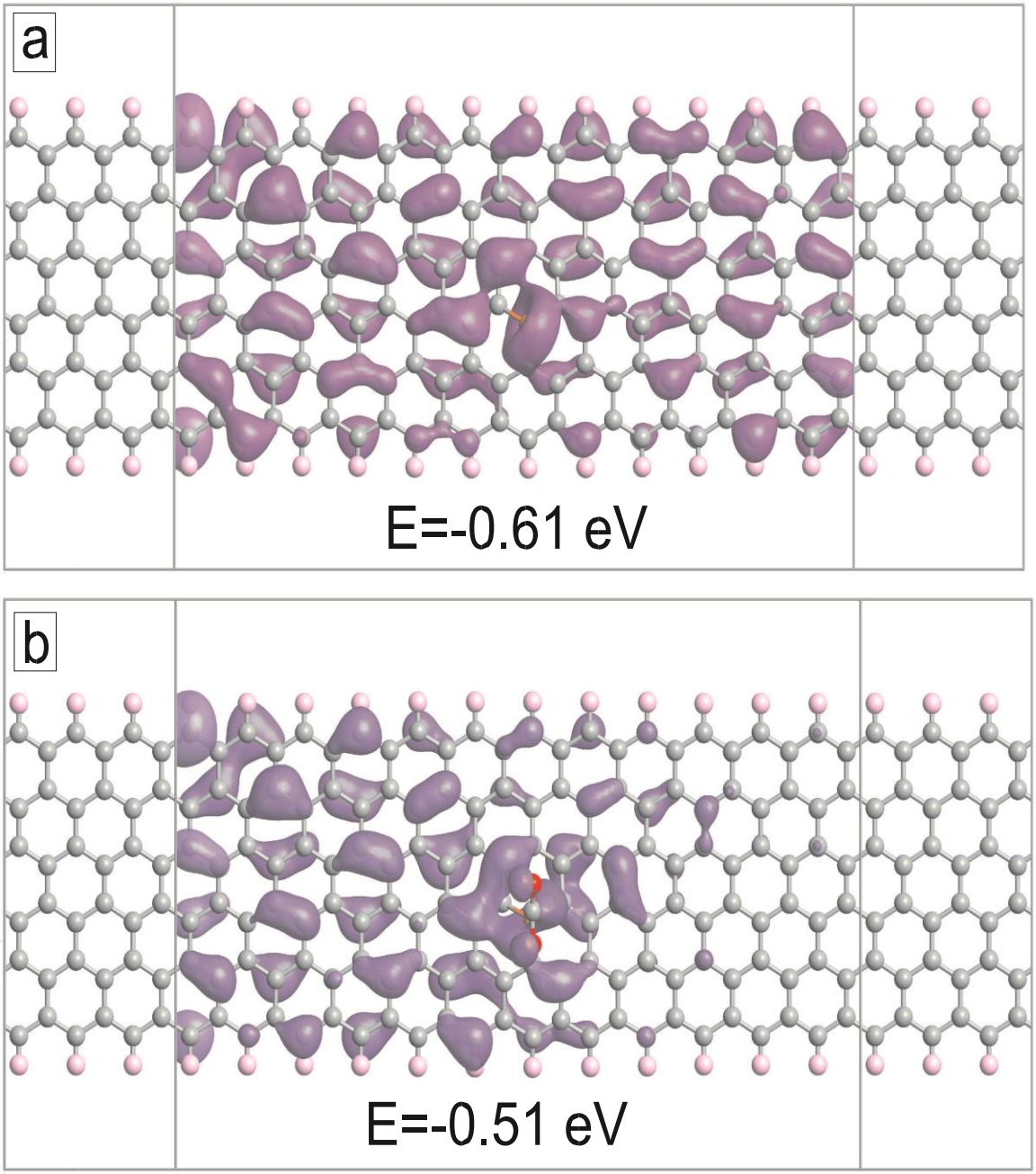

Figure 14: Isosurface plots of the projected self-consistent Hamiltonian eigenstates for the sFe-graphene (a) and sFe-graphene+CO_2 (b) systems. The isovalues are 0.01 ˚A−3/2. The energies of the corresponding isoplots are given in each panel.

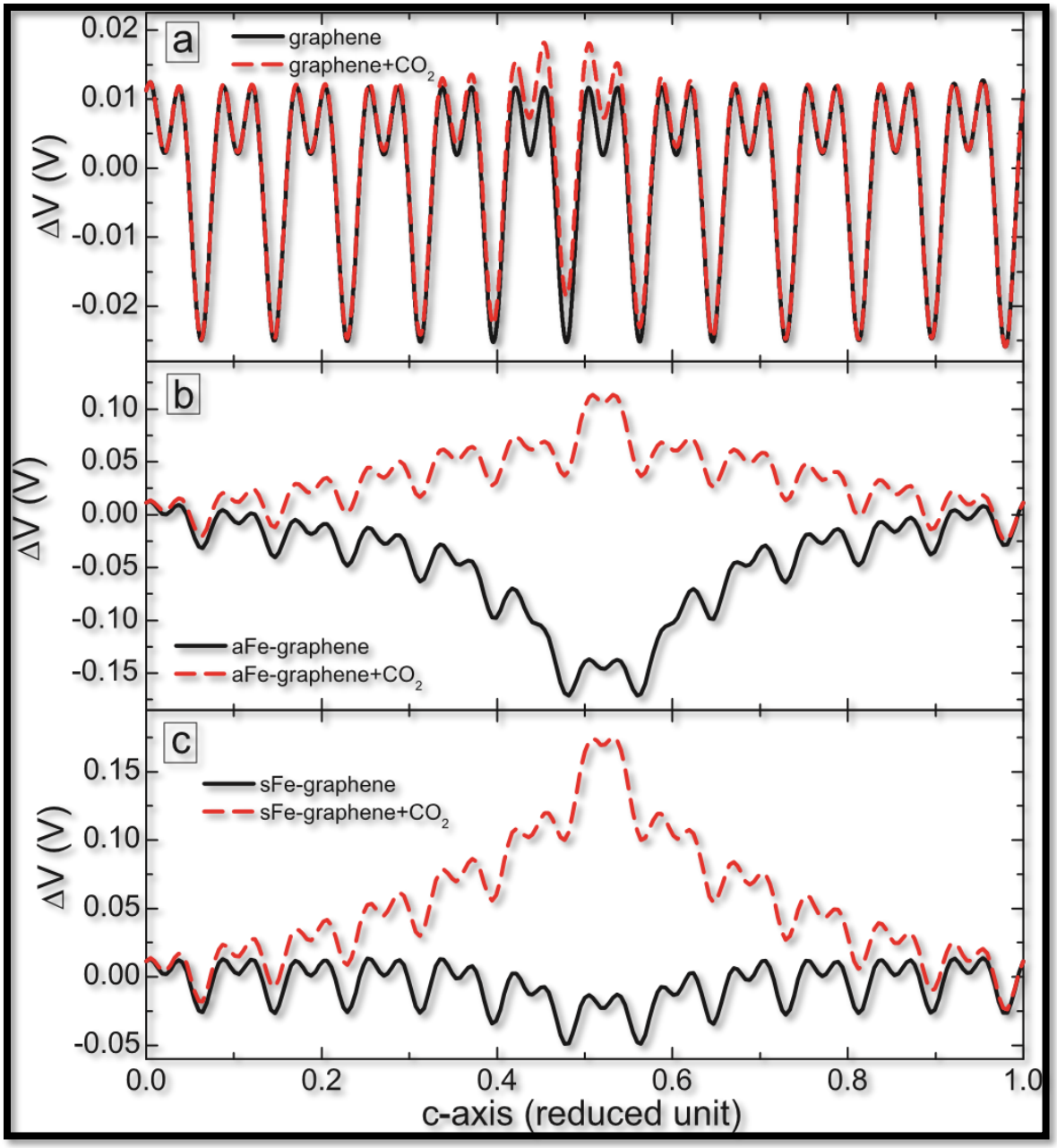

Figure 15: Electrostatic difference potential along the transport direction for zero bias across the samples. The results are shown for pristine graphene (a), aFe-graphene (b) and sFe-graphene (c) without (solid-black curves) and with CO_2 molecule (dashed-red curves).

(c-axis) at zero voltage biasing for pristine graphene (a), aFe-graphene (b) and sFe-graphene(c). The results are presented without (solid-black curves) and with (dashedred curves) the CO_2 molecule. For the pristine graphene we obtained periodic oscillations with double minima in each period (solid-black curve in Fig. 15(a)). The gas molecule adsorption results in small increase in the amplitude of the potential oscillations near the molecule. The electrostatic potential is strongly affected by the Fe atom adsorbed on the hollow site of the graphene (solid black curve in Fig. 15(b)): a potential difference of 0.17 V can be created in the system. Scattering of the electrons from such a large barrier can reduce their transport across the system. The adsorption of the gas molecule on the Fe atom reduces this large potential variation: ΔV reduces to 0.13 V. The potential difference reduces more than 3 times in the case of sFe-graphene sample (solid black curve in Fig. 15(c)). Contrary to the aFe-graphene system, the gas molecule adsorption increases the potential variation in the sFe-graphene sample more than 3 times (dashed-red curve in Fig. 15(c)). These findings also indicate the larger sensitivity of sFe-graphene as compared to aFe-graphene in terms of the change of the electronic transmission.

Finally, we study the effect of finite voltage biasing on the electronic transport in the pristine and doped-graphene nanoribbons. As a typical example, we present in Figure 16 the transmission spectra of all considered samples without (solid black curves) and with a single CO_2 molecule attached for the voltage difference $\Delta V = 0.5$ V. In the case of pristine graphene (solid-black curve in Fig. 16(a)), the voltage biasing results in the appearance of zero transmission area near the Fermi level due to the gap opening. The

CO_2 adsorption results in negligible changes in the transmission spectrum (dashed-red curve in Fig. 16(a)) as in the case of zero biasing. The zero transmission area remains in the case of aFe-graphene (solid-black curve in Fig. 16(b)). Strong reduction of the transmission is obtained away from the Fermi level. As in the case of the zero-voltage biasing, the CO_2 adsorption has minor effect on the transmission spectrum of aFe-graphene (dashed-red curve in Fig. 16(b)). Interestingly, a finite transmission is obtained at the Fermi energy in the case of sFe-graphene (solid-black curve in Fig. 16(c)). Several transmission minima is obtained near the Fermi level, which can also be related to the localization of the electronic states. The system is still sensitive to the CO_2 molecule: extra minima are obtained near the Fermi level together with enhanced transmission for the electron energies away from the Fermi level (see dashed-red curve in Fig. 16(c)).

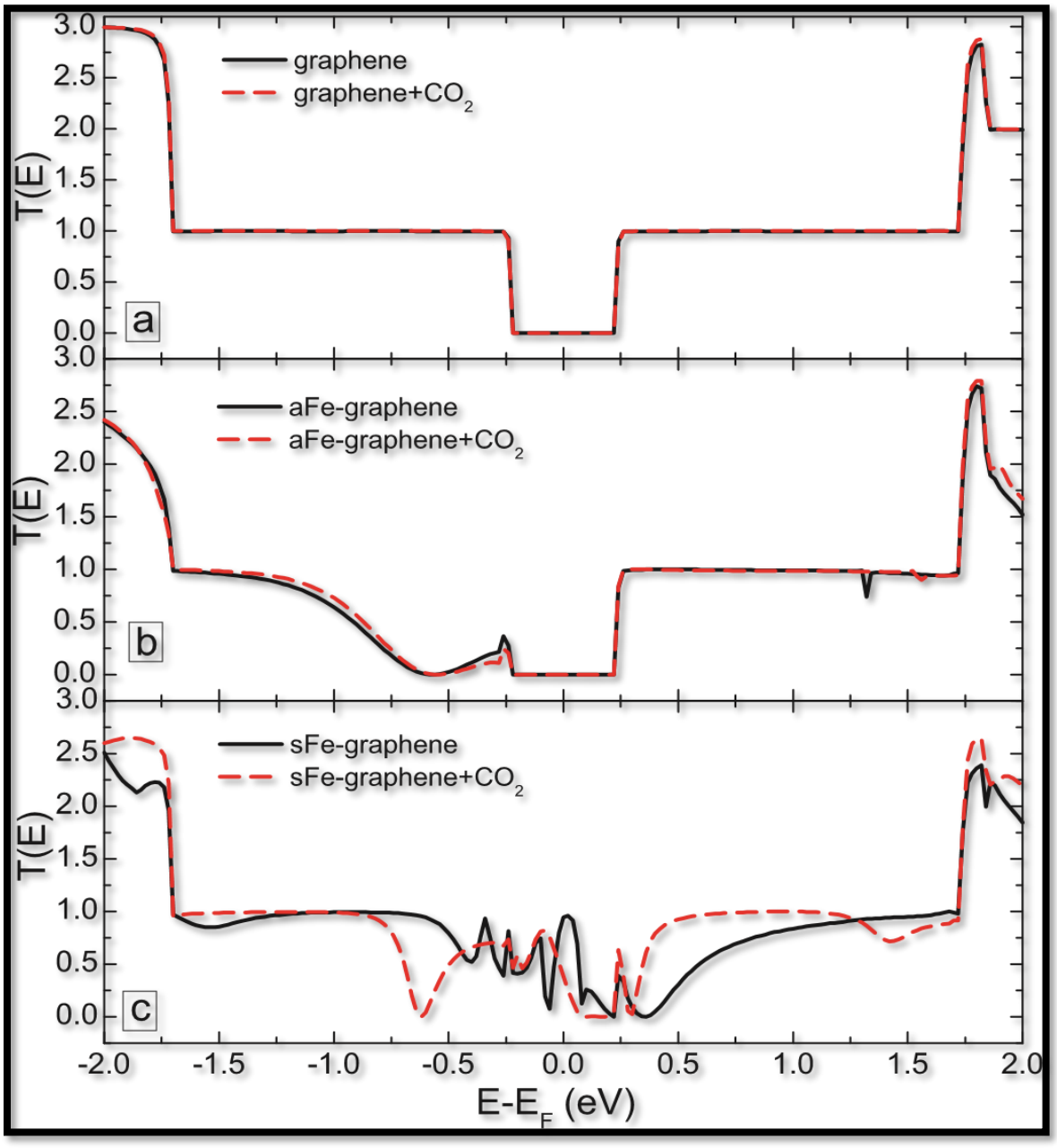

Figure 16: Transmission spectra of graphene (a), aFe-graphene (b) and sFe-graphene (c) without (solid-black curve) and with a single CO_2 molecule adsorbed (dashed-red curve) 0.5 V. for the voltage biasing V=

3.4 Conclusion

Using DFT calculations in combination with the nonequilibrium Green's function formalism we study the electronic transport properties of Fe-doped graphene nanoribbon to explore its properties for CO_2 detection. We found that the electronic transport in such hybrid system strongly depends on how metal atoms are attached to graphene. For example, the sFe-graphene system, where the metal atom replaces one carbon atom, shows better electronic transport as compared to the aFe -graphene sample with the Fe atom adsorbed on the hollow site. The latter system is also less sensitive to the gas molecule adsorption, whereas the transmission of the former sample exhibits extra features due to the CO_2 attachment. The obtained changes in the electronic transmission originate from the nanoscale charge localizations in the system. Our findings indicate the importance of the metal atom attachment for developing graphene-based gas sensors.

CHAPTER 4

ADSORPTION OF H2 ON GRAPHITIC ZNO

The adsorption of H_2 molecules on graphitic ZnO-2d is investigated using the self-consistent-charge density-functional tight-binding (SCC-DFTB) method, in which atomic relaxations are carried out with incorporation of the van de Waals (vdW) interactions but in exclusion of heat effects (i.e., at T = 0 ^{o}K). We focus to inspect the chemical activity of (a) Zn site, (b) O site, (iii) bridge site, (iv) hollow site, and (v) oxygen-vacancy "V_O" site. The results show that the chemisorption can occur only if H_2 molecule lands on the oxygen site. In that case, the H_2 molecules gets dissociated into two separate hydrogen atoms, one bonded to the underneath O atom and the other one bounded to the neighboring Zn atom. Moreover, oxygen vacancies do intentionally exist in real samples as native defects. Our simulations show that the relaxed oxygen vacancy in ZnO-2d would lead to construct an extended defect, formed by a triangle of three Zn atoms surrounded by three pentagon rings of ZnO. Such defect is found to introduce a triplet of donor states and a singlet of acceptor state as well as to shift Fermi level upper than the donor states (i.e., $E_F \geq E_D$). Furthermore, the chemisorption of H_2 on oxygen site yields to formation of one shallow donor state (attributed to O-H bond) and one deep acceptor state (attributed to Zn-H bond). These two scenarios would simultaneously enhance the majority charge carrier density and yield a degenerate n-type ZnO. Because of these reasons, our results show an enhanced conductance and sensitivity versus gas dose, and clearly display the suitability of ZnO for H_2 gas sensing.

4.1 Introduction

Gas detection based on metal-oxide semi$_{co}$nductors has attracted massive research attention in the past two decades. Zinc oxide (ZnO) and tin dioxide (SnO_2) have been widely chosen as sensing materials because of their excellent characteristics such as low cost, high sensitivity, rapid response, and fast recovery [87-89]. In particular, ZnO crystallizes in wurtzite structure having a wide band gap (3.37 eV) with tendency to n-type doping because of native defects of oxygen vacancies and has an exceptionally large exciton-binding energy (60 meV) at room temperature [90]. The breakthrough discovery of achieving p-doping [91] has recently extended the fields of applications of ZnO to comprise: (i) photonics: ZnO has large band-gap suitable for blue and ultraviolet optical devices and became rather a strong competitor to GaN. ZnO has been used in the fabrications of LED [92] and high-efficient dye-sensitized solar-energy cells [93], (ii) electronics: dual-gate ZnO-nanorod-based MOSFET was fabricated [94],(iii) piezoelectrics: having a wurtzite structure, ZnO can easily be functionalized for piezoelectric device applications[95, 96], (iv) photo-catalysis: ZnO is shown to have huge potential activity as a photo-catalyst to induce reactions of water splitting and hydrogen production [97-99] , (v) biomedical: ZnO nano-particles (NPs) have been utilized in medical imaging and therapy. ZnO NPs have recently been favored in especially drug delivery to treat cancer-tumor cells because of their high-luminescence efficiency and least toxicity properties [100-103], and (vi) gas sensing: At all times, ZnO has been a competitor to SnO_2 as a suitable material for sensing hazardous and toxic gases. ZnO has

rather shown some superiority in selective gas sensing; for instance ZnO nanotubes have been shown to reach very high sensitivity toward sensing H_2S with an outstanding resolution at scale of 1 ppb (part per billion) scale at room temperature[104, 105]. It is well known that the exposure to a dose of 10 ppm for 8 hours would endanger the human's life [106]. Then such sensitivity of ZnO-based sensor should be of a great achievement. Furthermore, ZnO has further been used in biosensors to detect glucose [107].

Recently, increasing attention has been paid to the utilization of hydrogen as a renewable and clean energy source because it provides a timely solution to the future supply in addition to other renewable energies [108, 109]. From this perspective, hydrogen detection measurements became an essential step for safety in industrial and household places to alert the formation of potentially explosive mixtures with air[110] . Another significant demand on rapid and accurate sensors able to monitor and control hydrogen concentration is in industrial processes where it is used in synthesis or chemical reactions, as well as for nuclear reaction safety [110]. The main challenges in hydrogen sensor technology are to aim higher sensitivity, higher selectivity, and faster response time. Although the currently existing hydrogen sensors are suitable for many industrial applications [111, 112], some of them are not appropriate for fuel cells, household, biomedical and transportation applications because of their sizes, high-temperature operation, slow response, high cost, and energy input [113]. In this perspective, 1D metal-oxide structures have become promising candidates for hydrogen-sensing applications [114-118]. It is worth emphasizing that operating at high temperatures

should be avoided because the H_2 may burn in air before even reaching the surface of the sensing material if temperatures > 500 ^oC [119]. Thus, for H_2 sensor applications the ZnO nanostructures should demonstrate improved performances, integrated-circuit compatibility, and the ability to work at room temperature.

The conventional gas sensing mechanism is such that upon exposure to the target gas, in case of occurrence of chemisorption, charge transfer occurs between the adsorbed gas species and the surface of semiconducting metal oxides. This charge transfer will either increase or decrease the concentration (or mobility) of the majority charge carriers in the metal oxides, depending on the semiconductor type and gas molecules, thereby increasing or decreasing the electrical conductance of the sensor under operating conditions. Usually, if the metal oxide is an n-type semiconductor (like our case of ZnO), the resistance increases in the presence of oxidizing gases, such as nitrogen monoxide (NO), nitrogen dioxide (NO_2) and ozone (O_3); while the resistance decreases in the case of reducing gases, like carbon monoxide (CO) and methane (CH_4) [120]. On the other hand, the reverse is true for p-type surface. In our present case, we will show that the adsorption of H_2 molecules on n-type ZnO would enhance the conductivity, as H atom plays a role of donor to oxygen atom composing the adsorbent bed.

In the computational side, density functional theory (DFT) has proven itself to be the most reliable method suitable for adsorption and gas-sensing problems. This method has the ability to predict the ground state properties such as atomic relaxation and conductivity, which are the main ingredients of adsorption and gas sensing, respectively

[121, 122]. In the present work, we employ the self-consistent-charge density-functional tight-binding (SCC-DFTB) technique, which uses DFT and has the ability to deal with large systems containing thousands of atoms, and perform accurate atomic relaxation in an efficient way [53, 54]. The aim is also to relax defects like oxygen vacancy, then to relax H_2 molecules on various sites. As output, we calculate the global-minimum total energy and obtain the fully relaxed structures as well as their corresponding band structures and density of states (DOS). From total energy calculations, one can estimate the binding energy of H_2 molecule. On the other hand, from DOS calculations, one can estimate the DOS at Fermi level from which conductance and gas detection sensitivity are evaluated. The model of conductivity assumes a metallic behavior of the sample and this is ensured as degenerate n-type ZnO can be reached through both the existence of oxygen vacancies and the chemisorption of H_2 molecules, simultaneously. This chapter is organized as follows: Section 2 describes the computational method. Section 3 gives a detailed discussion of the results. The last section summarizes the main findings.

4.2 Computational Method

In the present work, we use the self-consistent-charge density-functional tight-binding (SCC-DFTB) method [53, 54], as implemented in the DFTB+ package. This method is used to perform relaxations of atomic structures, including super-cell size in order to release pressure for a further minimization of the total energy. In this method, we use Slater-Koster (SK) parameter files [65] from the ‘znorg-0-1’ [123] set to parameterize the inter-atomic interactions. Van der Waals (vdW) interaction was accounted for by using

the Lenard-Jones dispersion model as in DFTB+ with parameters taken from the universal force field (UFF) [53, 54]. On one hand, approximating and parameterizing Fock-Matrix elements, an effective one-electron Kohn-Sham (KS) Hamiltonian is derived from density-functional theory (DFT) calculations. On the other hand, DFTB is in close connection to tight-binding method. So, it can be seen as tight-binding method, parameterized from DFT, and this overcomes the problem of parameters' transferability and makes the method more accurate. So, its basis set does not rely on plane-waves nor does it on Gaussian functions, but rather is a minimal basis set based on pseudo-atomic orbitals (Slater orbitals and spherical harmonics). Based on this basis set, DFTB gains its speed and ability to deal with large systems. So, in contrast to "full" DFT methods such as quantum Espresso, DFTB can easily handle calculations of large systems with reasonably large Monkhorst-Pack (MP) grid and perform atomic relaxations. Furthermore, DFTB was augmented by a self-consistency treatment based on atomic charges in the so-called self-consistent charge density-functional tight-binding (SCC-DFTB) method; where charge density is expressed in terms of Milliken charges [69]. Because the wave functions in DFTB are well defined as KS-like orbitals, one can easily derive expressions for any property in the same way as within a "full" DFT scheme. This has indeed paved the way for DFTB to extend its domain of applications to even comprise biological systems [70]. Its strength stems from the transparent derivation, the inclusion of electron correlation on the DFT-GGA level and the updating parameterization process. This led to a robust method that predicts molecular geometries quite reliably. Nevertheless, among the existing limitations in DFTB is the incomplete availability of Slater-Koster files for all elements in the periodic table and this fact remains among the main challenges in the next years.

Relaxed structures were determined through minimization of the total energy until Hellmann-Feynman forces on each atom became smaller than 0.03 eV/Å in magnitude. The 2D sheet of ZnO was simulated using a super-cell geometry, with vacuum layer of 20 Å separating adjacent periodic images of the sheet. A supercell size of 6x6x1 unit cells (i.e., containing 72 atoms) is used as it is sufficient to include defects as well as to study the adsorption versus gas dose. The Brillouin zone (BZ) was sampled using the Monkhorst-Pack technique [64], with a mesh of 26x26x1 to comprise 301 k-vectors, selected from within the irreducible wedge of BZ, in sampling the Brillouin zone. This number of k-vectors is indeed sufficient for the full convergence of both density of states and charge density.

The binding energy of a single gas molecule (i.e., the adsorption energy, E_{bind}) is calculated using the following convention:

$$E_{bind} = E_{(molecule+ZnO)} - E_{(ZnO)} - E_{(molecule)} \quad (4.1)$$

where $E_{(molecule+ZnO)}$, $E_{(ZnO)}$, and $E_{(molecule)}$ stand for the total energies of the relaxed molecule on ZnO-2d system, isolated ZnO-2d sheet, and isolated molecule, respectively. In case of adsorption of several molecules (for instance N molecules), the binding energy per molecule would be defined as

$$E_{bind} = \frac{E_{(molecules+ZnO)} - E_{(ZnO)} - NE_{(molecule)}}{N} \quad (4.2)$$

As a matter of fact, the binding energy of molecule on a surface can be taken as a parameter which reveals the type of adsorption taking place between molecule and surface. Specifically, physisorption (i.e., weak van der Walls-like interaction) usually occurs with

$|E_{bind}| < 1.0$ eV, whereas chemisorption often takes place with $|E_{bind}| > 1.0$ eV [124, 125]. The physisorption is always reversible; whereas in the chemisorption the molecule may alter into a chemical reaction of dissociation, that is irreversible or after which the molecule cannot be recovered by any attempt of desorption.

The *sensitivity* of a gas sensor is studied by looking at the variation of the electrical conductance versus gas dose (i.e., variation of conductance versus number of molecules landed on the adsorbent). The conductivity is evaluated based on Drude formula [126, 127], which should be valid for transport in metals:

$$\sigma = \frac{ne^2\tau}{m^*} = ne\mu \tag{4.3}$$

where n is the number density of free electrons, e is the free electron charge, τ is the average collision time, m* is electron's effective mass, and μ is the electron mobility. This formula remains valid in the case of n-type ZnO, especially in case of heavily-degenerate n-type doping. Neglecting the heat effects (at 0 K) and assuming that the mobility of the adsorbent is independent of gas dose, the sensitivity [128-131] then would be proportional to the following quantity:

$$S = \frac{|I_g - I_o|}{I_o} \times 100\% = \frac{|G_g - G_o|}{G_o} \times 100\% \tag{4.4}$$

where the pairs of I_g, I_o and G_g, G_o stand for the electric current intensity and the

conductance in presence and absence of gas adsorption, respectively. Here, we take by assumption the validity of Ohm's law (i.e., $I=GV$, where V is the applied voltage). Under the same assumption, the conductance is related to conductivity by the relation: $G = \frac{1}{R} =$

$\sigma \frac{A}{L}$ and with consideration that the cross-sectional area A and length L of sample to be constant, the sensitivity becomes:

$$S = \frac{|\sigma_g - \sigma_a|}{\sigma_a} \times 100\% = \frac{|n_g - n_a|}{n_a} \times 100\% \quad (4.5)$$

Furthermore, it should be emphasized that the conductivity depends only on the properties of the electrons at the Fermi surface, not on the total number of electrons in the metal. The high conductivity of metals is to be ascribed to the high current, $\mathbf{j_F}=ne\mathbf{v}_F$, carried by the few electrons at the top of the Fermi distribution, rather than to the total density of free electrons (i.e, $\mathbf{v_F}$ is Fermi velocity, and electrons of lower energy than Fermi energy are slowly drifting). Thus, the electrical conductivity gains its main contribution from states near Fermi surface [126, 127]. Assuming that Fermi energy remains the same after the adsorption of a molecule, then the sensitivity might be written as:

$$S = \frac{\left|N_F^{(g)} - N_F^{(a)}\right|}{N_F^{(a)}} \times 100\% \quad (4.6)$$

where $N_F^{(g)}$ and $N_F^{(a)}$ are the density of states (DOS) at Fermi level with and without gas molecule, respectively.

The results of structural relaxations, electronic structure calculations, and both conductivity and *sensitivity* will be discussed in the next section.

4.3 Results and Discussions

4.3.1 Relaxation and Atomic Structures

Figure 17 displays the atomic structures of adsorbent and adsorbate systems after being relaxed by the DFTB+ code. In all our calculations a super-cell containing 6x6 primitive cells (i.e., about 72 atoms) is used to describe the adsorbent bed of ZnO-2d. This supercell is chosen as being the optimum size to host relaxed extended defect (such as case of oxygen vacancy V_O), as well as to carry relaxations of several H_2 molecules in case of studying sensitivity versus gas dose. Furthermore, it is worth noting that a honeycomb supercell consisting of multiples of 3 of primitive cells along both directions would have a Brillouin zone with K-point folded into Γ-point [132], so E_g can be calculated just at center of BZ if need be. In this section, we focus on assessing the chemical activity of various sites of pristine ZnO-2d towards the adsorption of H_2 molecule, namely on: (i) Zn-site, (ii) O-site, (iii) bridge site, and (iv) hollow site. Adsorption of H_2 molecule on defect sites (.e.g., like on the vicinity of oxygen vacancy) will be discussed later below.

	Top-view	Side-view
(a) H_2 on Zn-site	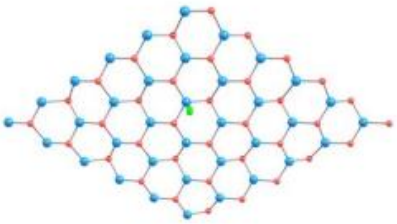	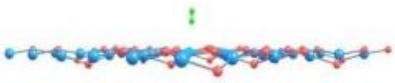 Physisorption
(b) H_2 on O-site	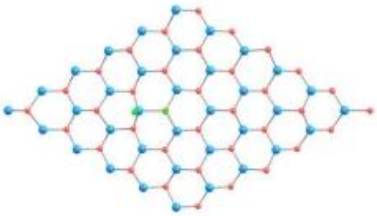	Chemisorption
(c) H_2 on Bridge-site	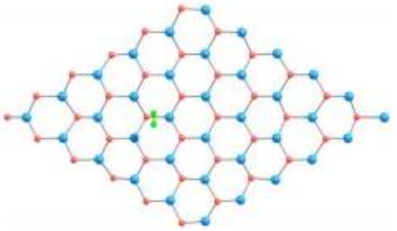	Physisorption
(d) H_2 on Hollow-site	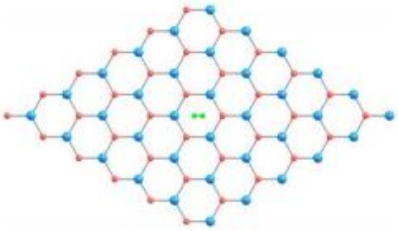	Physisorption

Figure 17: Both top-view and side-view of relaxed atomic structures of H_2 molecule on ZnO-2d starting from putting the H_2 molecule on: (a) Zn-site; (b) O-site; (c) Bridge-site; and (iv) Hollow-site. Only case (b) is found to yield chemisorption.

Table 5 summarizes the results of energetics and geometry of the previously-mentioned four configurations after getting fully relaxed. First of all, the honeycomb pristine ZnO relaxes to have an equilibrium bond length of b = 1.905 Å, which is consistent with the existing value in literature; for instance using DFT in Quantum-Espresso code Topsakal and coworkers [133] reported b = 1.895 Å, which is very close to our value within an error of less than 1%. Concerning the relaxations of H_2 on the proposed four sites, the results showed that all of them yielded physisorption except in case of relaxing H_2 on O-site, which generated a chemisorption. The O-site appeared to be the most chemically active and even more active than the vicinity of oxygen vacancy (V_O), on which the H_2 relaxation produced a physisorption (see more details below).

Table 5 : Summary of energetics and geometry results of relaxations of H_2 molecule on: (i) Zn-site; (ii) O-site; (iii) Bridge-site; and (iv) Hollow-site. Both EF and Ebind are in eV-units; whereas the Zn-H and O-H distances are in Å-units.

System	E_F (eV)	E_{bind} (eV)	D_{Zn-H} (Å)	D_{O-H} (Å)	Type of Adsorption
H_2 on Zn-site	-0.244	-0.331	2.386,3.128	----	Physisorption
H_2 on O-site	-0.363	-0.606	1.804	0.986	Chemisorption
H_2 on Bridge-site	-0.251	-0.337	2.665	3.041	Physisorption
H_2 on Hollow-site	-0.101	-0.065	2.761	2.647	Physisorption

Figure 17 shows that all adsorption processes to be associated with buckling of ZnO-sheet except in case of relaxing H_2 on a hollow site. Results are summarized in Table-1 and can be described as follows: (i) The relaxation of H_2 on Zn-site yielded a physisorption with a binding energy E_{bind} = -0.331 eV and the H_2 molecule hanging up the ZnO-2d sheet by a distance of about 2.386 Å and 3.128 Å from Zn to both sides of H_2 molecule; (ii) The relaxation of H_2 on O-side yielded a chemisorption, as an exceptional case, with a binding energy E_{bind} = -0.606 eV which included the dissociation of the molecule into two hydrogen atoms bonded to O-atom and Zn-atom neighboring the O-site responsible for the dissociation. The bond lengths of these latter single bonds are b(O-H) = 0.986 Å and b(Zn-H) = 1.804 Å, respectively. One should further emphasize that the binding energy includes the dissociation energy of H_2 molecule (which is about 4.52 eV per bond [134]); (iii) The relaxation of H_2 on bridge site led to a physisorption with a binding energy a bit better than the case of Zn-site (i.e., E_{bind} = -0.337 eV) accompanied with similar buckling of the adsorbent surface. The H_2 molecule hangs up within a distances of D(Zn-H)= 2.665 Å and D(O-H) = 3.041 Å. Nevertheless, H_2 molecule being in midway between Zn-O seems to be more stable than being above Zn-site; (iv) The relaxation of H_2 on the hollow site yielded the weakest physisorption with a binding energy E_{bind} = - 0.065 eV. The effects of such weak van der Waals like interaction is revealed not only through the weak binding energy but also through the large distances D(Zn-H) = 2.761 Å and D(O-H) = 2.647 Å and the complete absence of buckling in the ZnO-sheet.

4.3.2 Density of States

Among the important output results of the relaxation is the electronic density of states (DOS). Such calculation requires the inclusion of 301 k-vectors from within the irreducible wedge of BZ. We made sure that further increase of k-vectors would not change the DOS profile as a signature of achieving the full convergence. Figure 18 takes Fermi level as an energy reference and shows the results of DOS of: (a) pristine ZnO-sheet containing 72 atoms (36-Zn and 36-O atoms). It is worth emphasizing that using DFTB+ with the currently-available SK_files of reference [123] would yield reliable atomic structure but with an over-estimated band-gap energy (i.e., Eg = about 5.814 eV). Thus, one should keep in mind to apply a renormalization of the relative energies with a ratio of about 3.3/5.814 = 0.568. This looks kind of weird but normally DFT underestimate band gaps by an order of magnitude whereas DFTB+ does the opposite; it overestimate the band gap by about an order of magnitude. (b) H_2 molecule showing two states (i.e., bonding and anti-bonding states of about ± 8.0 eV around Fermi level). (c) H_2 chemisorbed on ZnO-2d after a start being on O-site. The chemisorption is associated with a dissociation of the H_2 molecule to form O-H and Zn-H single bonds. These latter single bonds are represented by a donor "E_D" and acceptor "E_A" states in the gap, respectively. Such behavior occurred because of the orders in electronegativity values which are as follows [135]: $\chi(Zn) = 1.6 < \chi(H) = 2.1 < \chi(O) = 3.5$ in units of Pauling. Based on these electronegativity values, one can expect that: (i) H-atom can attract the electron more than Zn-atom does in the Zn-H single bond, so that H-atom plays the role of an acceptor and would yield "E_A" state in the gap; whereas

(ii) O-atom can attract the electron more than H-atom does in the O-H single bond, so that H-atom plays the role of a donor and would yield "E_D" state in the gap.

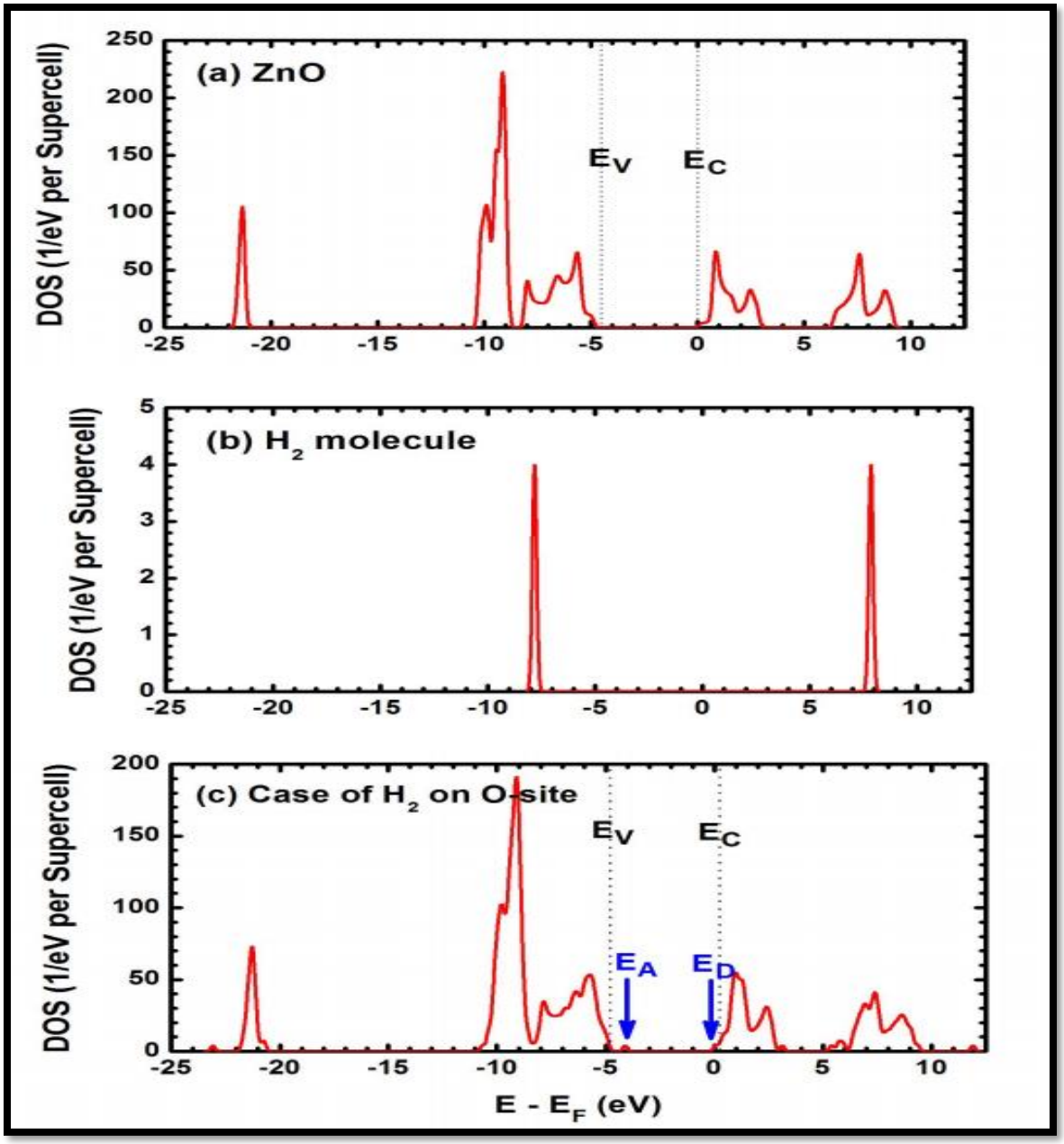

Figure 18: Density of electronic states of relaxed: (a) pristine ZnO containing 6x6 primitive cells (72 atoms); (b) isolated H_2 molecule; and (c) H_2 molecule chemisorbed on ZnO associated with its dissociation and the formation of Zn-H and O-H single bonds. These latter two bonds form acceptor and donor states, respectively. Fermi level is taken as an energy reference.

4.3.3 Simulation of Gas Sensing

Traditionally, gas sensing is based on measurements of conductance before the exposure of the sample (or adsorbent) to the target gas and after. The response function (named sensitivity) is proportional the normalized variation of conductance. Definitely, in absence of chemisorption no variation in conductance should be expected. In our current case of study, a gas sensing of H_2 on ZnO-2d should be expected as there exists at least one case of occurrence of chemisorption, which is the one of adsorption of H_2 on O-site. For this reason, we have considered the relaxations of N = 1-4 H_2 molecules on scattered O-sites and assessed their possible effects on the density of states at Fermi level (N_F) and the sensitivity, thereafter. Figure 19 shows the relaxed atomic structures of N = 1-4 H_2 molecules on pristine ZnO-2d starting from putting H_2 molecule(s) on O-site(s). Both top-view and side-view are shown for each relaxed configuration. The H_2 molecules are shown to exhibit chemisorption processes with dissociation of H_2 molecules; where each H_2 molecule split to form Zn-H and O-H single bonds. Our simulation of relaxation also included the supercell primitive vectors (i.e., relaxation of supercell's size to reduce the pressure and consequently minimize further the total energy) and yielded the shown structures in Figure-19. All structures are shown to exhibit buckling.

	Top-view	Side-view
(a) 1 H_2 on O-site	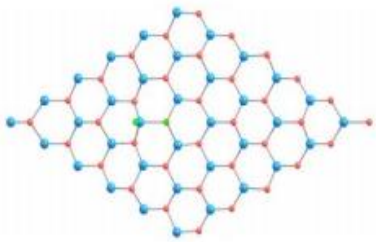	
(b) 2 H_2 on O-sites	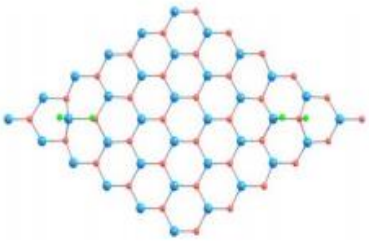	
(c) 3 H_2 on O-sites	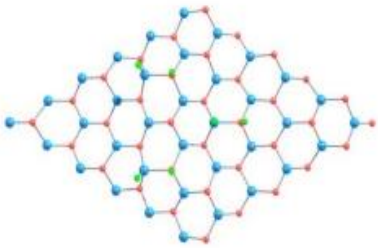	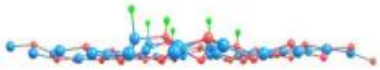
(d) 4 H_2 on O-sites	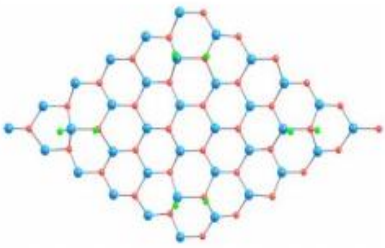	

Figure 19: Relaxed structures of H_2 molecule(s) on ZnO, starting from on O-sites and leading to chemisorption versus gas dose (i.e., versus N = 1-4 molecules).

Figure 20 shows the DOS of the four relaxed structures of (a) 1 H_2 molecule; (b) 2 H_2 molecules; (c) 3 H_2 molecules ; and (d) 4 H_2 molecules after being chemisorbed on ZnO-2d. As we mentioned in Figure-18, the chemisorption of each H_2 molecule is associated with a dissociation of the molecule into two separate H-atoms which make Zn-H and O-H single bonds. These two bonds form E_A and E_D states in the gap, respectively. Consequently, Fermi level shifts upper than E_D (i.e., $E_F \geq E_D$). As the number of H_2 molecules increases, the DOSs at energies E_A, E_D and E_F increase (see Table-6).

Table 6: Density of states at Fermi level (NF) and the response-function (i.e., gas sensitivity) are shown versus gas dose (i.e., N = 1-4 molecules).

Number of H_2 molecules	**E_F (eV)**	**E_{bind} (eV) per molecule**	**N_F (1/eV per Supercell)**	**Relative Sensitivity (%)**
1	-0.363	-0.606	3.37	Reference
2	-0.441	-0.853	83.31	23.72
3	-0.690	-0.731	163.72	47.58
4	-0.597	-0.775	243.21	71.17

Figure 20e and Table-6 summarize the variations of both DOS at Fermi level (N_F) and the response function (or named “sensitivity”). It should be emphasized that in evaluating the sensitivity, one needs a reference for the N_F before the exposure of the sample to the target gas. We have considered the case of 1 H_2-chemisorbed to ZnO as that reference. In real life, ZnO behaves as n-type and oxygen vacancies inevitably exist in ZnO samples.

So, one could take the case of V_O as a reference for N_F. In any case, based on our assumption, the sensitivity is shown to vary linearly with gas dose (i.e., with the number of H_2 molecule chemisorbed on ZnO-2d). Such behavior confirms that ZnO defected with V_O would be a good gas sensor of H_2.

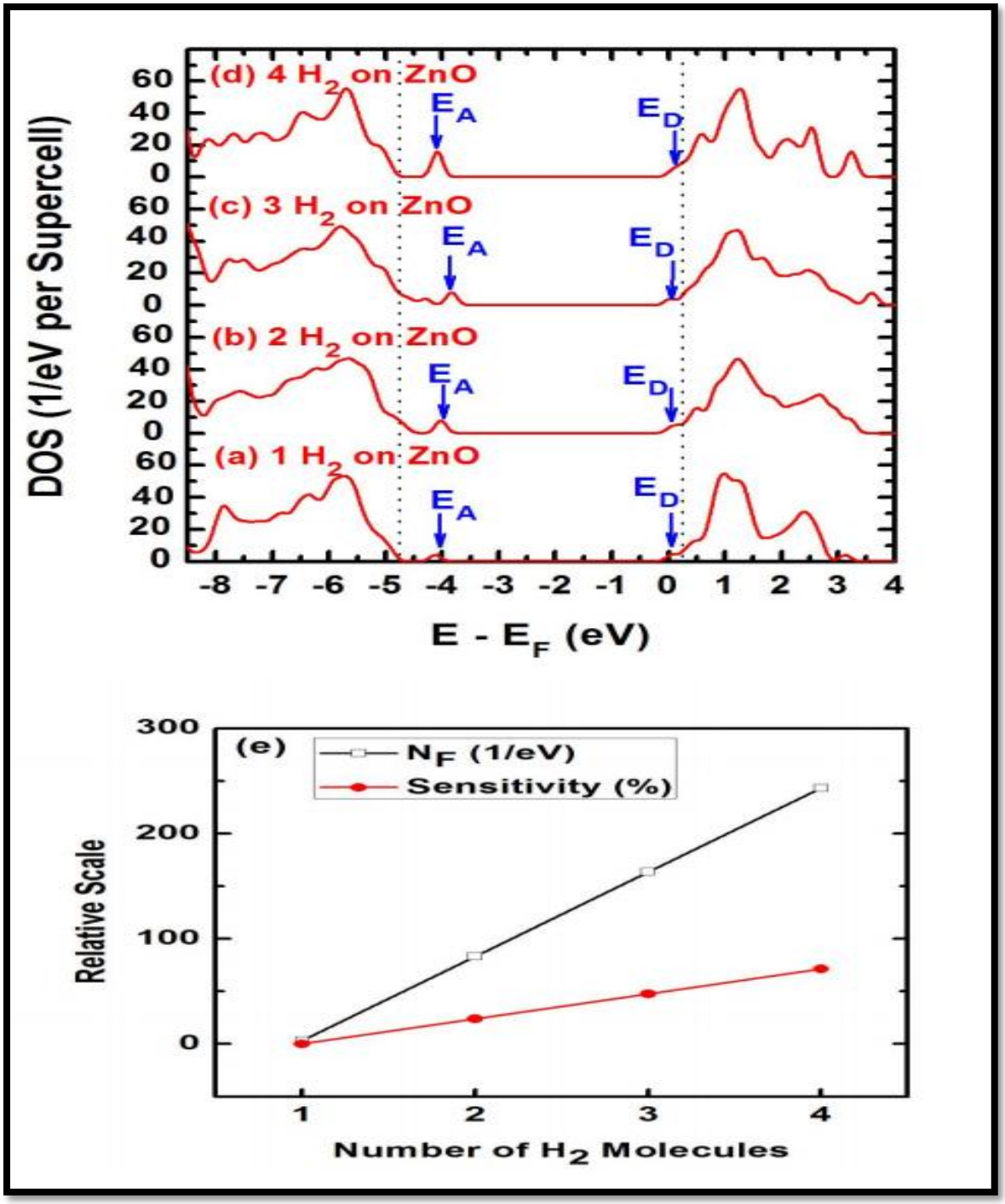

Figure 20: (a-d) DOS of relaxed structures of Figure 19. Fermi level is taken as an energy reference. (e) The DOS at Fermi level and sensitivity are shown versus number of H_2 molecules (i.e., versus gas dose).

4.3.4 Defected ZnO

Among the defects and perhaps the most abundant and important one is the oxygen vacancy. Here, we considered the case of single oxygen vacancy and performed atomic relaxation using DFTB+ code. (a) The result of atomic structure, without H_2 molecule, is shown in Figure 21a. It seems that the relaxed structure remains to be 2 dimensional and does not contain any buckling; meanwhile it includes a formation of an extended defect composed of a triangle of three Zn-atoms surrounded by three pentagon rings of ZnO. As shown DOS of Figure 21c, such extended defect forms 1 acceptor state at about ($E_A - E_V$) $\approx$ 0.225 eV and 3 donor states: 2 degenerate E_{D1} states below one single state E_{D2} by about 0.238 eV, and this latter state is below the conduction band by about (E_C-E_{D2}) $\approx$ 0.751 eV. Of course, these values are over-estimated using DFTB+ code and in real life they should be much smaller or renormalized. (b) The relaxation of one H_2 molecule on the extended defect (i.e., on the reconstructed oxygen vacancy) has predicted the occurrence of a physisorption, in which H_2 molecule hangs upper the triangle of Zn-atoms by distances: D(Zn-H) = 2.834 Å, 2.834 Å, and 2.420 Å. Actually the polarity of the new surface, after the formation of extended defect, would induce a dipole moment into H_2 molecule. Such a weak van-der-Waals interaction has a minor effect of the DOS as can been in Figure 21c.

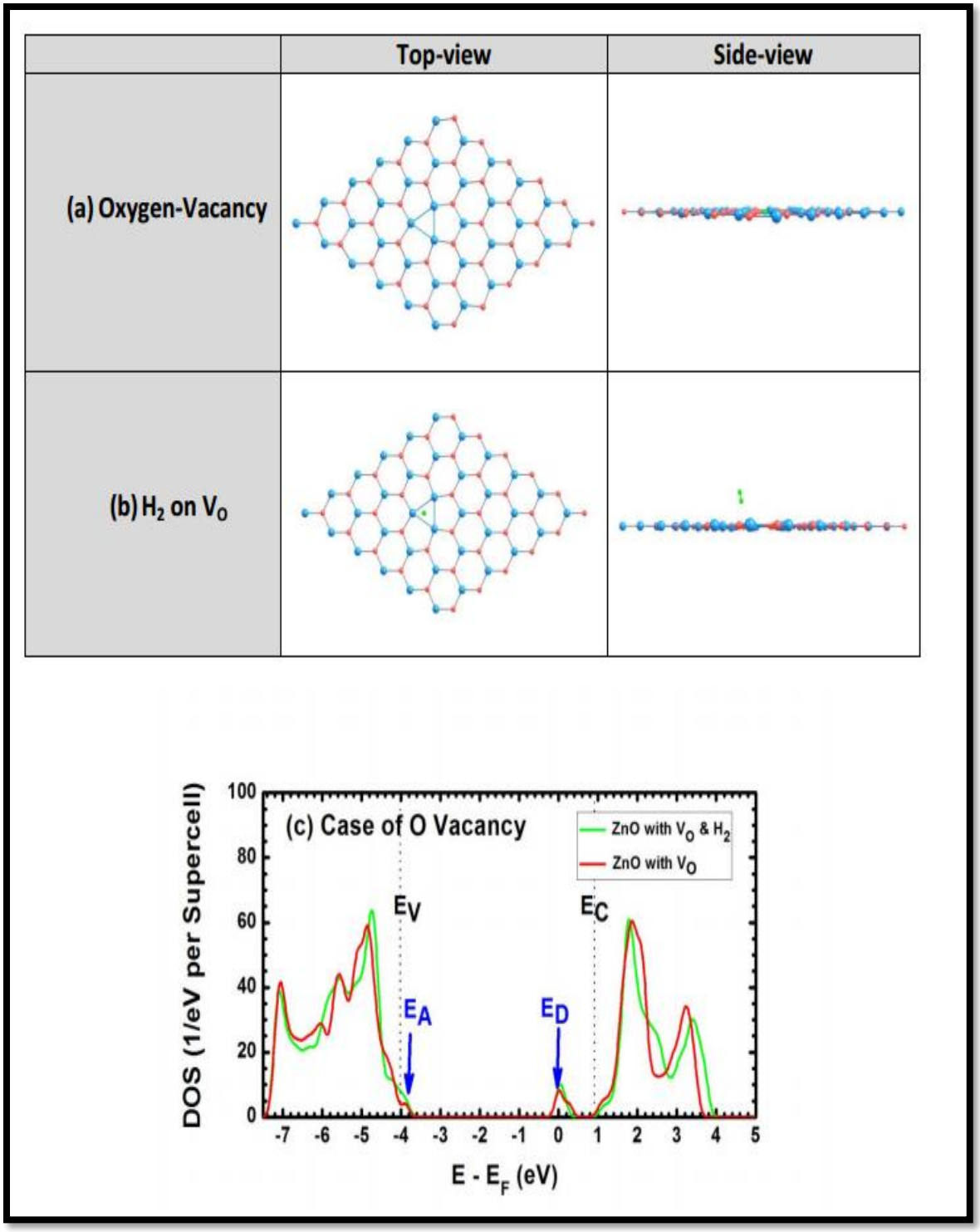

Figure 21: Relaxed atomic structures of ZnO with VO (a) and with H_2 molecule (b). The corresponding DOSs to (a-b) are shown in (c), with Fermi level as an energy reference.

4.3.5 Band Structures

For accurate readings of the energetics of relaxed structures, one needs to show the band structures for various cases. Figure 22 shows the bands structures along three high-symmetry lines along the irreducible wedge of the BZ: (a) Pristine ZnO; (b) H_2 chemisorbed on ZnO starting its relaxation from the top of O-site; (c) ZnO containing single oxygen vacancy after a relaxation leading to the formation of extended defect; and (d) H_2 in a physisorption on V_O-defected ZnO. The results clearly show the following: (i) The chemisorption of H_2 on O-site would lead to the formation of a shallow donor state (E_C-E_D) ≈ 0.153 eV due to formation of O-H bond in which H plays the role of a donor; also it leads to formation of a deep acceptor state (E_A-E_V) ≈ 0.672 eV due to formation of Zn-H bond in which H plays the role of an acceptor. Of course, it should be understood that these values are overestimated using DFTB+ code. (ii) The reconstruction of the oxygen vacancy leads to a formation of an extended defect, composed of a triangle of three Zn atoms surrounded by 3 pentagon rings of ZnO. The results of bands for such an extended defect are shown in Figure 22c. The extended defect produces an acceptor state of (E_A-E_V) ≈ 0.225 eV and a doublet and singlet of donor states E_{D1} and E_{D2}, respectively. (E_{D1}-E_{D2}) ≈ 0.238 eV and (E_C-E_{D2}) ≈ 0.751 eV. Again, these values are overestimated when using DFTB+ code. (iii) The occurrence of physisorption of H_2 on reconstructed V_O would not affect much the locations of the donor and acceptor states as shown in Figure 22d. The interaction between the extended defect and H_2 molecule is via van der Walls weak dipole-dipole interaction.

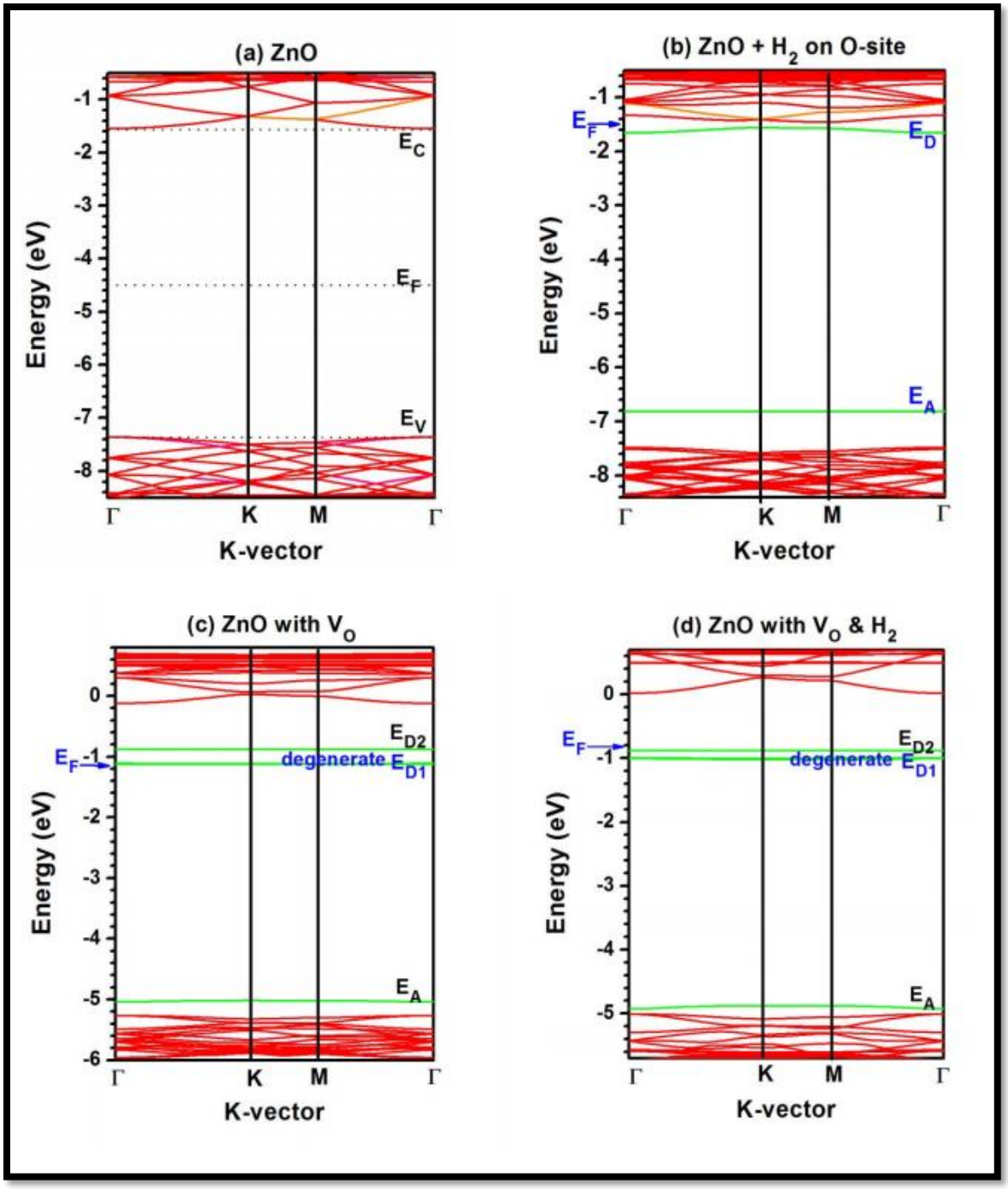

Figure 22: Band structures are shown for: (a) Pristine ZnO-2d; (2) Relaxed H_2 on ZnO in case of chemisorption (i.e., stating from on O-site); (c) Reconstructed oxygen vacancy; (d) relaxed H_2 on reconstructed VO, which yields physisorption.

4.4 Conclusions

The adsorption of H_2 gas molecule on graphitic ZnO-2d is investigated using DFTB, with the inclusion of van der Waals interaction and exclusion of heat effects (i.e., T = 0 ^oK). The chemical activities of many sites were assessed, namely by putting H_2 molecule on: (i) Zn-site, (ii) O-site, (iii) bridge-site, (iv) hollow-site, and (v) oxygen-vacancy site. The results show the following:

(1) The only case for occurrence of chemisorption is when H_2 molecule is put on O-site. The chemisorption is associated with a dissociation of H_2 molecule into two separate atoms that make single bonds to O and Zn atoms. These two bonds (O-H and Zn-H) produce a shallow donor and a deep acceptor states in the gap, respectively;

(2) The reconstruction of oxygen vacancy would form an extended defect consisting of a triangle of three Zn atoms, surrounded by three pentagon rings of ZnO. Such defect produces one singlet shallow acceptor state and a triplet of deep donor states. Consequently, Fermi level raises upper than the donor states due to such extended defect;s

(3) The estimations of band gap energy as well as relative energies of donor and acceptor states are overestimated using DFTB with the currently-available Slater-Koster files. In more realistic calculations, one should expect the following scenarios: (i) The reconstruction of oxygen vacancy leading to extended defect would introduce shallow donor states and make the material n-type; Then (ii) The chemisorption of H_2 molecules on O-site leading to formation of shallow donor and

deep acceptor states would definitely enrich the negative-charge carrier density and make the n-type semiconductor heavily-doped n-type. In this case Drude formula of conductivity would be validated and the estimation of conductivity would be reliable;

(4) Under the assumption of validity of metallic conductivity because of heavily-degenerated n-doping due to the chemisorption of H_2 molecules on O-sites, the sensitivity is shown to linearly increase versus the H_2 gas dose. Such behavior demonstrates the sensitivity of n-type ZnO towards detecting H_2 gas;

(5) This study is of great importance in the field of energy production and environmental protection, where ZnO can be used for both storage and detection of H_2 gas, respectively.

CHAPTER 5

CONCLUSIONS

This chapter restates the conclusions of the three studies conducted in this thesis.

For the first problem, the self-consistent-charge density-functional tight-binding (SCC-DFTB) method was employed to study the adsorption properties of CO_2 molecules on both pristine graphene and pure conducting ac-CNT, after being decorated with Fe metal-catalyst atoms. It was found that the catalyst plays a crucial role in inducing and enhancing the interaction to a level of achieving chemisorption state. The results of chemisorption of CO_2 molecule on G-Fe and ac-CNT-Fe compounds can be summarized as follows:

(1) It is recommended to deposit Fe atoms in a scattered manner on the surface of graphene or CNT, since any clustering of Fe atoms yields less binding to the surface and less coupling with CO_2 molecules. Thus, the clustering is found to yield lower sensitivity. The Fe atoms should be scattered and their ratio should be restricted with respect to the total number of existing carbon atoms. The optimum number should not exceed the order of a doping density in semiconductors (i.e., much less than 1% of total number of carbon atoms). Below that limit, Fe will enhance the DOS at Fermi level and lead to considerable reduction of NF by the chemisorption of CO_2 molecules. The reduction of NF will enhance both the surface electrical resistance and sensitivity versus gas dose.

(2) The atomic relaxations demonstrate that the deposition of Fe on hollow site yields the most stable configuration. Additionally, the ac-CNT were found to have sensitivity much higher than those of graphene and zz-CNT. Thus, our study of sensitivity and selectivity was focused only on ac-CNT.

(3) In the study of sensitivity, CO_2 molecules were deposited on ac-CNT-Fe compound one by one (N = 0-5 molecules). NF was found to decrease, resulting in enhancement of resistance and sensitivity. The C=O double bonds were found to partially break down and become weaker and longer than those in free CO_2 molecule. The O-C-O angle was found to decrease to 154^o (this angle is likely dependent on curvature). Meanwhile, the average charge of oxygen increases against gas dose, because oxygen has higher electronegativity than carbon and would drain more charge from Fe atom with increasing gas dose.

(4) On the issue of selectivity, ac-CNT-Fe compound was found to be highly sensitive and selective towards three gases (CO, CO_2 and H_2O) to a greater degree than any other gas studied (such as O_2, N_2, H_2). The cost of production of ac-CNT-Fe systems being relatively low, would make them promising candidates for mass production of ac-CNT-Fe based sensors, filters, and storage devices.

For the second problem, using DFT calculations in combination with the non-equilibrium Green's function formalism we study the electronic transport properties of Fe-doped graphene nanoribbon to explore its properties for CO_2 detection. We found that the electronic transport in such hybrid system strongly depends on how metal atoms are attached to graphene. For example, the sFe-graphene system, where the metal atom

replaces one carbon atom, shows better electronic transport as compared to the aFe - graphene sample with the Fe atom adsorbed on the hollow site. The latter system is also less sensitive to the gas molecule adsorption, whereas the transmission of the former sample exhibits extra features due to the CO_2 attachment. The obtained changes in the electronic transmission originate from the nanoscale charge localizations in the system. Our findings indicate the importance of the metal atom attachment for developing graphene-based gas sensors.

For the third problem, the adsorption of H_2 gas molecule on graphitic ZnO-2d is investigated using DFTB, with the inclusion of van der Waals interaction and exclusion of heat effects (i.e., T = 0 ^oK). The chemical activities of many sites were assessed, namely by putting H_2 molecule on: (i) Zn-site, (ii) O-site, (iii) bridge-site, (iv) hollow-site, and (v) oxygen-vacancy site. The results show the following:

(1) The only case for occurrence of chemisorption is when H_2 molecule is put on O-site. The chemisorption is associated with a dissociation of H_2 molecule into two separate atoms that make single bonds to O and Zn atoms. These two bonds (O-H and Zn-H) produce a shallow donor and a deep acceptor states in the gap, respectively;

(2) The reconstruction of oxygen vacancy would form an extended defect consisting of a triangle of three Zn atoms, surrounded by three pentagon rings of ZnO. Such defect produces one singlet shallow acceptor state and a triplet of deep donor states. Consequently, Fermi level raises higher than the donor states due to such extended defects.

(3) The estimations of band gap energy as well as relative energies of donor and acceptor states are overestimated using DFTB with the currently-available Slater-Koster files. In more realistic calculations, one should expect the following scenarios: (i) The reconstruction of oxygen vacancy leading to extended defect would introduce shallow donor states and make the material n-type; Then (ii) The chemisorption of H_2 molecules on O-site leading to formation of shallow donor and deep acceptor states would definitely enrich the negative-charge carrier density and make the n-type semiconductor heavily-doped n-type. In this case Drude formula of conductivity would be validated and the estimation of conductivity would be reliable;

(4) Under the assumption of validity of metallic conductivity because of heavily-degenerated n-doping due to the chemisorption of H_2 molecules on O-sites, the sensitivity is shown to linearly increase versus the H_2 gas dose. Such behavior demonstrates the sensitivity of n-type ZnO towards detecting H_2 gas;

(5) This study is of great importance in the field of energy production and environmental protection, where ZnO can be used for both storage and detection of H_2 gas, respectively.

APPENDIX

METALLIC CONDUCTIVITY AND GAS SENSITIVITY

In a free-electron gas, such as in metals, Ohm's law relates the current density to the electric field (j=σE, where σ is the electric conductivity). Within the picture of the classical Drude's model [127], the only possible interaction of a free electron with its environment is through instantaneous collisions. The average time between subsequent collisions is τ, and conductivity is given by the formula:

$$\sigma = \frac{ne^2\tau}{m^*} = ne\mu \qquad \text{(A-1)}$$

where *n* is the number density of free electrons, *e* and *m* are charge and mass of free electron, and μ is the electron mobility. This formula is derived under assumptions of an applied static electric field and uniform temperature.

It should be further emphasized that the above conductivity depends only on the properties of the electrons at the Fermi surface, not on the total number of electron in the metal. The high conductivity of metals is to be ascribed to the high current, $\boldsymbol{j_F} = n\, e\, \boldsymbol{v_F}$, carried by the few electrons at the top of the Fermi surface, rather than to the total density of free electrons (i.e,$\boldsymbol{v_F}$ vF is Fermi velocity, and electrons of lower energy than

Fermi energy are slowly drifting). Thus, the electrical conductivity gains its main contribution from states near Fermi surface and may be written as [50]:

$$\sigma = \frac{1}{3} j_F^2 \tau g(E_F) \quad \text{(A-2)}$$

$g(E_F)$ is the density of states at Fermi level and E_F is Fermi energy.

From another perspective, using free-electron model at 0 K temperature, the density of states at Fermi level is given [127] by:

$$g(E_F) = \frac{3n}{2E_F} \quad \text{(A-3)}$$

Furthermore, it should be emphasized that in Ohm's law, the resistance R is connected to the resistivity ρ by:

$$R = \rho \frac{L}{A} \quad \text{(A-4)}$$

where L and A are the length and cross-sectional area of the sample. The counter-part of resistance is the conductance (G = 1/R) and the counter-part of resistivity is conductivity (σ = 1/ρ); so the conductance may be written as:

$$G = \sigma \frac{A}{L} \quad \text{(A-5)}$$

In gas-sensing, the concept of gas sensitivity "S" is based on the variation of resistance between two states (before and after exposure to gas). It is customary to define the sensitivity as follows [128-130]:

$$S = \frac{|I_g - I_o|}{I_o} \times 100\% = \frac{|G_g - G_o|}{G_o} \times 100\% \quad \text{(A-6)}$$

where the pairs of I_g, I_a, G_g, and G_a are the electric current intensity and the conductance before and after gas exposure, respectively. If we assume that the mobility of electron, its relaxation time, and samples size (L and A) to be gas independent, then the sensitivity may be written as:

$$S = \frac{|\sigma_g - \sigma_a|}{\sigma_a} \times 100\% = \frac{|n_g - n_a|}{n_a} \times 100\% \quad \text{(A-7)}$$

where n_g and n_a are the respective densities of electrons in presence and absence of gas. These densities should concern the electrons most responsible for conduction. As shown in equation (A-3), and neglecting the variation of Fermi energy before and after the landing of a gas molecule on the sample, the sensitivity can be written as:

$$S = \frac{\left|N_F^{(g)} - N_F^{(a)}\right|}{N_F^{(a)}} \times 100\% \quad \text{(A-8)}$$

where $N_F^{(g)}$ and $N_F^{(a)}$ are the density of states (DOS) at Fermi level with and without gas molecule, respectively. Furthermore, total DOS of either pristine graphene or CNT should be normalized (such as 8 electrons per hexagon) in order to keep a reference in dealing with ratio in equation (A-8).

REFERENCES

[1] Z. Liu, D. Guan, W. Wei, S. J. Davis, P. Ciais, J. Bai*, et al.*, "Reduced carbon emission estimates from fossil fuel combustion and cement production in China," *Nature,* vol. 524, pp. 335-338, 2015.

[2] A. B. Rao and E. S. Rubin, "A Technical, Economic, and Environmental Assessment of Amine-Based CO2Capture Technology for Power Plant Greenhouse Gas Control," *Environmental Science & Technology,* vol. 36, pp. 4467-4475, 2002/10 2002.

[3] G. F. Fine, L. M. Cavanagh, A. Afonja, and R. Binions, "Metal Oxide Semi-Conductor Gas Sensors in Environmental Monitoring," *Sensors,* vol. 10, pp. 5469-5502, 2010/06/01 2010.

[4] P. Nugent, Y. Belmabkhout, S. D. Burd, A. J. Cairns, R. Luebke, K. Forrest*, et al.*, "Porous materials with optimal adsorption thermodynamics and kinetics for CO2 separation," *Nature,* vol. 495, pp. 80-84, 2013/02/27 2013.

[5] O. Shekhah, Y. Belmabkhout, Z. Chen, V. Guillerm, A. Cairns, K. Adil*, et al.*, "Made-to-order metal-organic frameworks for trace carbon dioxide removal and air capture," *Nature Communications,* vol. 5, 2014/06/25 2014.

[6] M. S. Shafeeyan, W. M. A. W. Daud, A. Houshmand, and A. Shamiri, "A review on surface modification of activated carbon for carbon dioxide adsorption," *Journal of Analytical and Applied Pyrolysis,* vol. 89, pp. 143-151, 2010/11 2010.

[7] N. Zouadi, S. Messaci, S. Sam, D. Bradai, and N. Gabouze, "CO2 detection with CNx thin films deposited on porous silicon," *Materials Science in Semiconductor Processing,* vol. 29, pp. 367-371, 2015/01 2015.

[8] A. K. Mishra and S. Ramaprabhu, "Nano magnetite decorated multiwalled carbon nanotubes: a robust nanomaterial for enhanced carbon dioxide adsorption," *Energy Environ. Sci.,* vol. 4, pp. 889-895, 2011.

[9] K. K. Paulla and A. A. Farajian, "Concentration Effects of Carbon Oxides on Sensing by Graphene Nanoribbons: Ab Initio Modeling," *The Journal of Physical Chemistry C,* vol. 117, pp. 12815-12825, 2013/06/20 2013.

[10] K. Sumida, D. L. Rogow, J. A. Mason, T. M. McDonald, E. D. Bloch, Z. R. Herm*, et al.*, "Carbon Dioxide Capture in Metal–Organic Frameworks," *Chemical Reviews,* vol. 112, pp. 724-781, 2012/02/08 2012.

[11] L. I. Bendavid and E. A. Carter, "CO2Adsorption on Cu2O(111): A DFT+U and DFT-D Study," *The Journal of Physical Chemistry C,* vol. 117, pp. 26048-26059, 2013/12/12 2013.

[12] H. J. Yoon, D. H. Jun, J. H. Yang, Z. Zhou, S. S. Yang, and M. M.-C. Cheng, "Carbon dioxide gas sensor using a graphene sheet," *Sensors and Actuators B: Chemical,* vol. 157, pp. 310-313, 2011/09 2011.

[13] M. Rahimi, J. K. Singh, and F. Müller-Plathe, "CO2Adsorption on Charged Carbon Nanotube Arrays: A Possible Functional Material for Electric Swing Adsorption," *The Journal of Physical Chemistry C,* vol. 119, pp. 15232-15239, 2015/07/09 2015.

[14] S. Iijima, "Helical microtubules of graphitic carbon," *Nature,* vol. 354, pp. 56-58, 1991/11/07 1991.

[15] M. S. Dresselhaus, G. Dresselhaus, and P. C. Eklund, "Applications of Carbon Nanostructures," in *Science of Fullerenes and Carbon Nanotubes*, ed: Elsevier BV, 1996, pp. 870-917.

[16] F. Schedin, A. K. Geim, S. V. Morozov, E. W. Hill, P. Blake, M. I. Katsnelson*, et al.*, "Detection of individual gas molecules adsorbed on graphene," *Nature Materials,* vol. 6, pp. 652-655, 2007/07/29 2007.

[17] O. Leenaerts, B. Partoens, and F. M. Peeters, "Adsorption of H 2 O , N H 3 , CO, N O 2 , and NO on graphene: A first-principles study," *Physical Review B,* vol. 77, 2008/03/17 2008.

[18] F. Xia, V. Perebeinos, Y.-m. Lin, Y. Wu, and P. Avouris, "The origins and limits of metal–graphene junction resistance," *Nature Nanotechnology,* vol. 6, pp. 179-184, 2011/02/06 2011.

[19] K. R. Ratinac, W. Yang, S. P. Ringer, and F. Braet, "Toward Ubiquitous Environmental Gas Sensors—Capitalizing on the Promise of Graphene," *Environmental Science & Technology,* vol. 44, pp. 1167-1176, 2010/02/15 2010.

[20] S. S. Varghese, S. Lonkar, K. K. Singh, S. Swaminathan, and A. Abdala, "Recent advances in graphene based gas sensors," *Sensors and Actuators B: Chemical,* vol. 218, pp. 160-183, 2015/10 2015.

[21] Y. Zhao, X.-g. Li, X. Zhou, and Y.-n. Zhang, "Review on the graphene based optical fiber chemical and biological sensors," *Sensors and Actuators B: Chemical,* vol. 231, pp. 324-340, 2016/08 2016.

[22] T. Wang, D. Huang, Z. Yang, S. Xu, G. He, X. Li*, et al.*, "A Review on Graphene-Based Gas/Vapor Sensors with Unique Properties and Potential Applications," *Nano-Micro Letters,* vol. 8, pp. 95-119, 2015/11/26 2015.

[23] P. T. Yin, S. Shah, M. Chhowalla, and K.-B. Lee, "Design, Synthesis, and Characterization of Graphene–Nanoparticle Hybrid Materials for Bioapplications," *Chemical Reviews,* vol. 115, pp. 2483-2531, 2015/04/08 2015.

[24] F.-L. Meng, Z. Guo, and X.-J. Huang, "Graphene-based hybrids for chemiresistive gas sensors," *TrAC Trends in Analytical Chemistry,* vol. 68, pp. 37-47, 2015/05 2015.

[25] S. Gupta Chatterjee, S. Chatterjee, A. K. Ray, and A. K. Chakraborty, "Graphene–metal oxide nanohybrids for toxic gas sensor: A review," *Sensors and Actuators B: Chemical,* vol. 221, pp. 1170-1181, 2015/12 2015.

[26] J. E. Castellanos Águila, H. H. n. Cocoletzi, and G. H. n. Cocoletzi, "A theoretical analysis of the role of defects in the adsorption of hydrogen sulfide on graphene," *AIP Advances,* vol. 3, p. 032118, 2013.

[27] S. Wang, H. Sun, H. M. Ang, and M. O. Tadé, "Adsorptive remediation of environmental pollutants using novel graphene-based nanomaterials," *Chemical Engineering Journal,* vol. 226, pp. 336-347, 2013/06 2013.

[28] S. Mubeen, T. Zhang, N. Chartuprayoon, Y. Rheem, A. Mulchandani, N. V. Myung*, et al.*, "Sensitive Detection of H2S Using Gold Nanoparticle Decorated Single-Walled Carbon Nanotubes," *Analytical Chemistry,* vol. 82, pp. 250-257, 2010/01 2010.

[29] T. J. Bandosz, "On the Adsorption/Oxidation of Hydrogen Sulfide on Activated Carbons at Ambient Temperatures," *Journal of Colloid and Interface Science,* vol. 246, pp. 1-20, 2002/02 2002.

[30] R. Yan, D. T. Liang, L. Tsen, and J. H. Tay, "Kinetics and Mechanisms of H2S Adsorption by Alkaline Activated Carbon," *Environmental Science & Technology,* vol. 36, pp. 4460-4466, 2002/10 2002.

[31] J.-H. Tsai, F.-T. Jeng, and H.-L. Chiang, "Removal of H2S from exhaust gas by use of alkaline activated carbon," *Adsorption,* vol. 7, pp. 357-366, 2001.
[32] R. Martel, T. Schmidt, H. R. Shea, T. Hertel, and P. Avouris, "Single- and multi-wall carbon nanotube field-effect transistors," *Applied Physics Letters,* vol. 73, p. 2447, 1998.
[33] S. J. Tans, A. R. Verschueren, and C. Dekker, "Room-temperature transistor based on a single carbon nanotube," *Nature,* vol. 393, pp. 49-52, 1998.
[34] H. Choi, H. Kim, S. Hwang, W. Choi, and M. Jeon, "Dye-sensitized solar cells using graphene-based carbon nano composite as counter electrode," *Solar Energy Materials and Solar Cells,* vol. 95, pp. 323-325, 2011/01 2011.
[35] P. Avouris, Z. Chen, and V. Perebeinos, "Carbon-based electronics," *Nature Nanotechnology,* vol. 2, pp. 605-615, 2007/09/30 2007.
[36] X. Li, X. Liu, J. Huang, Y. Fan, and F.-z. Cui, "Biomedical investigation of CNT based coatings," *Surface and Coatings Technology,* vol. 206, pp. 759-766, 2011/11 2011.
[37] J.-S. Jeong and H.-W. Lee, "Curvature-enhanced spin-orbit coupling in a carbon nanotube," *Physical Review B,* vol. 80, 2009/08/07 2009.
[38] T. Zhang, S. Mubeen, N. V. Myung, and M. A. Deshusses, "Recent progress in carbon nanotube-based gas sensors," *Nanotechnology,* vol. 19, p. 332001, 2008/07/07 2008.
[39] R. K. Roy, M. P. Chowdhury, and A. K. Pal, "Room temperature sensor based on carbon nanotubes and nanofibres for methane detection," *Vacuum,* vol. 77, pp. 223-229, 2005/02 2005.
[40] C. Lu, H. Bai, B. Wu, F. Su, and J. F. Hwang, "Comparative Study of CO2Capture by Carbon Nanotubes, Activated Carbons, and Zeolites," *Energy & Fuels,* vol. 22, pp. 3050-3056, 2008/09/17 2008.
[41] F. Su, C. Lu, W. Cnen, H. Bai, and J. F. Hwang, "Capture of CO2 from flue gas via multiwalled carbon nanotubes," *Science of The Total Environment,* vol. 407, pp. 3017-3023, 2009/04 2009.
[42] Y. Jin, S. C. Hawkins, C. P. Huynh, and S. Su, "Carbon nanotube modified carbon composite monoliths as superior adsorbents for carbon dioxide capture," *Energy & Environmental Science,* vol. 6, p. 2591, 2013.
[43] M. Rahimi, D. J. Babu, J. K. Singh, Y.-B. Yang, J. J. Schneider, and F. Müller-Plathe, "Erratum: “Double-walled carbon nanotube array for CO2 and SO2 adsorption” [J. Chem. Phys. 143, 124701 (2015)]," *The Journal of Chemical Physics,* vol. 143, p. 169901, 2015/10/28 2015.
[44] G. Neri, "First Fifty Years of Chemoresistive Gas Sensors," *Chemosensors,* vol. 3, pp. 1-20, 2015/01/05 2015.
[45] M. D. Ganji and N. Danesh, "Adsorption of H2S molecules by cucurbit[7]uril: an ab initio vdW-DF study," *RSC Advances,* vol. 3, p. 22031, 2013.
[46] A. I. Ayesh, Z. Karam, F. Awwad, and M. A. Meetani, "Conductometric graphene sensors decorated with nanoclusters for selective detection of Hg2+ traces in water," *Sensors and Actuators B: Chemical,* vol. 221, pp. 201-206, 2015/12 2015.
[47] J. Dai, J. Yuan, and P. Giannozzi, "Gas adsorption on graphene doped with B, N, Al, and S: A theoretical study," *Applied Physics Letters,* vol. 95, p. 232105, 2009.
[48] M. Zhou, Y.-H. Lu, Y.-Q. Cai, C. Zhang, and Y.-P. Feng, "Adsorption of gas molecules on transition metal embedded graphene: a search for high-performance graphene-based catalysts and gas sensors," *Nanotechnology,* vol. 22, p. 385502, 2011/08/26 2011.

[49] L. Ma, J.-M. Zhang, K.-W. Xu, and V. Ji, "A first-principles study on gas sensing properties of graphene and Pd-doped graphene," *Applied Surface Science,* vol. 343, pp. 121-127, 2015/07 2015.
[50] H.-p. Zhang, X.-g. Luo, H.-t. Song, X.-y. Lin, X. Lu, and Y. Tang, "DFT study of adsorption and dissociation behavior of H2S on Fe-doped graphene," *Applied Surface Science,* vol. 317, pp. 511-516, 2014/10 2014.
[51] A. S. Alshammari, L. Chi, X. Chen, A. Bagabas, D. Kramer, A. Alromaeh*, et al.*, "Visible-light photocatalysis on C-doped ZnO derived from polymer-assisted pyrolysis," *RSC Advances,* vol. 5, pp. 27690-27698, 2015.
[52] J. Xue, S. Ma, Y. Zhou, and Z. Zhang, "Facile synthesis of ZnO–C nanocomposites with enhanced photocatalytic activity," *New Journal of Chemistry,* vol. 39, pp. 1852-1857, 2015.
[53] T. Frauenheim, G. Seifert, M. Elstner, T. Niehaus, C. Köhler, M. Amkreutz*, et al.*, "Atomistic simulations of complex materials: ground-state and excited-state properties," *Journal of Physics: Condensed Matter,* vol. 14, pp. 3015-3047, 2002/03/08 2002.
[54] P. Koskinen and V. Mäkinen, "Density-functional tight-binding for beginners," *Computational Materials Science,* vol. 47, pp. 237-253, 2009/11 2009.
[55] R. A. Betts, O. Boucher, M. Collins, P. M. Cox, P. D. Falloon, N. Gedney*, et al.*, "Projected increase in continental runoff due to plant responses to increasing carbon dioxide," *Nature,* vol. 448, pp. 1037-1041, 2007/08/30 2007.
[56] J. Meyer, "Crisis reading," *Nature,* vol. 455, pp. 733-733, 2008/10/09 2008.
[57] D. W. Keith, "Why Capture CO2 from the Atmosphere?," *Science,* vol. 325, pp. 1654-1655, 2009/09/24 2009.
[58] R. S. Haszeldine, "Carbon Capture and Storage: How Green Can Black Be?," *Science,* vol. 325, pp. 1647-1652, 2009/09/24 2009.
[59] S. Chu and A. Majumdar, "Opportunities and challenges for a sustainable energy future," *Nature,* vol. 488, pp. 294-303, 2012/08/15 2012.
[60] T. Zhu and E. Ertekin, "Resolving anomalous strain effects on two-dimensional phonon flows: The cases of graphene, boron nitride, and planar superlattices," *Physical Review B,* vol. 91, 2015/05/20 2015.
[61] T. Zhu and E. Ertekin, "Generalized Debye-Peierls/Allen-Feldman model for the lattice thermal conductivity of low-dimensional and disordered materials," *Physical Review B,* vol. 93, 2016/04/11 2016.
[62] C. Dekker, S. J. Tans, and A. R. M. Verschueren, *Nature,* vol. 393, pp. 49-52, 1998/05/07 1998.
[63] A. K. Mishra and S. Ramaprabhu, "Magnetite decorated graphite nanoplatelets as cost effective CO2 adsorbent," *Journal of Materials Chemistry,* vol. 21, p. 7467, 2011.
[64] H. J. Monkhorst and J. D. Pack, "Special points for Brillouin-zone integrations," *Physical review B,* vol. 13, p. 5188, 1976.
[65] J. C. Slater and G. F. Koster, "Simplified LCAO method for the periodic potential problem," *Physical Review,* vol. 94, p. 1498, 1954.
[66] M. Elstner, D. Porezag, G. Jungnickel, J. Elsner, M. Haugk, T. Frauenheim*, et al.*, "Self-consistent-charge density-functional tight-binding method for simulations of complex materials properties," *Physical Review B,* vol. 58, p. 7260, 1998.
[67] T. A. Niehaus, M. Elstner, T. Frauenheim, and S. Suhai, "Application of an approximate density-functional method to sulfur containing compounds," *Journal of Molecular Structure: THEOCHEM,* vol. 541, pp. 185-194, 2001.

[68] G. Zheng, H. A. Witek, P. Bobadova-Parvanova, S. Irle, D. G. Musaev, R. Prabhakar*, et al.*, "Parameter calibration of transition-metal elements for the spin-polarized self-consistent-charge density-functional tight-binding (DFTB) method: Sc, Ti, Fe, Co, and Ni," *Journal of chemical theory and computation,* vol. 3, pp. 1349-1367, 2007.

[69] C. Goringe, D. Bowler, and E. Hernandez, "Tight-binding modelling of materials," *Reports on Progress in Physics,* vol. 60, p. 1447, 1997.

[70] M. Elstner, "The SCC-DFTB method and its application to biological systems," *Theoretical Chemistry Accounts: Theory, Computation, and Modeling (Theoretica Chimica Acta),* vol. 116, pp. 316-325, 2006.

[71] P. Giannozzi, S. Baroni, N. Bonini, M. Calandra, R. Car, C. Cavazzoni*, et al.*, "QUANTUM ESPRESSO: a modular and open-source software project for quantum simulations of materials," *Journal of physics: Condensed matter,* vol. 21, p. 395502, 2009.

[72] D. Vanderbilt, "Soft self-consistent pseudopotentials in a generalized eigenvalue formalism," *Physical Review B,* vol. 41, p. 7892, 1990.

[73] J. P. Perdew, K. Burke, and M. Ernzerhof. (1997). *Generalized Gradient Approximation Made Simple*.

[74] S. Grimme, "Semiempirical GGA-type density functional constructed with a long-range dispersion correction," *Journal of computational chemistry,* vol. 27, pp. 1787-1799, 2006.

[75] V. I. Hegde, S. N. Shirodkar, N. Tit, U. V. Waghmare, and Z. H. Yamani, "First principles analysis of graphene and its ability to maintain long-ranged interaction with H 2 S," *Surface Science,* vol. 621, pp. 168-174, 2014.

[76] S. Kouser, U. V. Waghmare, and N. Tit, "Adsorption and splitting of H 2 S on 2D-ZnO 1− x N y: first-principles analysis," *Physical Chemistry Chemical Physics,* vol. 16, pp. 10719-10726, 2014.

[77] J. Dai and J. Yuan, "Adsorption of molecular oxygen on doped graphene: Atomic, electronic, and magnetic properties," *Physical Review B,* vol. 81, 2010/04/08 2010.

[78] B. Wanno and C. Tabtimsai, "A DFT investigation of CO adsorption on VIIIB transition metal-doped graphene sheets," *Superlattices and Microstructures,* vol. 67, pp. 110-117, 2014/03 2014.

[79] C. Chen, X.-D. Yang, Z.-Y. Zhou, Y.-J. Lai, M. Rauf, Y. Wang*, et al.*, "Aminothiazole-derived N,S,Fe-doped graphene nanosheets as high performance electrocatalysts for oxygen reduction," *Chem. Commun.,* vol. 51, pp. 17092-17095, 2015.

[80] X. Li, X. Wang, L. Zhang, S. Lee, and H. Dai, "Chemically Derived, Ultrasmooth Graphene Nanoribbon Semiconductors," *Science,* vol. 319, pp. 1229-1232, 2008/02/29 2008.

[81] Y.-W. Son, M. L. Cohen, and S. G. Louie, "Energy Gaps in Graphene Nanoribbons," *Physical Review Letters,* vol. 97, 2006/11/22 2006.

[82] C. QuantumWise company, Denmark.

[83] G. Berdiyorov, M. Milošević, F. Peeters, and A. C. van Duin, "Stability of CH 3 molecules trapped on hydrogenated sites of graphene," *Physica B: Condensed Matter,* vol. 455, pp. 60-65, 2014.

[84] G. Berdiyorov, H. Bahlouli, and F. Peeters, "Effect of substitutional impurities on the electronic transport properties of graphene," *Physica E: Low-dimensional Systems and Nanostructures,* vol. 84, pp. 22-26, 2016.

[85] B. Zhou, B. Zhou, X. Chen, and G. Zhou, "Electronic transport for impurity-doped armchair-edge graphene nanoribbons," *The European Physical Journal B,* vol. 85, p. 121, 2012.

[86] X. Zheng, I. Rungger, Z. Zeng, and S. Sanvito, "Effects induced by single and multiple dopants on the transport properties in zigzag-edged graphene nanoribbons," *Physical Review B,* vol. 80, p. 235426, 2009.
[87] C. Wang, L. Yin, L. Zhang, D. Xiang, and R. Gao, "Metal oxide gas sensors: sensitivity and influencing factors," *Sensors,* vol. 10, pp. 2088-2106, 2010.
[88] Y.-F. Sun, S.-B. Liu, F.-L. Meng, J.-Y. Liu, Z. Jin, L.-T. Kong*, et al.*, "Metal oxide nanostructures and their gas sensing properties: a review," *Sensors,* vol. 12, pp. 2610-2631, 2012.
[89] D. R. Miller, S. A. Akbar, and P. A. Morris, "Nanoscale metal oxide-based heterojunctions for gas sensing: a review," *Sensors and Actuators B: Chemical,* vol. 204, pp. 250-272, 2014.
[90] Y. Chen, D. Bagnall, and T. Yao, "ZnO as a novel photonic material for the UV region," *Materials Science and Engineering: B,* vol. 75, pp. 190-198, 2000.
[91] A. Tsukazaki, A. Ohtomo, T. Onuma, M. Ohtani, T. Makino, M. Sumiya*, et al.*, "Repeated temperature modulation epitaxy for p-type doping and light-emitting diode based on ZnO," *Nature materials,* vol. 4, p. 42, 2005.
[92] D.-K. Hwang, S.-H. Kang, J.-H. Lim, E.-J. Yang, J.-Y. Oh, J.-H. Yang*, et al.*, "p-ZnO/n-GaN heterostructure ZnO light-emitting diodes," *Applied Physics Letters,* vol. 86, p. 222101, 2005.
[93] S. H. Ko, D. Lee, H. W. Kang, K. H. Nam, J. Y. Yeo, S. J. Hong*, et al.*, "Nanoforest of hydrothermally grown hierarchical ZnO nanowires for a high efficiency dye-sensitized solar cell," *Nano letters,* vol. 11, pp. 666-671, 2011.
[94] H.-J. Kim, C.-H. Lee, D.-W. Kim, and G.-C. Yi, "Fabrication and electrical characteristics of dual-gate ZnO nanorod metal–oxide semiconductor field-effect transistors," *Nanotechnology,* vol. 17, p. S327, 2006.
[95] Ü. Özgür, Y. I. Alivov, C. Liu, A. Teke, M. Reshchikov, S. Doğan*, et al.*, "A comprehensive review of ZnO materials and devices," *Journal of applied physics,* vol. 98, p. 11, 2005.
[96] S. R. Anton and H. A. Sodano, "A review of power harvesting using piezoelectric materials (2003–2006)," *Smart materials and Structures,* vol. 16, p. R1, 2007.
[97] A. Kudo and Y. Miseki, "Heterogeneous photocatalyst materials for water splitting," *Chemical Society Reviews,* vol. 38, pp. 253-278, 2009.
[98] K. Maeda, T. Takata, M. Hara, N. Saito, Y. Inoue, H. Kobayashi*, et al.*, "GaN: ZnO solid solution as a photocatalyst for visible-light-driven overall water splitting," *Journal of the American Chemical Society,* vol. 127, pp. 8286-8287, 2005.
[99] X. Wang, K. Maeda, A. Thomas, K. Takanabe, G. Xin, J. M. Carlsson*, et al.*, "A metal-free polymeric photocatalyst for hydrogen production from water under visible light," *Nature materials,* vol. 8, pp. 76-80, 2009.
[100] R. Singh and H. S. Nalwa, "Medical applications of nanoparticles in biological imaging, cell labeling, antimicrobial agents, and anticancer nanodrugs," *Journal of biomedical nanotechnology,* vol. 7, pp. 489-503, 2011.
[101] J. W. Rasmussen, E. Martinez, P. Louka, and D. G. Wingett, "Zinc oxide nanoparticles for selective destruction of tumor cells and potential for drug delivery applications," *Expert opinion on drug delivery,* vol. 7, pp. 1063-1077, 2010.
[102] C. Hanley, J. Layne, A. Punnoose, K. Reddy, I. Coombs, A. Coombs*, et al.*, "Preferential killing of cancer cells and activated human T cells using ZnO nanoparticles," *Nanotechnology,* vol. 19, p. 295103, 2008.

[103] O. Bondarenko, K. Juganson, A. Ivask, K. Kasemets, M. Mortimer, and A. Kahru, "Toxicity of Ag, CuO and ZnO nanoparticles to selected environmentally relevant test organisms and mammalian cells in vitro: a critical review," *Archives of toxicology,* vol. 87, pp. 1181-1200, 2013.
[104] C. Wang, X. Chu, and M. Wu, "Detection of H 2 S down to ppb levels at room temperature using sensors based on ZnO nanorods," *Sensors and Actuators B: Chemical,* vol. 113, pp. 320-323, 2006.
[105] M. Kaur, N. Jain, K. Sharma, S. Bhattacharya, M. Roy, A. Tyagi*, et al.*, "Room-temperature H 2 S gas sensing at ppb level by single crystal In 2 O 3 whiskers," *Sensors and Actuators B: Chemical,* vol. 133, pp. 456-461, 2008.
[106] Y. S. Patil, F. C. Raghuvanshi, and I. D. Patil, "Zinc Oxide Nanorods as H2S Gas Sensor," *International Journal of Scientific Research,* vol. 5, 2016.
[107] J. Wang, X. W. Sun, A. Wei, Y. Lei, X. Cai, C. M. Li*, et al.*, "Zinc oxide nanocomb biosensor for glucose detection," *Applied Physics Letters,* vol. 88, p. 233106, 2006.
[108] J. M. Bockris, "Hydrogen economy in the future," *International Journal of Hydrogen Energy,* vol. 24, pp. 1-15, 1999.
[109] L. Barreto, A. Makihira, and K. Riahi, "The hydrogen economy in the 21st century: a sustainable development scenario," *International Journal of Hydrogen Energy,* vol. 28, pp. 267-284, 2003.
[110] T. Hübert, L. Boon-Brett, G. Black, and U. Banach, "Hydrogen sensors–a review," *Sensors and Actuators B: Chemical,* vol. 157, pp. 329-352, 2011.
[111] V. Aroutiounian, "Metal oxide hydrogen, oxygen, and carbon monoxide sensors for hydrogen setups and cells," *International Journal of Hydrogen Energy,* vol. 32, pp. 1145-1158, 2007.
[112] V. M. Aroutiounian, "Hydrogen detectors," *Int. Sci. J. Altern. Energy Ecol,* vol. 3, pp. 21-31, 2005.
[113] F. Rumiche, H.-H. Wang, and J. Indacochea, "Development of a fast-response/high-sensitivity double wall carbon nanotube nanostructured hydrogen sensor," *Sensors and Actuators B: Chemical,* vol. 163, pp. 97-106, 2012.
[114] G. Shen, "Fabrication and characterization of metal oxide nanowire sensors," *Recent patents on nanotechnology,* vol. 2, pp. 160-168, 2008.
[115] O. Lupan, G. Chai, and L. Chow, "Fabrication of ZnO nanorod-based hydrogen gas nanosensor," *Microelectronics Journal,* vol. 38, pp. 1211-1216, 2007.
[116] O. Lupan, G. Chai, and L. Chow, "Novel hydrogen gas sensor based on single ZnO nanorod," *Microelectronic Engineering,* vol. 85, pp. 2220-2225, 2008.
[117] O. Lupan, V. Ursaki, G. Chai, L. Chow, G. Emelchenko, I. Tiginyanu*, et al.*, "Selective hydrogen gas nanosensor using individual ZnO nanowire with fast response at room temperature," *Sensors and Actuators B: Chemical,* vol. 144, pp. 56-66, 2010.
[118] S. N. Das, J. P. Kar, J.-H. Choi, T. I. Lee, K.-J. Moon, and J.-M. Myoung, "Fabrication and characterization of ZnO single nanowire-based hydrogen sensor," *The Journal of Physical Chemistry C,* vol. 114, pp. 1689-1693, 2010.
[119] P. Patnaik, *A comprehensive guide to the hazardous properties of chemical substances*: John Wiley & Sons, 2007.
[120] Q.-H. Wu, J. Li, and S.-G. Sun, "Nano SnO2 gas sensors," *Current Nanoscience,* vol. 6, pp. 525-538, 2010.

[121] L. Ling, Z. Zhao, B. Wang, M. Fan, and R. Zhang, "Effects of CO and CO 2 on the desulfurization of H 2 S using a ZnO sorbent: a density functional theory study," *Physical Chemistry Chemical Physics,* vol. 18, pp. 11150-11156, 2016.
[122] G. Berdiyorov, H. Abdullah, M. Al Ezzi, G. Rakhmatullaeva, H. Bahlouli, and N. Tit, "CO2 adsorption on Fe-doped graphene nanoribbons: First principles electronic transport calculations," *AIP Advances,* vol. 6, p. 125102, 2016.
[123] N. H. Moreira, G. Dolgonos, B. Aradi, A. L. da Rosa, and T. Frauenheim, "Toward an accurate density-functional tight-binding description of zinc-containing compounds," *Journal of chemical theory and computation,* vol. 5, pp. 605-614, 2009.
[124] J. Rouquerol, F. Rouquerol, P. Llewellyn, G. Maurin, and K. S. Sing, *Adsorption by powders and porous solids: principles, methodology and applications*: Academic press, 2013.
[125] M. Batzill and U. Diebold, "Surface studies of gas sensing metal oxides," *Physical Chemistry Chemical Physics,* vol. 9, pp. 2307-2318, 2007.
[126] N. W. Ashcroft and N. W. Mermin, "Solid State Physics," D. G. Crane, Ed., ed: Harcourt College Pubishers, 1976, p. 29.
[127] J. M. Ziman, "Principles of the theory of solids," 2nd ed: Cambridge University Press, 1979, p. 211.
[128] A. I. Ayesh, "Linear hydrogen gas sensors based on bimetallic nanoclusters," *Journal of Alloys and Compounds,* vol. 689, pp. 1-5, 2016.
[129] A. I. Ayesh, A. F. Abu-Hani, S. T. Mahmoud, and Y. Haik, "Selective H 2 S sensor based on CuO nanoparticles embedded in organic membranes," *Sensors and Actuators B: Chemical,* vol. 231, pp. 593-600, 2016.
[130] M. A. Haija, A. I. Ayesh, S. Ahmed, and M. S. Katsiotis, "Selective hydrogen gas sensor using CuFe 2 O 4 nanoparticle based thin film," *Applied Surface Science,* vol. 369, pp. 443-447, 2016.
[131] N. Tit, M. M. Al Ezzi, H. M. Abdullah, M. Yusupov, S. Kouser, H. Bahlouli*, et al.*, "Detection of CO 2 using CNT-based sensors: Role of Fe catalyst on sensitivity and selectivity," *Materials Chemistry and Physics,* 2016.
[132] P. P. Shinde and V. Kumar, "Direct band gap opening in graphene by BN doping: Ab initio calculations," *Physical Review B,* vol. 84, p. 125401, 2011.
[133] M. Topsakal, S. Cahangirov, E. Bekaroglu, and S. Ciraci, "First-principles study of zinc oxide honeycomb structures," *Physical Review B,* vol. 80, p. 235119, 2009.
[134] B. Darwent, "Bond dissociation energies in simple molecules," *NSRDS-NBS NO. 31, U. S. DEPT. COMMERCE, WASHINGTON, D. C. JAN. 1970, 48 P,* 1970.
[135] L. Pauling, "The transition from one extreme bond type to another," *J. Am. Chem. Soc,* vol. 54, pp. 3570-3582, 1932.

VITAE

Name :Mohammed Mohammed Esmail Alezzi

Nationality :Yemeni

Date of Birth : 29/07/1991

Email :Mohammed.elezzi2015@gmail.com

Address : Ibb - Yemen

Academic Background :

Masters of Science, Physics (Sep, 2015- May, 2017).

Bachelor of Science, Physics (Jan,2011-May, 2015). Honor Student

Bachelor of Science, Mechanical Engineering (Jan,2011-May, 2015). Honor Student